ASSESSING THE PREDICTABILITY OF THE BEAUFORT SEA MINIMUM ICE EXTENT IN A CHANGING ARCTIC CLIMATE REGIME

A Thesis

by

LAURA MARIE QUIRK

Submitted to the Office of Graduate and Professional Studies of
Texas A&M University
in partial fulfillment of the requirements for the degree of

MASTER OF SCIENCE

Chair of Committee,	Oliver Frauenfeld
Committee Members,	Steven Quiring
	Andrew Dessler
Head of Department,	Vatche Tchakerian

May 2014

Major Subject: Geography

ABSTRACT

Understanding the climatic drivers of changes in sea ice extent in the Arctic has become increasingly important as record minima in the September sea ice extent continue to be reached. This research therefore addresses the question of which synoptic scale climatological features are most important in affecting changes in sea ice extent in the Beaufort Sea. First, three measures of sea ice extent—the Barnett Severity Index, the Beaufort Sea minimum sea ice extent, and the Arctic-wide minimum sea ice extent—are compared to assess their degree of agreement and consistency using goodness of fit techniques. Secondly, a number of atmospheric predictor variables are analyzed using a composite approach to identify the most relevant predictors of sea ice in the region. Thirdly, monthly statistical forecast models are created based on multiple regressions and classification and regression trees (CART) to predict the minimum sea ice extent beginning in October of the previous year.

Many differing measures have been used to quantify sea ice conditions in the Beaufort Sea, although no study has assessed these measures for consistency. When compared, all three measures indicate the same level of agreement according to the goodness of fit tests. This indicates that the choice of measure can be determined based on the specific application, as no measure outperforms another. In addition to differing measures of sea ice extent, differing predictor variables have been utilized to predict summer sea ice conditions. This study assesses all potentially relevant predictor variables and indicates that upper atmospheric air temperatures at 850 hPa, 700 hPa, and

500 hPa, monthly mean surface air temperatures, freezing degree days, thawing degree days, sea level pressure, total ice concentration, and multiyear ice concentration showed the strongest relationships with sea ice. Various teleconnection patterns including the Arctic Oscillation, the North Atlantic Oscillation, and the Pacific-North American pattern also showed strong relationships with these variables and are therefore believed also have some predictive utility. Finally, monthly multiple linear regression and CART models are created to predict the September sea ice extent using a number of climatic predictor variables. The results of these models suggest that antecedent sea ice conditions (total and multiyear ice concentration) and surface air temperature are the most important variables in predicting summer sea ice extent. The potential predictive power of the forecasts increases as predictions are made closer to the September minimum sea ice extent, with the most precise predictions made during July. This research confirms previous studies and provides a useful compilation of the state of the knowledge on the drivers of sea ice changes in the Beaufort Sea.

NOMENCLATURE

AA	Arctic Amplification
AO	Arctic Oscillation
AW	Arctic-Wide Minimum Ice Extent
BS	Beaufort Sea Minimum Ice Extent
BSI	Barnett Severity Index
CART	Classification and Regression Trees
CPC	Climate Prediction Center
d	Index of Agreement
DOE	Department of Energy
EA	East Atlantic Teleconnection Index
EAWR	East Atlantic/Western Russian Teleconnection Index
ENSO	El Niño/Southern Oscillation
EOF	Empirical Orthogonal Function
EPNP	East Pacific-North Pacific Teleconnection Index
FDD	Freezing Degree Days
GOF	Goodness of Fit
HDD	Heating Degree Days
IHO	International Hydrographic Organization
MAE	Mean Absolute Error
MLR	Multiple Linear Regression

MYI	Multiyear Ice Concentration
NAO	North Atlantic Oscillation
NCEP	National Centers for Environmental Prediction
NIC	National Ice Center
NOAA	National Oceanic and Atmospheric Administration
NSIDC	National Snow and Ice Data Center
PC	Principal Component
PCA	Principal Component Analysis
PDO	Pacific Decadal Oscillation
PE	Polar/Eurasian Teleconnection Index
PNA	Pacific-North American Teleconnection Pattern
rho	Spearman-Rank Correlation
r	Pearson's Product Moment Correlation Coefficient
R^2	Coefficient of Determination
R/O	Range-Offset
RMSE	Root Mean Square Error
SAT	Surface Air Temperature
SLP	Sea Level Pressure
SLR	Stepwise Linear Regression
SOI	Southern Oscillation Index
SOM	Self-Organizing Map
SST	Sea Surface Temperatures

TDD	Thawing Degree Days
TI	Total Ice Concentration
VIF	Variance Inflation Factor
WP	Western Pacific Teleconnection Index

TABLE OF CONTENTS

Page

ABSTRACT……..... ii

NOMENCLATURE……. iv

TABLE OF CONTENTS……. vii

LIST OF FIGURES…….. x

LIST OF TABLES……... xvi

CHAPTER I INTRODUCTION AND LITERATURE REVIEW……..... 1

I.1 Importance of the Cryosphere……. 2
I.2 Sea Ice……. 3
I.3 Arctic Amplification……... 6
I.4 Prediction Techniques……. 9
I.5 State and Limitation of Statistical Predictions in the Beaufort Sea…… 10
I.6 Research Objectives…… 11

CHAPTER II ASSESSMENT OF MEASURES OF SEA ICE EXTENT…….. 14

II.1 Introduction……... 14
II.2 Study Area……. 15
II.3 Data…… 15
II.4 Methods……. 19
II.4.1 Evaluation Techniques……... 19
II.5 Results……... 22
II.5.1 Goodness-of-Fit Measures…….. 25
II.4.2 Linear Regression……... 29
II.6 Discussion and Conclusions…….. 31

CHAPTER III ANALYSIS OF PREDICTOR VARIABLES……. 34

III.1 Introduction…….. 34
III.1.1 Research Objective…… 37
III.1.2 Atmosphere Variable Selection……. 38
III.1.3 Teleconnection Selection…….. 40
III.1.4 Long-Term Teleconnection Analysis…… 41
III.2 Study Region…… 42

III.3 Data……..... 42
III.3.1 National Snow and Ice Data Center (NSIDC) Sea Ice Data…. 42
III.3.2 Multiyear Ice Data……. 43
III.3.3 National Centers for Environmental Prediction (NCEP)/Department of Energy (DOE) Reanalysis 2……... 43
III.3.4 Teleconnections……. 45
III.4 Methods…… 46
III.4.1 Part 1: Composite Analysis……... 46
III.4.2 Part 2: Teleconnections……. 48
III.4.3 Part 3: Long-Term Teleconnection Relationships…… 48
III.5 Results…….. 50
III.5.1 Part 1: Composite Analysis……... 50
III.5.2 Part 2: Predictor Variable Correlations with Teleconnections…… 76
III.5.3 Part 3: Long-Term Teleconnection Relationships…… 107
III.6 Conclusions…….. 121
III.6.1 Part 1: Composite Analysis……... 121
III.6.2 Part 2: Teleconnections……. 123
III.6.3 Part 3: Long-Term Teleconnection Relationships…… 124
III.6.4 Final Conclusions…….. 125

CHAPTER IV PREDICTING SEPTEMBER SEA ICE EXTENT……. 126

IV.1 Introduction…….. 126
IV.1.1 Limitations of Statistical Forecasts of Sea Ice Extent……... 128
IV.2 Study Regions…….. 131
IV.3 Data…….. 132
IV.4 Methods…… 133
IV.4.1 Part 1: Principal Component Analysis…….. 133
IV.4.2 Part 2: Stepwise Linear Regression…….. 133
IV.4.3 Part 3: Classification and Regression Trees (CART)……... 135
IV.5 Results…….. 135
IV.5.1 Part 1: Principal Component Analysis…….. 135
IV.5.2 Part 2: Stepwise Linear Regression…….. 136
IV.5.3 Part 3: Classification and Regression Trees…….. 142
IV.6 Discussion and Conclusions……. 146
IV.6.1 Comparison to Previous Studies……... 147

CHAPTER V SUMMARY AND CONCLUSIONS……... 150

V.1 Assessment of Measures of Sea Ice Extent……... 151
V.2 Analysis of Predictor Variables……. 152
V.3 Predicting September Sea Ice Extent…… 154
V.4 Final Conclusions…….. 155

REFERENCES……. 157

LIST OF FIGURES

		Page
Figure 1	Map of study area. Basemap from ESRI online Basemaps in ArcMap 10. Blue lines outline the definition of the Beaufort Sea from the IHO. Black box outlines the study area utilized in Chapter III…….	16
Figure 2	Ice extent values for each measure from 1980 through 2012…….	17
Figure 3	Standardized ice extent for each measure from 1979 through 2012. BSI values are inverted……..	22
Figure 4	Comparisons of the standardized values of each measure. A shows the Beaufort Sea and Arctic, B shows the Beaufort Sea and the Barnett Severity Index, C shows the Arctic and the Barnett Severity Index……..	23
Figure 5	Correlation coefficients between the three measures. Bars indicate the 95% confidence intervals……	26
Figure 6	Linear regression equations for each measure. The top panel represents the Beaufort Sea minimum ice extent, the middle panel represents the Arctic-wide ice extent, and the bottom panel represents the Barnett Severity Index…….	30
Figure 7	Air temperature difference maps during April (left column), May (middle column), and June (right column) at four pressure levels (from top to bottom: 300 hPa, 500 hPa, 700 hPa, 850 hPa). Black dots represent the center point of grid cells with significant differences…….	52

Figure 8 Air temperature anomaly maps during July for the heavy ice years (left column) and the light ice years (right column) at four pressure levels (from top to bottom: 300 hPa, 500 hPa, 700 hPa, 850 hPa)……. 55

Figure 9 Air temperature standard deviation maps for the heavy ice years (left column) and the light ice years (right column) at 500 hPa during February (top row), July (middle row), and November (bottom row)……... 56

Figure 10 Geopotential height difference maps during June (left column), October (middle column), and December (right column) at four pressure levels (from top to bottom: 300 hPa, 500 hPa, 700 hPa, 850 hPa). Black dots represent the center point of grid cells with significant differences…… 59

Figure 11 Geopotential height anomaly maps during March (left group) and during September (right group). The right column of each group represents the light ice anomalies and the right column represents the heavy ice anomalies. Maps are displayed for four pressure levels (from top to bottom: 300 hPa, 500 hPa, 700 hPa, 850 hPa)…… 61

Figure 12 Difference maps for surface air temperatures (top row) and TDD (bottom row) during June, July, August (from left to right). Black dots represent the center point of grid cells with significant differences…… 64

Figure 13 Anomaly maps during January (left group), August (middle group), and October (right group) for SAT (top row) and FDD (for January and October) or TDD (August)

(bottom row). Light ice anomalies are shown in the left column of each group and heavy ice anomalies are shown in the right column…… 66

Figure 14 Difference maps for SLP (top row) and surface wind (bottom row) during March, June, and November (from left to right). Black dots represent the center point of grid cells with significant differences…… 68

Figure 15 Anomaly maps during March (left group), July (middle group), and October (right group) for SLP (top row) and surface wind (bottom row). The left column of each group represents light ice anomalies and the right column represents heavy ice anomalies……... 70

Figure 16 TI (top row) and MYI (bottom row) for February (left group) and August (right group) during heavy ice (left column) and light ice (right column) years……... 72

Figure 17 Difference maps for TI (top row) and MYI (bottom row) during March (left) and September (right). Black dots represent the center point of each grid cell with significant differences…….. 74

Figure 18 Air temperature correlation maps with AO during December (left) and January (right) at four pressure levels (from top to bottom: 300 hPa, 500 hPa, 700 hPa, 850 hPa). Cells with correlations significant at the 95% confidence level are plotted……... 77

Figure 19 Air temperature correlation maps with PNA during January (left) and

October (right) at four pressure levels (from top to bottom: 300 hPa, 500 hPa, 700 hPa, 850 hPa). Cells with correlations significant at the 95% confidence level are plotted……. 79

Figure 20 Air temperature correlation maps with EAWR during May (left) and December (right) at four pressure levels (from top to bottom: 300 hPa, 500 hPa, 700 hPa, 850 hPa). Cells with correlations significant at the 95% confidence level are plotted……... 81

Figure 21 Air temperature correlation maps with EPNP during March (left), July (middle), and November (right) at four pressure levels (from top to bottom: 300 hPa, 500 hPa, 700 hPa, and 850 hPa). Cells with correlations significant at the 95% confidence level are plotted…….. 83

Figure 22 Geopotential height correlation maps with AO during October (left) and NAO during September (middle) and October (right) at four pressure levels (from top to bottom: 300 hPa, 500 hPa, 700 hPa, 850 hPa). Cells with correlations significant at the 95% confidence level are plotted……... 86

Figure 23 Geopotential height correlation maps with PNA during September (left) and December (right) at four pressure levels (from top to bottom: 300 hPa, 500 hPa, 700 hPa, 850 hPa). Cells with correlations significant at the 95% confidence level are plotted…… 88

Figure 24 Geopotential height correlation maps with EAWR during February (left) and November (right) at four pressure

levels (from top to bottom: 300 hPa, 500 hPa, 700 hPa, 850 hPa). Cells with correlations significant at the 95% confidence level are plotted……... 90

Figure 25 Geopotential height correlation maps with EA during July (left) and EPNP during January (middle) and August (right) at four pressure levels (from top to bottom: 300 hPa, 500 hPa, 700 hPa, 850 hPa). Cells with correlations significant at the 95% confidence level are plotted…….. 91

Figure 26 Correlation maps with AO during January (left) and October (middle), and with NAO during October (right) for SAT (top row) and FDD (bottom row). Cells with correlations significant at the 95% confidence level are plotted…… 93

Figure 27 Correlation maps with PNA during August (left) and September (right) for SAT (top), FDD (middle), and TDD (bottom). Cells with correlations significant at the 95% confidence level are plotted……. 95

Figure 28 Correlation maps with EPNP during February (left), July (middle), and November (right) for SAT (top) and FDD (for February and November) and TDD (for July) (bottom). Cells with correlations significant at the 95% confidence level are plotted……... 97

Figure 29 Correlation maps for AO (left group) and NAO (right group) during March (left) and October (right) for SLP (top), wind speed (middle), and wind direction (bottom). Cells with correlations significant at the 95% confidence level are plotted……... 98

Figure 30 Correlation maps with PNA during

	February (left) and August (right) for SLP (top), wind speed (middle), and wind direction (bottom). Cells with correlations significant at the 95% confidence level are plotted……..	100
Figure 31	Correlation maps with EPNP during January (left) and July (right) for SLP (top), wind speed (middle), and wind direction (bottom). Cells with correlations significant at the 95% confidence level are plotted……	101
Figure 32	Correlation maps with AO during January (left) and August (right) for TI (top) and MYI (bottom). Cells with correlations significant at the 95% confidence level are plotted……	103
Figure 33	Correlation maps with NAO during July (left), August (middle), and December (right) for TI (top) and MYI (bottom). Cells with correlations significant at the 95% confidence level are plotted……..	104
Figure 34	Correlation maps with PNA during January (left) and September (right) for TI (top) and MYI (bottom). Cells with correlations significant at the 95% confidence level are plotted……..	105
Figure 35	PC maps for PC1, PC2, and PC3 for 850 hPa geopotential height (top group) and 850 hPa air temperature (bottom group) during January……	137

LIST OF TABLES

		Page
Table 1	Timing of light ice and heavy ice years…….	24
Table 2	Goodness-of-fit measures showing the level of agreement between the three measures of sea ice extent……..	25
Table 3	Percentage of grid cells with significant differences at the 95% confidence level…….	51
Table 4	The proportion of variance explained by the first five PCs for each predictor variable……..	108
Table 5	Concurrent correlations between the teleconnection patterns and PC1……	110
Table 6	Concurrent correlations between the teleconnection patterns and PC2……	110
Table 7	Concurrent correlations between the teleconnection patterns and PC3……	111
Table 8	Significant correlations for PC1 during the 1-month and 2-month lags……	112
Table 9	Significant correlations for MYI between PC1 and AO,NAO, and EAWR…….	114
Table 10	Significant correlations between teleconnection indices and PC1 for the 12-month lag……	114
Table 11	Significant correlations for PC2 during the 1-month and 2-month lags……	116
Table 12	Significant correlations for PC3 during the 1-month and 2-month lags……	117
Table 13	Results of the forward method SLR for each forecast month……..	139
Table 14	Results of the backward method SLR for	

each forecast month…… 141

Table 15 CART model results for each forecast month…… 143

Table 16 Ranked variable importance for each forecast month…… 145

CHAPTER I

INTRODUCTION AND LITERATURE REVIEW

Arctic climatology is strongly affected by those features of the cryosphere (portions of the Earth where water is in its solid form) that are present in the northern hemisphere (Lemke et al. 2007). The Arctic can be defined in many ways, including the area above the Arctic Circle (66.5°N) (Lemke et al. 2007), the area in the northern hemisphere where permafrost is present, or the area above the 50°F isotherm (Serreze and Barry 2005). Arctic climatology includes studies of glaciers, ice caps, ice sheets, sea ice, and frozen ground (Lemke et al. 2007). Although Arctic research began in the 1600s with explorations hoping to find new passages that linked the eastern and western hemispheres, quantitative studies focused on understanding the Arctic climate system did not begin until the late 1900s (World Climate Research Programme 2007). With the rise of the satellite era in the late 1970s, more detailed and reliable data could be obtained over larger spatial scales (World Climate Research Programme 2007). This allowed for more exhaustive studies to be performed and alleviated the accessibility problems that prevented extensive research before this time (World Climate Research Programme 2007).

The geography of the Arctic is characterized by the Arctic Ocean, located above 70°N, which is almost entirely surrounded by the landmasses of North America and Eurasia (Serreze and Barry 2005). This geography makes the Arctic unique compared to the Antarctic, which consists of a large landmass at the highest latitudes surrounded by

an ocean. Because of its high latitude, the Arctic has a very low energy state throughout the year. The least amount of thermal energy is received during winter, when the region above the Arctic Circle experiences 24-hour darkness. During the summer, the Arctic experiences 24-hour daylight. Throughout the year, the Arctic Ocean is covered by sea ice, which is mobile and shows a distinct seasonal cycle. The seasonal cycle is dependent on the surface air temperatures in the Arctic, which show large amounts of variation throughout the region depending on the geographic location. For example, surface air temperatures in the central Arctic Ocean are moderated throughout the year by heat exchanges between the ocean water and the overlying atmosphere, while some land areas experience large temperature ranges throughout the year (Serreze and Barry 2005).

I.1 Importance of the Cryosphere

The cryosphere plays an important role in the global climate system. It contains approximately 80% of all freshwater, with frozen ground representing the largest areal component (Lemke et al. 2007). Because it represents such a large area, aspects of the cryosphere such as snow cover and sea ice have important influences on the global energy budget. Some of the components of the cryosphere (e.g., snow and ice) have very high albedos, meaning they reflect most of the incoming solar radiation that reaches the surface, up to 80–90%. These surfaces thus prevent the absorption of this solar radiation and cool the surrounding area as well as the global climate (Lemke et al. 2007). Additionally, the components of the cryosphere can insulate ocean and land surfaces. The snow and ice holds in heat, which slows the transfer of energy from these covered

surfaces (either land or ocean water) to the overlying atmosphere (Serreze and Barry 2005). The Arctic also has important implications for the thermohaline circulation, which is driven by global oceanic temperature and salinity gradients (Serreze and Barry 2005). These gradients are influenced by the amount of freshwater that exits the Arctic. If larger quantities of freshwater are exported from the Arctic, it is possible that this circulation will break down or change in some way (Serreze and Barry 2005, Lemke et al. 2007). For this reason, it is critically important to understand the ways in which the Arctic adapts to global climatic changes.

I.2 Sea Ice

Sea ice extent in the Arctic has been steadily declining since the 1960s, and following slight increases in extent during the 1990s, has shown drastic decreases in the past decade (from 2002 onward) (Lemke et al. 2007, National Research Council 2012, Stroeve et al. 2011, Drobot and Maslanik 2003, Stroeve et al. 2008). Annual mean ice extent anomalies, calculated throughout the entire Arctic from 1978 to 2005, show a significant decreasing trend of $-33 \pm 7.4 \times 10^3$ km^2 yr^{-1} (-2.7 ± 0.6% per decade), with summer minimum ice extent, calculated from 1979 to 2005, showing an even stronger trend of $-60 \pm 20 \times 10^3$ km^2 yr^{-1} (-7.4 ± 2.4% per decade) (Lemke et al. 2007). While decreasing trends in ice extent are observed throughout the year, the most significant trends are observed in summer, where the six lowest ice extents on record have been observed in the last six summers (from 2007 to 2012) (National Research Council 2012, Stroeve et al. 2011, Serreze et al. 2007).

Observed decreases in sea ice extent, especially during September, can be explained through a combination of many distinct, yet interacting processes. The September sea ice extent can be linked to internal climate variability in surface air temperatures, circulation patterns in the atmosphere and ocean, the surface energy and hydrologic budgets, and human-induced changes as a result of increased concentrations of greenhouse gases (Serreze et al. 2007a, b, Stroeve et al. 2011, Serreze and Barry 2005). Although the basic physical explanations behind many of these processes are understood, the interaction between them is still a topic that needs further research. One of the most important unanswered questions in Arctic sea ice research is whether or not humans have induced an unprecedented change in Arctic sea ice and how this change will influence the global climate in the future (Stroeve et al. 2011, Serreze and Barry 2005, Lemke et al. 2007).

Of these Arctic-wide reductions in ice extent, the greatest decreases have been observed in the Beaufort and Chukchi seas and in the Kara and Laptev Seas (National Research Council 2012). Specifically, drastic ice extent decreases in the Beaufort Sea will have important impacts on international shipping legislation, as an ice-free Beaufort Sea signifies the opening of the Northwest Passage, a shipping lane connecting the Atlantic and Pacific Oceans (Griffiths 1987). The opening of this sea will represent the first battleground for unprecedented international shipping legislation, as countries compete for shipping privileges as well as exploration opportunities.

As the minimum ice extent continues to decline, more open water is present during the summer months. This increase in open water is accompanied by a host of

changes that may contribute a non-linear decline in ice extent in the coming years (Stroeve et al. 2011). More open water in September is accompanied by thinner first-year ice that is more susceptible to summer melt than older and thicker multiyear ice (Stroeve et al. 2011, National Research Council 2012). Multiyear ice is ice that survives the summer melt and is therefore thicker and more stable than first-year ice (Maslanik et al. 2007). Decreases in the amount of multiyear ice (increases in the amount of first-year ice) suggest that less ice is able to survive the summer melt and therefore more susceptible to yearly melting and continued decreases in ice extent. With thinner ice cover, open water is able to develop earlier in the year, which leads to an increase in the importance of the ice-albedo feedback mechanism (Stroeve et al. 2011). As ice cover decreases and more open water is present, albedo is decreased because the darker water absorbs more solar energy than the lighter ice (Deser et al. 2000). This increased absorption leads to further warming and melting of the ice (Deser et al. 2000). Also, in areas previously covered by ice the upper ocean is warmer and fresher and biological productivity at the base of the food chain has increased (National Research Council 2012). Sea-ice dependent marine mammals such as seals, whales, and walruses continue to lose habitat (National Research Council 2012, Drobot and Maslanik 2003) and increased open water along the coasts may increase the risks associated with storm surge and coastal erosion (Drobot and Maslanik 2003). In the Beaufort Sea, decreasing ice extent also has implications for indigenous populations, fishing communities, offshore oil exploration, and commercial shipping (Drobot and Maslanik 2003, Drobot 2003, National Research Council 2012). Because of the possibility of extreme changes

associated with decreasing summer ice extent, it has become increasingly important to understand and predict interannual variations.

I.3 Arctic Amplification

Arctic Amplification (AA) is the idea that the Arctic is warming disproportionately compared to overall global average warming (Serreze and Francis 2006, Serreze and Barry 2011). Although warming has been observed throughout the northern hemisphere, the Arctic has shown larger warming trends (Serreze and Barry 2011). At the time of carbon dioxide doubling, the Arctic warming (calculated for the region from 60°N to 90°N) was a large as 1.9 times greater than the global average warming (Winton 2006). This phenomenon has been observed in the temperature records for the past 50 years and has become increasingly noticeable in the last decade, especially during autumn and winter (Serreze and Francis 2006, Serreze and Barry 2011). Evidence suggests that AA will continue to increase and may have implications not only for Arctic regions, but for the overall global climate (Lawrence et al. 2008). AA is thought to be a response to human practices that have induced planetary warming and has particular importance for studies of Arctic sea ice.

Although AA is caused by a host of different physical processes, sea ice plays a critical role in this phenomenon. Throughout most of the year, sea ice insulates the Arctic Ocean water from the cold atmosphere. When sea ice is thick (during all seasons excluding summer), it is difficult for heat to be transferred from the warm ocean waters to the cold overlying atmosphere (Serreze and Barry 2005). In this way, sea ice dampens the warming that could occur from this transfer of heat from the ocean. If sea ice thins or

disappears entirely at the end of summer, this heat will be able to escape and ultimately warm the atmosphere (Francis and Hunter 2006). Analogously, the ice-albedo feedback will allow ocean waters to absorb more solar radiation (because they are exposed for longer during the summer), which will allow for increased heating. If the ocean becomes warmer, the temperature gradient between the ocean and cold atmosphere will become more pronounced, and a greater amount of heat will be released into the atmosphere, contributing to atmospheric warming (Serreze et al. 2011). This process explains AA in general, and also why AA is most pronounced during autumn and winter. The largest amount of ocean water is exposed during the summer, when the sea ice reaches its minimum extent. Therefore, the ocean heats up the most during the summer months. The highest air temperatures in the Arctic also occur during summer, so the temperature gradient between the ocean and air is small and therefore less energy transfer occurs. When temperatures start to plummet during autumn and winter because of significantly shorter day lengths, this temperature gradient becomes more extreme and the large amount of heat stored in the oceans can be transferred to the atmosphere (Serreze et al. 2009, Screen and Simmonds 2010, Serreze et al. 2011). This ultimately contributes to the pronounced AA signal during autumn and winter.

Because of the importance of sea ice changes in understanding AA, most scientists believe that AA is a surface-based phenomenon, meaning the signature of AA is most pronounced in the lower troposphere, with its influence becoming less noticeable as the distance to the surface is increased (Serreze et al. 2009, Serreze et al. 2011). The influence of AA on surface climatology, in the Arctic and in the northern hemisphere as

a whole, has already been observed. Studies have found that increased transfer of heat into the lower atmosphere has potentially weakened the polar jet stream (Overland and Wang 2010). Lui et al. (2012) and Francis et al. (2009) found that changes have occurred in the northern hemisphere atmospheric circulation, which can be attributed to AA, and that these new patterns resemble distinct phases of the Arctic Oscillation and North Atlantic Oscillation. Bhatt et al. (2010) suggest that AA has an influence on tundra vegetation growth, with increased air temperatures allowing for more vegetation to grow at high latitudes. Francis and Vavrus (2012) go even further and suggest that AA has contributed to observed changes in Rossby waves over North America. They suggest that AA could weaken zonal winds and increase wave amplitude. This would cause the Rossby waves to progress more slowly, increasing the possibility of extreme weather events in North America, such as flooding, drought, and heat waves (Fancis and Vavrus 2012). Although evidence of the existing impacts of AA has been discussed, these impacts are not fully accepted or understood (see Barnes 2013).

The potential impacts of AA in the future have been studied extensively using model simulations, although no consistent pattern of changes has been observed in the many studies that have been conducted. Depending on the input parameters (the expected ice conditions, changes in greenhouse gas concentrations, etc.), different results are observed. Many studies, including Alexander et al. 2004, Yamamato et al. 2006, Deser et al. 2010, and Higgins and Cassano 2009, find that the impacts of AA are confined to the Arctic itself, although the magnitude of these impacts vary widely between studies. Other studies suggest that the impacts of AA will be more widespread

(Seierstad and Bader 2008, Petoukhov and Semenov 2010, Lawrence et al. 2008). Although it is unknown exactly how AA will influence global climate in the future, it is clear that this phenomenon is critical in understanding the importance of Arctic sea ice change.

I.4 Prediction Techniques

To predict changes in sea ice extent, two modeling approaches are utilized: dynamical models and statistical models. Dynamical models utilize known physical relationships based on physics to make long-term projections about the state of the climate. Statistical models utilize statistical relationships between variables to make shorter-term predictions about climatic conditions. For sea ice forecasting, these statistical models rely on information about the seasonality of ice conditions and allow for forecasting up to a year in advance. The minimum ice extent is reached during September of each year, with ice beginning to refreeze in October as temperatures begin to decrease. The minimum extent in September represents the most noticeable change in ice conditions as a result of climate change and is therefore a useful proxy for the ice conditions each year. Starting with October climatological data, sea ice conditions for the following summer can be forecasted starting almost a year in advance and forecasts can be made up to one month in advance of the summer minimum. In the past, these statistical models have used a number of measures of summer sea ice conditions including the September minimum sea ice extent for the Beaufort Sea, the Barnett Severity Index, and the opening date of the Prudhoe Bay shipping lane (Drobot et al. 2009, Barnett 1980, Drobot 2003). A more detailed explanation of the utility of each of

these measures is provided in chapter II. The utility of statistical models is that they are easily adaptable to changing ice conditions and can be recreated every year with different predictor variables to improve upon predictions (National Research Council 2012).

I.5 State and Limitations of Statistical Predictions in the Beaufort Sea

Although several studies have examined the predictability of Beaufort Sea summer sea ice extent (Barnett 1980, Walsh 1980, Drobot and Maslanik 2003, Drobot 2003, Drobot 2007, Lindsay et al. 2008, Drobot et al. 2009), further research is needed to increase understanding of how predictor variables interact and how predictor relationships may change. Throughout these studies, many potential predictor variables have been examined, but no study has attempted to combine all useful variables. A more detailed analysis of the predictor variables utilized in these studies and the relative fit of these previous statistical models are provided in Chapter III and Chapter III. Studies have found that sea ice concentration (Drobot 2003, Drobot 2007, Lindsay 2008), surface air temperature (Walsh 1980, Drobot and Maslanik 2003, Drobot 2003, Drobot et al. 2009), sea level pressure (Walsh 1980, Barnett 1980, Drobot and Maslanik 2003, Drobot et al. 2009), teleconnections indices (Dumas et al. 2003, Drobot 2003), and ocean temperatures at varying depths (Lindsay et al. 2008) all have potential predictive ability, but no study has utilized all of these variables together. By combing all suggested variables, the predictive ability of seasonal forecasting models in the Beaufort Sea for all months can be improved.

Because of the chaotic nature of the Arctic and the state of the knowledge about drivers of sea ice changes, there are many limitations to this type of seasonal forecasting method (National Research Council 2012, Lemke et al. 2007). Firstly, the precision of predictions is hindered by our incomplete understanding of the complex interactions between sea ice, the ocean, and the atmosphere (National Research Council 2012, Stroeve et al. 2011). Secondly, a regime shift from thicker multiyear ice to thinner first year ice may limit the predicative ability of known climate variables (National Research Council 2012, Maslanik et al. 2007 b, Stroeve et al. 2007). With recent unprecedented sea ice melt and warming of the Arctic, it is possible that statistical relationships between sea ice extent and predictor variables are changing (Holland and Stroeve 2011). For example, Maslanik et al. (2007 b) and Holland and Stroeve (2011) suggest that the precision of the predictive relationship between AO and summer ice extent may be decreasing. Thirdly, the feedback processes between AA and sea ice are relatively unknown and it is therefore possible that more pronounced AA will have unknown impacts on Arctic sea ice, which could hinder our ability to accurately predict sea ice extent using statistical models (Serreze and Francis 2006, Serreze et al. 2011). Our predictive relationships rely on historical data, so as the Arctic shifts to predominately first year ice it is possible that the same relationships do not exist.

I.6 Research Objectives

This research addresses the question, which combination of synoptic scale climatological features drive summer sea ice extent in the Beaufort Sea? The purpose of this study is to evaluate the measures of ice conditions in the Beaufort Sea and to

determine the climatological features with the most skill in predicting these sea ice conditions in the following summer. This research intends to assess the predictive skill at differing time scales, from eleven months in advance to one month in advance, to assess the utility of longer-scale predictions and the degree to which the predictive ability of climatic variables changes throughout the year. The following objectives will be used to answer this question:

1. Determine the yearly minimum sea ice extent in the Beaufort Sea and evaluate this as a measure of sea ice conditions (chapter II),
2. identify relevant climatic predictor variables (chapter III), and
3. utilize relevant climatic predictor variables to determine the predictability of minimum ice extent in the following summer using monthly statistical models (chapter IV).

Commonly used measures of sea ice extent will be compared in Chapter II to determine the most appropriate measure as well as improve understanding of how previous studies utilizing different measures can be compared. Previous works have utilized various measures to represent summer sea ice conditions, but no comparative study has been made. In this way, comparisons between studies are difficult. Chapter II addresses this problem by comparing three of the most commonly used measures. In Chapter III, an assessment of all relevant predictor variables will be made to identify which variables show the most promise in improving statistical forecasts of sea ice extent. In previous statistical models, only a small number of predictor variables were utilized as input variables, meaning the predictive ability of these models was potentially

incomplete. A comprehensive study utilizing a large number of variables is necessary to determine which aspects of the climate system have the strongest predictive relationships with sea ice. In Chapter IV, a large number of potentially relevant variables will be assessed for a comprehensive overview. Finally, Chapter IV will utilize these predictor variables in creating statistical forecast models up to 11 months in advance of the September minimum sea ice extent. Using a large number of predictor variables, this assessment will provide useful information on the importance of specific predictor relationships in forecasting sea ice conditions up to a year in advance. This represents an updated assessment of the predictability of the Beaufort Sea minimum sea ice extent, which will provide critical information on the changes in the predictability of sea ice extent that have potentially occurred in recent years. As the Arctic continues to change, information regarding the potential decrease in the predictability of sea ice extent as well as changes in predictor relationships is critical in understanding and forecasting further modifications of sea ice.

CHAPTER II

ASSESSMENT OF MEASURES OF SEA ICE EXTENT

II.1 Introduction

Previous studies have examined changes in summer ice extent using various measures of summer sea ice extent, such as the Arctic-wide minimum ice extent (Lindsay et al. 2008, Stroeve et al. 2007) and the Barnett Severity Index (BSI) (Barnett 1980, Drobot and Maslanik 2003, Drobot 2003, Drobot et al. 2009). Although these measures have been widely used to quantify summer sea ice extent, the utility of each is largely unknown. The Arctic-wide minimum extent, because it includes information for a large area, may not accurately reflect the sea ice conditions in the Beaufort Sea. The BSI describes ice extent using attributes of the summer shipping season (Barnett 1980), and therefore may not be climatologically significant. This measure also includes information about the shipping lane throughout the summer, which may not accurately reflect the minimum ice extent, which is reached in September. This portion of my thesis will establish a new dataset of minimum ice extent values for the Beaufort Sea, following the procedure used by the National Snow and Ice Data Center (NSIDC) for the Sea Ice Index. This measure will represent the minimum ice extent (similar to the Arctic-wide extent) for only the Beaufort Sea, and is expected to represent Beaufort Sea ice changes more accurately than previously used measures. Specifically, this chapter will quantitatively compare these three different measures of summer minimum ice extent in the Beaufort Sea to assess the level of agreement between measures. This will provide

insight into the level of agreement between measures and can facilitate more direct comparisons between studies utilizing these different measures. This research will also provide a new measure of sea ice extent for the Beaufort Sea that can be utilized in future studies.

II.2 Study Area

The extent of the Beaufort Sea was determined using the limits defined by the International Hydrographic Organization (IHO) (Figure 1). The northern edge of the sea is defined by the line from Point Barrow, Alaska to Lands End, Prince Patrick Island (IHO 1953). The easternmost edge of the sea is defined as the line from Lands End through the southwest coast of Prince Patrick Island, then following the coast of Banks Island, and then to the mainland (IHO 1953). For this study the easternmost edge is defined as 124°W, the longitude of Lands End. The southernmost edge is truncated at 70°N. For the northern edge, all grid cells that intersect the line defined by the IHO are used. This includes all grid cells from 124°W to 156°W for latitudes 70°N to 72°N, from 124°W to 154°W for latitudes 72°N to 73°N, from 124°W to 149°W for latitudes 73°N to 74°N, from 124°W to 144°W for latitudes 74°N to 75°N, from 124°W to 135°W for latitudes 75°N to 76°N, and from 124°W to 130°W for latitudes 76°N to 77°N.

II.3 Data

In this study, three measures of ice extent are used: the Beaufort Sea minimum ice extent (BS), the Arctic-Wide minimum ice extent (AW), and the BSI. The time period of 1979 to 2012 will be used for comparison (Figure 2).

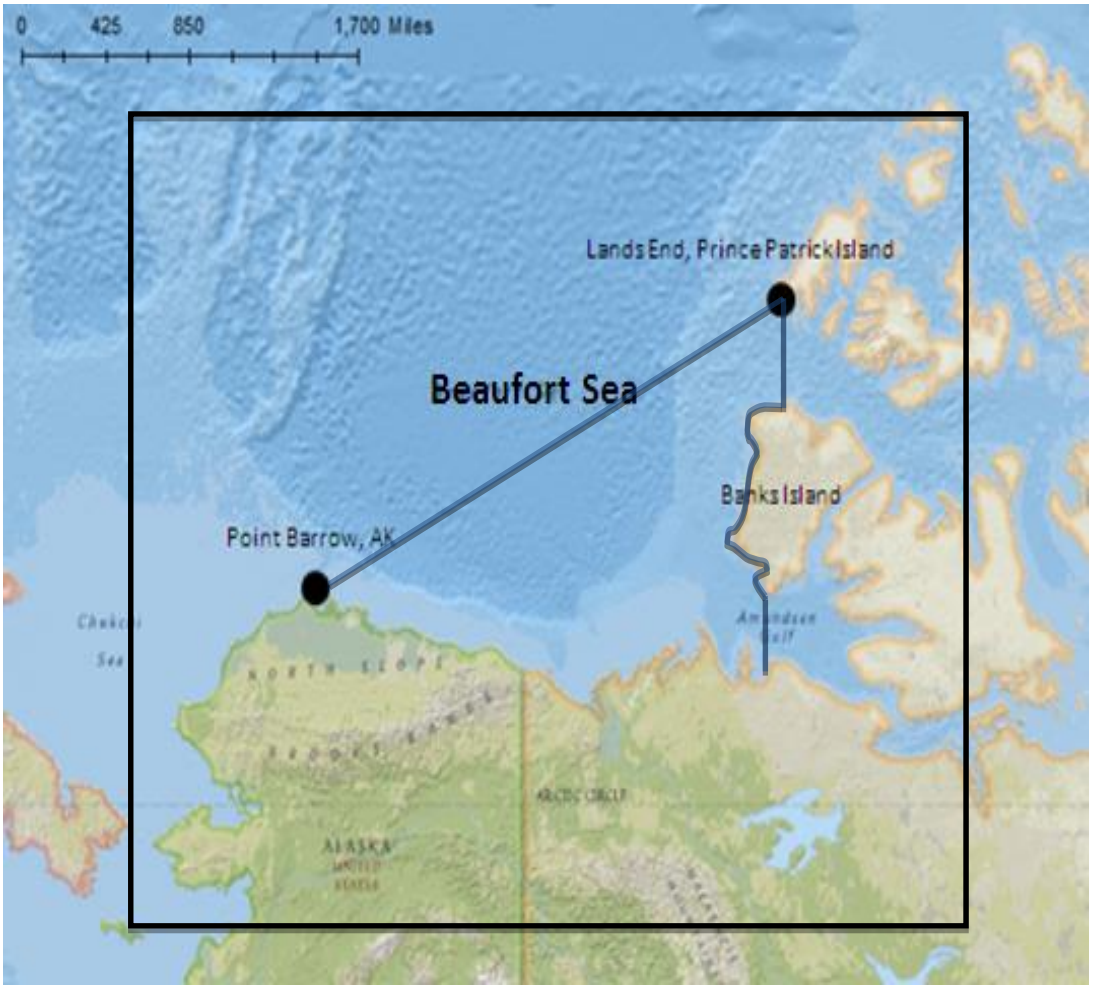

Figure 1: Map of study area. Basemap from ESRI online Basemaps in ArcMap 10. Blue lines outline the definition of the Beaufort Sea from the IHO. Black box outlines the study area utilized in Chapter III.

Daily sea ice concentration data for September of every year were obtained from the NSIDC Sea Ice Concentrations from Nimbus-7 Scanning Multichannel Microwave Radiometer (SMMR) and Defense Meteorological Satellite Program (DMSP) -F8, -F11

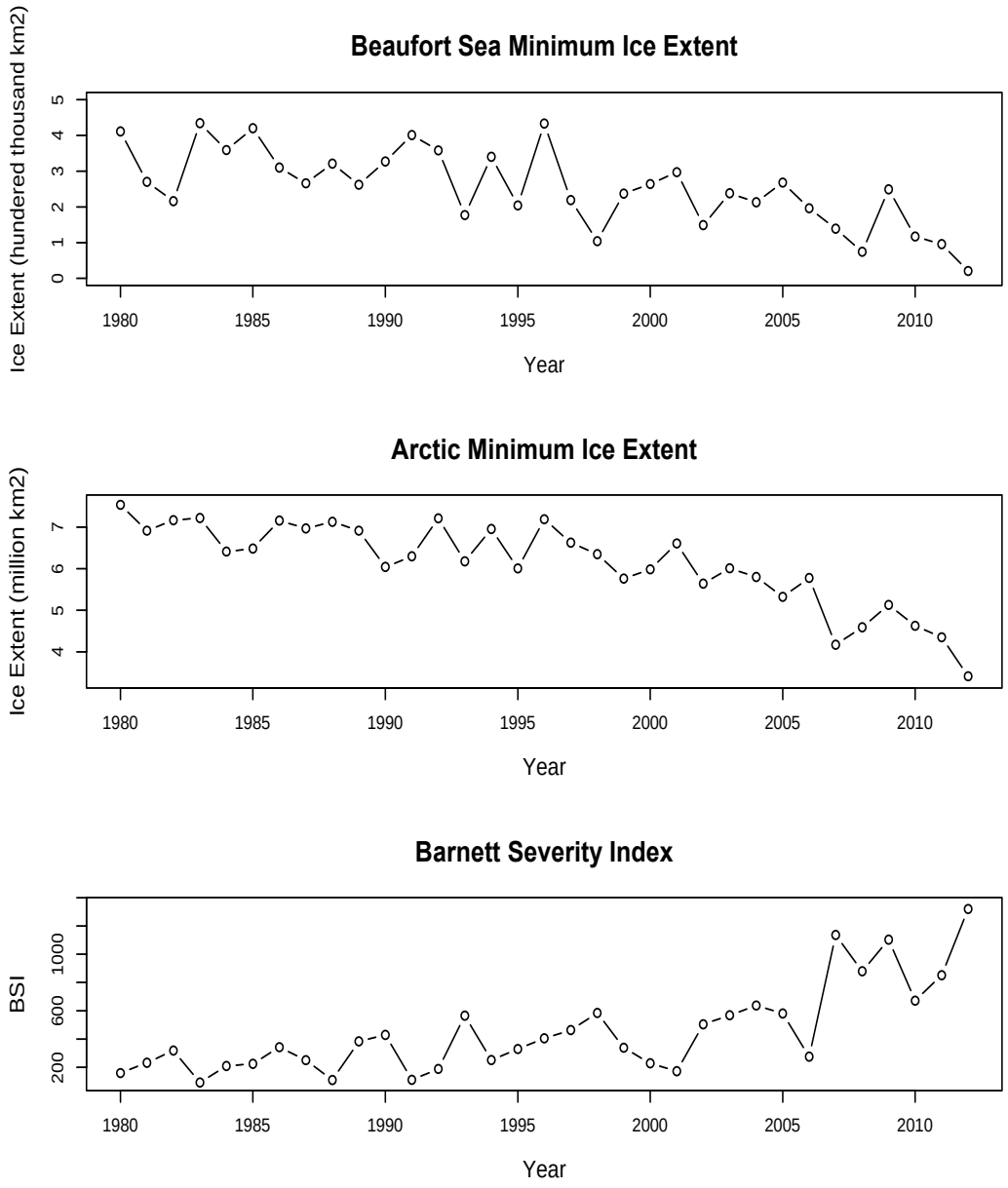

Figure 2: Ice extent values for each measure from 1980 through 2012.

and -F13 Special Sensor Microwave/Imagers (SSM/Is), and the DMSP-F17 Special Sensor Microwave Imager/Sounder (SSMIS) Passive Microwave Dataset for 1979 through 2012 (Cavalieri et al. 1996). The SMMR was operational every other day for the

period of 1980 through 1987. Starting in July of 1987, the two satellites (SSMR and SSM/I) are merged and provide daily sea ice concentrations. Concentration data are provided on a 25 km by 25 km grid as the percentage of each grid cell covered by ice. The daily minimum ice extent is defined as the total area of all grid cells in the study area with a sea ice concentration of 15% or greater, as used by the NSIDC for minimum ice extent calculations. BS is defined as the single day within the month of September when the minimum ice extent is reached.

AW is obtained from the Sea Ice Concentrations from Nimbus-7 SSMR and DMSP SSM/I Passive Microwave Data (Cavalieri et al. 1996). The daily minimum ice extent is defined as the total area of all grid cells with a sea ice concentration of 15% or greater. The daily minimum ice extent for the entire Arctic is defined as the single day within the month of September when the minimum ice extent is reached.

The BSI, obtained from the National Ice Center (NIC) in Washington D.C., is a unitless measure describing ice extent in the Beaufort Sea based on five parameters: (1) the distance (in nautical miles) from Point Barrow, AK northward to the ice edge on 15 September, (2) the distance from Point Barrow, AK northward to the boundary of 4/8 ice concentration on 15 September, (3) the initial date the entire sea route to Prudhoe Bay, AK is less than or equal to 4/8 ice concentration, (4) the number of days the entire sea route to Prudhoe Bay, AK is ice-free, and (5) the number of days the entire sea route to Prudhoe Bay, AK is less than or equal to 4/8 ice concentration (Barnett 1980). These five values are added to form the BSI, where smaller BSI values indicate larger ice extent and larger BSI values indicate a smaller ice extent (Figure 2).

II.4 Methods

II.4.1 Evaluation Techniques

Evaluation of the different measures of ice extent will consist of four parts: (1) comparison of long-term means, (2) analysis of the timing of heavy and light ice years, (3) goodness-of-fit measures, and (4) linear regression. Because the three measures describe ice extent using different scales, they are converted into Z-scores to allow for direct comparison. For each measure, the standardized value is calculated by subtracting the mean value from each individual yearly value and then dividing by the standard deviation of the dataset. BSI data represent ice extent inversely (higher BSI values indicate less ice), so the inverse of the BSI data are used for analysis to allow for direct comparison with the other two measures.

II.4.1.1 Long-Term Means

The long-term mean ice extent value for each measure is determined. This is done using the non-standardized values and is intended to show the differences in magnitude between the three datasets.

II.4.1.2 Analysis of the timing of light ice and heavy ice years

Using the standardized values, heavy and light ice years are determined for each measure and then compared for consistency. For each measure, a light ice year is any year with a standardized value less than or equal to −1 and a heavy ice year is any year with a standardized value greater than or equal to 1 (Rogers 1978, Drobot and Maslanik 2003).

II.4.1.3 Goodness-of -Fit Measures

Goodness-of-fit (GOF) measures are used to determine the degree of association between the different measures of ice extent. GOF analysis is performed for each combination of measures (BS with AW, BS with BSI, and AW with BSI) for both the standardized datasets and detrended datasets. For the detrended datasets, the residuals obtained from linear regression equations for each measure are utilized. The GOF measures used are the Pearson's product-moment correlation coefficient (r), the coefficient of determination (R^2), the Spearman-Rank correlation (rho), the root mean square error (RMSE), the mean absolute error (MAE), the index of agreement (d), and the range-offset (R/O).

The correlation coefficient and coefficient of determination describe the strength of the relationship between the two measures used. The coefficient of determination describes the proportion of the total variance in one measure than can be accounted for by the other. Both of these measures are more sensitive to outliers than to observations near the mean (Legates and Davis 1997) and are insensitive to additive and proportional differences between measures (Willmott 1984). They may thus not accurately reflect the amount of agreement between measures.

The Spearman-rank correlation is a nonparametric statistic that is less sensitive to outliers and therefore may provide a more robust characterization of the correlation between variables (Legates and McCabe 1999). A drawback of this nonparametric statistic is that because the data are converted to an ordinal (ranked) form, there is a loss of information (Legates and McCabe 1999).

The RMSE and MAE are commonly used to quantify the amount of error between datasets. For both the RMSE and the MAE, values closer to zero indicate better agreement between the two datasets. While the RMSE is a good indicator of agreement, it does not take into account the distribution of errors in the dataset, and is therefore sensitive to the distribution and magnitude of errors, as well as the sample size and outliers (Willmott and Matsuura 2005). The MAE is derived from the unaltered magnitude (absolute value) of difference between the two datasets (total error) divided by the number of observations (Willmott and Matsuura 2005).

The index of agreement (d) varies from 0.0 to 1.0, with higher values indicating better agreement between measures. This measure was developed to overcome the insensitivity of correlation-based measures to differences in the means of the two measures and variances (Willmott 1984). It represents an improvement over the coefficient of determination but is also sensitive to extreme values because it includes the squared differences between measures (Legates and McCabe 1999).

Finally, R/O represents the difference between the ranges of two datasets. Lower values indicate that the two datasets have similar ranges and therefore are likely to be in better agreement.

II.4.1.4 Linear Regression

Least-squares linear regression is performed for each measure and the resulting regression equations are compared. The slope will indicate the degree to which the datasets agree. If all measures are equal, it is expected that the regression equations (representing the overall trends in the datasets) would also be equal.

II.5 Results

All three measures of summer ice extent in the Beaufort Sea are similar (Figure 3). Figure 4 shows the standardized values of each measure plotted against one another. If the two measures were identical, the plotted points should fall along the 1 to 1 line. The greatest similarity is seen between the AW and the BSI. While these two measures

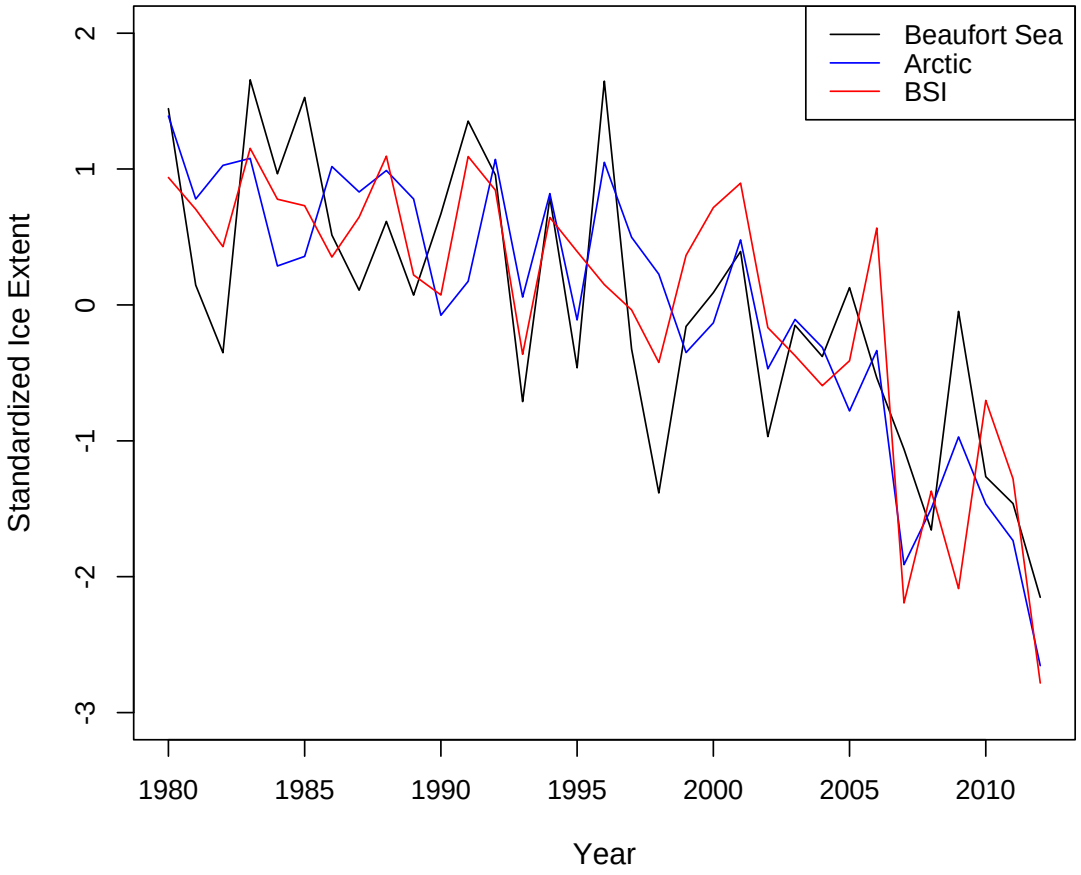

Figure 3: Standardized ice extent for each measure from 1979 through 2012. BSI values are inverted.

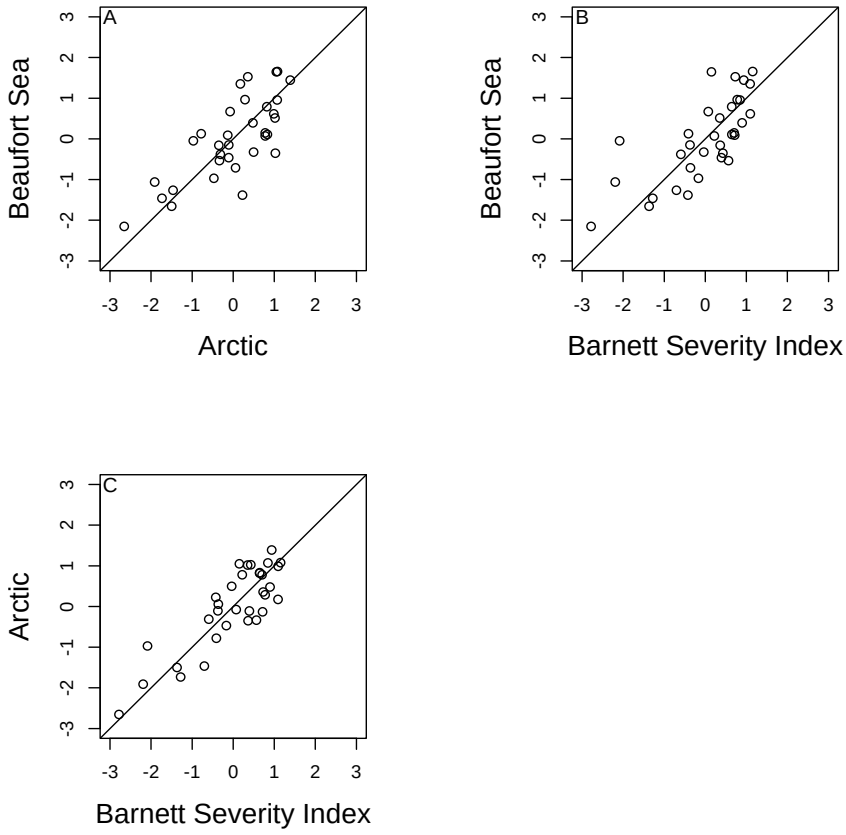

Figure 4: Comparisons of the standardized values of each measure. A shows the Beaufort Sea and Arctic, B shows the Beaufort Sea and the Barnett Severity Index, C shows the Arctic and the Barnett Severity Index.

show the strongest relationship, they each also show strong relationships with BS, suggesting that all three measures are related and depict summer ice extent variability in similar ways. When comparing the timing of light ice and heavy ice years, all three

measures agree for the light ice years of 2007, 2008, 2011, and 2012 (Table 1). All years selected for BS and AW match, while 2009 was only selected for BSI. Overall, the heavy ice years do not show as much consistency as the light ice years. For the heavy ice years, 1983 was the only year selected by all three measures.

Table 1: Timing of light ice and heavy ice years.

Light Ice Years			Heavy Ice Years		
Beaufort Sea	**BSI**	**Arctic**	**Beaufort Sea**	**BSI**	**Arctic**
2007	2007	2007	1980	1983	1980
2008	2008	2008	1983	1988	1982
2010	2009	2010	1985	1991	1983
2011	2011	2011	1991		1986
2012	2012	2012	1996		1992
					1996

The calculated long-term mean value for BS was 254,231 km^2, for AW was 6,119,515 km^2, and for BSI was 452. Because the AW represents a much larger area, it has a significantly larger mean value than the BS. The BSI values are much smaller because they do not represent the ice extent in km^2.

II.5.1 Goodness-of-Fit Measures

II.5.1.1 Standardized Datasets

All three variable combinations (BS and AW, BS and BSI, and AW and BSI) indicate statistically significant correlations at the 95% confidence level (Table 2a). The strongest correlation is between AW and BSI (r = 0.85), while the weakest correlation is for BS and BSI (r = 0.74). According to the correlation coefficients, BS is the variable least associated with the other two measures. Despite these differences in the r values, the 95% confidence intervals of all three variables overlap, which indicates that these

Table 2: Goodness-of-fit measures showing the level of agreement between the three measures of sea ice extent. A shows the results using the standardized datasets, B shows the results using the detrended datasets.

Goodness-of-Fit Measures									
A.						**Correlation**		**Spearman Rank**	
Measure	**R^2**	**RMSE**	**MAE**	**d**	**R/O**	**r**	**p-value**	**rho**	**p-value**
Beaufort Sea and Arctic	0.547	0.682	0.550	0.868	0.236	0.760	<0.001	0.545	<0.001
Beaufort Sea and BSI	0.458	0.710	0.579	0.854	0.127	0.740	<0.001	0.580	<0.001
Arctic and BSI	0.728	0.533	0.455	0.922	0.108	0.853	<0.001	0.557	<0.001
B.						**Correlation**		**Spearman Rank**	
Measure	**R^2**	**RMSE**	**MAE**	**d**	**R/O**	**r**	**p-value**	**rho**	**p-value**
Beaufort Sea and Arctic	0.192	0.667	0.530	0.658	0.714	0.438	0.011	0.367	0.036
Beaufort Sea and BSI	0.203	0.709	0.584	0.670	0.134	0.450	0.009	0.490	0.004
Arctic and BSI	0.377	0.525	0.447	0.770	0.580	0.614	<0.001	0.534	0.002

correlation coefficient values are not statistically significantly different (Figure 5).

Using rho, all three associations are again significant at the 95% confidence level and are similar in magnitude (Table 2a). The strongest correlation is between BS and

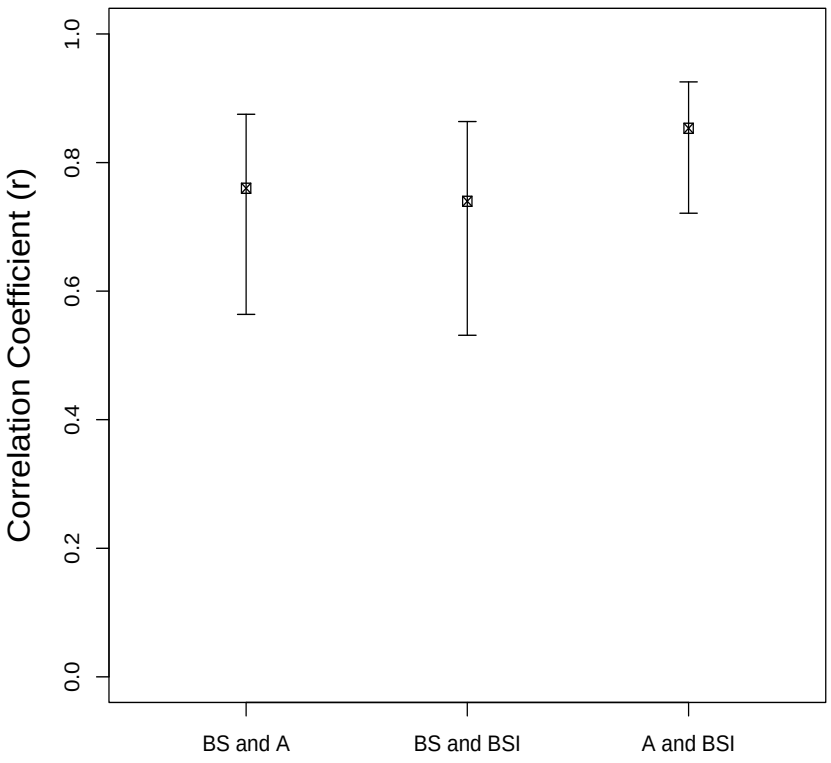

Figure 5. Correlation coefficients between the three measures. Bars indicate the 95% confidence intervals.

BSI (rho = 0.58), while the weakest correlation is for BS and AW (rho = 0.55). These Spearman-Rank correlations suggests that all three measures differ from each other by the same amount. This can be contrasted to the results from the correlation coefficient and coefficient of determination, which show that the largest discrepancies are seen in BS, with the greatest similarities seen between AW and BSI. These differences could be a result of the limitations in the correlation coefficient and coefficient of determination, which are sensitive to outliers and therefore may not accurately reflect associations

(Legates and Davis 1997), or because of the loss of data associated with rho (Legates and McCabe 1999).

The RMSE values (Table 2a) indicate that AW and BSI (RMSE = 0.53) are most similar, and BS and BSI (RMSE = 0.71) are least similar. These results agree with the correlation coefficient and coefficient of determination. Associations with BS show the greatest magnitude of errors (RMSE = 0.68 with AW and 0.71 with BSI), indicating the largest discrepancy. The MAE values (Table 2a) further confirm these results, with the strongest agreement between AW and BSI (MAE = 0.46) and the weakest agreement between BS and BSI (MAE = 0.58). The MAEs are smaller (0.46–0.58 vs. 0.53–0.71 for RMSE), due to the fact that the RMSE provides the square of the errors, which would exacerbate differences between the datasets.

The index of agreement (d) also indicates the strongest association between AW and BSI (d = 0.92) and the weakest association between BS and BSI (d = 0.854) (Table 2a).

The range-offset shows the greatest difference in range between BS and AW (R/O = 0.24) and the smallest difference between AW and BSI (R/O = 0.11) (Table 2a). The two associations with BSI show the lowest R/O's (0.11 with AW and 0.13 with BS). In general, the three values are very similar and indicate that all three measures have similar ranges.

II.5.1.2 Detrended Datasets

Table 2b shows the results from the goodness-of-fit measures for the detrended datasets. All three correlations are statistically significant at the 95% confidence level. In

all three cases, the correlation coefficient for the detrended datasets is weaker than the corresponding value for the standardized datasets, indicating that a common trend in all variables inflated the correlation magnitudes. As with the standardized datasets, the strongest correlation was seen between AW and BSI (r = 0.61), with weaker correlations between BS and AW (r = 0.44) and BS and BSI (r = 0.45). However, the overlapping confidence intervals (not shown) again suggest that these correlation magnitudes are not statistically significantly different. This is similar to the results seen with the standardized datasets.

The Spearman-Rank correlations for the detrended data differ from the standardized results. All three rho values are again significant at the 95% confidence level and the strongest correlation is again between AW and BSI (rho = 0.53). However, the weakest correlation is between BS and AW (rho = 0.37). The differences in rho between the standardized and detrended datasets again indicate that some of the associations observed in the standardized datasets are a product of a common (decreasing) trend in each of the three measures, and not a result of their degree of agreement.

The RMSE values for the detrended datasets (Table 2b) are very similar to the values obtained from the standardized datasets. For all three variable combinations, the detrended RMSEs are slightly lower than the standardized RMSEs, which suggests that the detrended datasets show slightly better agreement. The MAEs (Table 2b) again show similar results, with similar but slightly lower MAE values for the detrended BS–

AW and AW– BSI combinations. The MAE for BS and BSI is negligibly higher for the detrended data (MAE = 0.58).

For the detrended datasets, the index of agreement (d) is lower for all three combinations of measures when compared with the standardized d values (Table 2b). As for the standardized datasets, the strongest association is between AW and BSI (d = 0.77), although it is weaker than the corresponding value from the standardized data (d = 0.92). As with the standardized datasets, the d values for the associations between BS and AW (d = 0.66) and between BS and BSI (d = 0.67) are very similar.

The range-offset values for the detrended datasets (Table 2b) are larger than the standardized results for all three associations, which indicates that the negative trend in the standardized datasets may slightly skew the results of the analysis.

II.5.2 Linear Regression

Linear regression was performed for each sea ice measure (Figure 6). For all three linear regression equations, the slope is statistically significant at the 99% confidence level. The R^2 values indicate that the strongest level of agreement is seen for AW, where $R^2 = 0.72$. The weakest level of agreement is seen for BS, where $R^2 = 0.49$. For BSI, the R^2 value is 0.57. The BS and BSI represent summer ice extent in the Beaufort Sea, a much smaller area than represented by AW. These measures are therefore expected to show more interannual variation and should be less appropriate to represent using linear equations.

All three regression equations have approximately equal slopes (Figure 6). Because the three slopes are very similar, the three measures of summer ice extent and

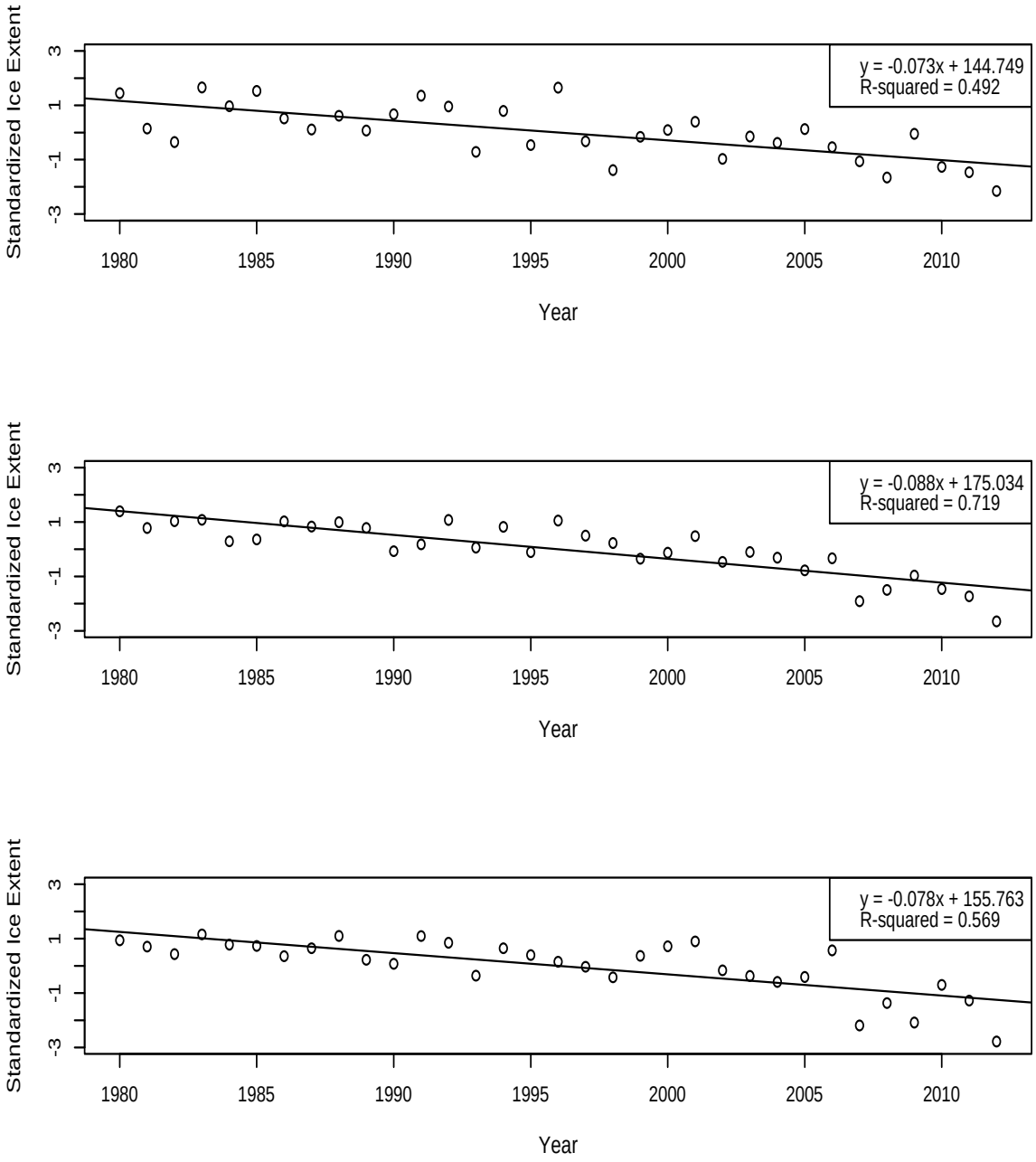

Figure 6: Linear regression equations for each measure. The top panel represents the Beaufort Sea minimum ice extent, the middle panel represents the Arctic-wide ice extent, and the bottom panel represents the Barnett Severity Index.

their temporal change are also very similar. If the input data for the three measures are very similar, the resulting regression equations are expected to be very similar as well.

The regression equations suggest that the three measures are indeed very similar (they all show about the same trends over time), although the distribution of AW may be more accurately reflected by the linear equation than the distributions of BS and BSI.

II.6 Discussion and Conclusions

This study examined the level of agreement between three different measures of summer sea ice extent: the Beaufort Sea minimum ice extent (BS), the Arctic-wide minimum ice extent (AW), and the Barnett Severity Index (BSI). The agreement between measures was assessed using an analysis of the timing of light ice and heavy ice years, goodness-of-fit measures, and linear regression. The following results were observed:

1. Of the goodness-of-fit measures, r, R^2, RMSE, MAE, d, and R/O indicate that the greatest amount of agreement is between AW and BSI, and less agreement with BS. This suggests that AW and BSI are the most similar of the measures and potentially provide more accurate representations of sea ice extent.
2. The goodness-of-fit measures indicate that while there may be slightly better agreement between AW and BSI than with BS, this difference is likely small enough to be negligible.
3. According to the results from the Spearman-Rank correlation (rho), the analysis of the timing of light ice and heavy ice years, and the linear regression, all three measures again show the same level of agreement. This indicates that any of the three measures could be used for an analysis of sea ice conditions and the same results would be expected.

4. An analysis of the detrended datasets indicates that the negative trend observed in all three datasets may have some effect on the results obtained from the goodness-of-fit measures, but this effect is very small.
5. Comparison of the timing of light ice and heavy ice years showed a stronger agreement between the three measures for the light ice years than for the heavy ice years. This suggests that the light ice events, occurring in the most recent years of record, are extreme enough to be captured by all three of these measures.
6. The linear regressions suggest that the trends are generally the same for all three measures. Because AW covers a larger area, a linear trend better captures the distribution of this data compared to the distributions of BS and BSI.

Overall, this research suggests that all three measures of summer sea ice extent represent summer ice conditions equally well. This means that the choice of which measure to use in future research can be made based on the specific intent of the study. AW characterizes sea ice conditions for the entire Arctic and therefore is most useful in larger-scale studies. The BSI utilizes shipping information in the Beaufort Sea and includes information about the entire summer shipping season, and is therefore most useful when studying ice conditions throughout the summer. BS represents the Beaufort Sea minimum ice conditions. This measure would be most useful in studies to determine specific conditions causing decreasing ice extent because it captures the region of most extreme ice loss in each year.

Because all three measures of ice extent represent different regions or time periods, it is interesting that they all show the same level of agreement. BS follows the

same general distribution as AW, even though AW represents a much larger area. Within the Arctic, specific seas show different trends in sea ice extent. Therefore it would be expected that certain smaller areas within the Arctic would have distributions that differ greatly from AW. It is therefore interesting that the Beaufort Sea follows the same general pattern of sea ice extent as the Arctic as a whole. The BSI does not incorporate any climatological measures to determine sea ice variability; it only uses the conditions of the shipping season to quantify sea ice extent. It is therefore interesting that the BSI shows a strong agreement with BS and AW. This indicates that even though the BSI may not be climatologically significant, it still represents the sea ice conditions well and is valid to use in climatological studies.

CHAPTER III

ANALYSIS OF PREDICTOR VARIABLES

III.1 Introduction

To predict changes in sea ice extent in the Beaufort Sea, previous studies have focused on creating statistical models. These models predict the summer ice conditions using a variety of different atmospheric and oceanic variables as input predictors (Barnett 1980, Walsh 1980, Drobot and Maslanik 2003, Drobot 2003, Drobot 2007, Lindsay et al. 2008, Drobot et al. 2009).

In one of the earliest studies applying a statistical prediction of sea ice extent, Barnett (1980) attempted to predict August extent in the Beaufort Sea using the strength of the Siberian High in April. Although he did not find any significant predictive skill using this high pressure system, he was able to define the BSI, which uses characteristics of the shipping lane north of Barrow, Alaska to quantify Beaufort Sea ice extent (Barnett 1980). This index became used in a number of statistical predictions (Drobot and Maslanik 2003, Drobot 2003, Drobot et al. 2009) and will be used in this study as a check on the minimum ice extent obtained from the National Snow and Ice Data Center (NSIDC), Boulder, Colorado.

Walsh (1980) attempted to use sea level pressure (SLP), surface air temperature (SAT), and prior sea ice extent anomalies to create monthly statistical models, lagged up to one year. He used empirical orthogonal functions and found the greatest predictive skill at a one month lag, and no significant predictive skill past a two month lag.

Drobot and Maslanik (2003) categorized ice extent into light and heavy ice years to identify the dynamic and thermodynamic mechanisms in winter and summer, which drive ice extent changes. In winter, a poorly defined Beaufort High (leading to a reduction in the Beaufort Gyre) and less multiyear ice lead to lighter ice summers (Drobot and Maslanik 2003). In summer, a well-defined Beaufort High (which results in strong easterlies and enhanced advection out of the Beaufort Sea) and elevated SAT lead to lighter ice conditions (Drobot and Maslanik 2003). Drobot and Maslanik (2003) also found a link between SLP and wind variations similar to phases of the Arctic Oscillation/ North Atlantic Oscillation (AO/NAO) and ice extent.

Drobot (2003) created monthly linear regression models to forecast BSI from October of the previous year through July of the prediction year. Input variables included teleconnections indices, heating degree days (HDD) from Barrow, Alaska station data, and total and multiyear ice concentration data from the NSIDC (Drobot 2003). HDD accumulate daily based on a comparison of the SAT to a threshold of 65°F, where a mean daily temperature, e.g., of 40°F would accumulate 25 HDD units (Drobot 2003). Total ice concentration data were only used for October, November, May, June, and July, when there was less than full ice coverage in the Beaufort Sea (Drobot 2003). Drobot (2003) found that the multiyear ice concentration gradient was the most significant predictor in every month, followed by the total ice concentration and the teleconnections indices (October East Atlantic index and March NAO). HDD also appeared as the final and least significant predictor variable retained in July (Drobot

2003). All monthly models had R^2 values above 0.74 (October), with the highest in the July prediction model (0.92) (Drobot 2003).

Drobot (2007) predicted the regional minimum sea ice extent in the Beaufort/Chukchi Seas, the Laptev/East Siberian Seas, the Kara/Barents Seas, and the Canadian Arctic Archipelago by creating multiple linear regression models. The predictor variables included mean monthly weighted indices of sea ice concentration, multiyear ice concentration, surface skin temperature, surface albedo, and downwelling longwave radiation flux at the surface as input variables. March and June regression equations were created for each region. For the Beaufort/Chukchi Sea, the March model retained multiyear ice concentration with an R^2 value of 0.52 and the June model retained multiyear ice concentration, June albedo, and June sea ice concentration with an R^2 vale of 0.80.

Lindsay et al. (2008) created monthly forecast models to predict the Arctic-wide September ice extent using historical information about the ocean and ice obtained from an ice-ocean model retrospective analysis. The strongest predictive skill was found in the 6-month lead (March) model, with a forecast skill of 0.77, and the 11 month lead (October), with a forecast skill of 0.75 (Lindsay et al. 2008). Ice concentration was the most important predictor for the first two months, and ocean temperature at a depth of 200 to 270 m was the most important for longer lead times (Lindsay et al. 2008).

Drobot et al. (2009) assessed the interannual variability in the opening date of the Prudhoe Bay shipping season (one of the inputs of the BSI) using ordinal regression to predict and early, normal, or late opening date. Input variables included Freezing Degree

Days (FDD), mean sea ice area in the Bering Sea, and the frequency of occurrence of self-organizing map (SOM) patterns described by Maslanik et al. (2007) (Drobot et al. 2009). FDD are similar to HDD, except that a threshold of 1.8°C is used (Drobot et al. 2009). Sea ice concentration and FDD were found to have value in predicting whether an opening date would be early, normal, or late, with a correct prediction made in 32 out of 53 years (Drobot et al. 2009).

Although these studies have examined varying predictor relationships between synoptic scale climatological variables and the minimum sea ice extent, these studies are lacking because of their use of only a small number of predictor variables. In each case, the predictive ability of only a select number of atmospheric variables was utilized. Though this does provide important information regarding the relationship between these select variables and the minimum sea ice extent, it does not reflect the greatest possible predictive ability. With a large number of variables included, the most useful combination of predictor variables can be obtained, yielding the most accurate predictions of sea ice extent. An extensive study using a large number of potential predictor variables is needed.

III.1.1 Research Objective

The purpose of this chapter is to provide a comprehensive assessment of all potential predictor variables. In previous studies, only a small subset of predictors had been utilized as inputs. Therefore, only an incomplete picture of the most important predictor variables as well as the total predictive ability of variables has been achieved. This chapter aims to incorporate a larger number of potential variables to provide a

detailed and complete representation of the predictability of the Beaufort Sea minimum sea ice extent. This complete assessment involves a detailed analysis of the changes occurring in each potential predictor variable over the year prior to the September minimum sea ice extent. Each variable is compared between heavy ice years and light ice years to understand how these variables change in the year prior to these extreme ice events. Next, the relationship between each predictor variable and selected teleconnection indices is assessed to identify the large scale patterns potentially driving each of the predictor variables and therefore driving observed changes in sea ice extent.

III.1.2 Atmospheric Variable Selection

The variables that have been shown to have to most predictive ability include SLP, SAT, HDD, FDD, thawing degree days (TDD), surface wind speed, total ice concentration (TI), and multiyear ice concentration (MYI) (Barnett 1980, Walsh 1980, Drobot and Maslanik 2003, Drobot 2003, Drobot 2007, Drobot et al. 2009, Rogers 1978). Surface albedo has been utilized as an input variable, but only appeared as a final predictive variable in one model for one forecast study (Drobot 2007). Surface albedo did not increase the predictive ability of the model by any appreciable amount, and is therefore not considered in this analysis. In addition to these atmospheric and ice condition variables, ocean temperature data at varying depths have been utilized in previous forecast studies (Lindsay et al. 2008). This study focuses on the atmospheric drivers of sea ice extent and therefore does not consider ocean temperatures as an input variable. In some forecasting studies, teleconnection indices have been utilized as input

variables. Specifically, the AO, NAO, and the East Atlantic (EA) index have been shown to have some predictive power (Drobot and Maslanik 2003, Drobot 2003).

In this study, 16 atmospheric and surface predictor variables and 10 teleconnection indices will be utilized. In previous studies, variables depicting the surface conditions in the Beaufort Sea region have been employed to create forecast models. Of the 16 predictor variables selected in this study, seven have been shown to have some utility in forecast models created in previous studies: SLP, SAT, FDD, TDD, wind speed, TI, and MYI (Barnett 1980, Walsh 1980, Drobot and Maslanik 2003, Drobot 2003, Drobot 2007, Lindsay et al. 2008, Drobot et al. 2009, Rogers 1978). One additional surface variable, wind direction, is included in this study because of the potential importance of ice motion in determining the sea ice extent during a given year.

The remaining eight predictor variables represent the upper atmospheric conditions in the Beaufort Sea region. Although these upper level variables have not been included in previous studies, it is likely that the atmospheric conditions in the region may have some appreciable influence on the yearly minimum sea ice extent. The link between upper atmospheric conditions and surface conditions in the Arctic has been studied extensively, and it is expected that the upper level conditions will influence and ultimately strengthen surface phenomena (Kunkel et al 1993, Palecki and Leathers 1993, Klein and Walsh 1983, Leathers et al. 1991). For this study, upper level air temperatures and geopotential height at 850 hPa, 700 hPa, 500 hPa, and 300 hPa are utilized. The 850 hPa level represents conditions near the surface and is expected to exhibit patterns most similar to the observed surface conditions. The 700 hPa pressure level is commonly used

in atmospheric studies as it represents conditions between the surface and the middle of the troposphere. The 500 hPa pressure level represents the level of non-divergence, which is the level in the atmosphere at which the horizontal velocity divergence is zero. Because of this, the 500 hPa level is expected to show a unique picture of the upper atmospheric conditions as well as represent characteristics of ridging and troughing in the atmosphere. The 300 hPa pressure level is expected to capture the influence of the polar jet stream as well as represent the upper tropospheric conditions, which may have some influence on the conditions observed at the surface.

III.1.3 Teleconnection Selection

In this study, ten teleconnection indices will be used. In previous statistical forecasts, the AO, NAO, and EA index have been shown to have some utility in predicting sea ice conditions (Drobot and Maslanik 2003, Drobot 2003, Rigor et al. 2002). Additionally, the Pacific-North American (PNA) pattern has also been shown to have a relationship with sea ice extent (L'Heureux et al. 2008). Beyond these four indices, little is known about the influence of other teleconnections on sea ice conditions in the Beaufort Sea region. It is likely that other high-latitude teleconnection indices may exert some influence on the region. Therefore, the East Atlantic/Western Russia (EAWR) pattern, the East Pacific-North Pacific (EPNP) pattern, the Polar/Eurasia (PE) pattern, the Western Pacific (WP) pattern, the Southern Oscillation Index (SOI), and the Niño3.4 index are included in this study. The EAWR, EPNP, PE, and WP patterns are included specifically because of their known links to high latitude processes, while the El Niño/Southern Oscillation (ENSO) measures are used due to their role in affecting

some teleconnections (e.g., PNA) as well as their general role in modulating extratropical Rossby waves.

ENSO refers to a large-scale mode of climate variability related to sea surface temperature (SST) and Walker circulation patterns in the tropical Pacific Ocean. It is represented by two distinct phases, the El Niño phase and the La Niña phase, which are characterized by opposite SST patterns. During the El Niño phase, positive SST anomalies are observed in the eastern Pacific, while anomalously negative SST anomalies are observed in that region during La Niña events. Although this phenomenon is observed in the tropics, it is possible that ENSO has some indirect influence on the other teleconnection indices, and therefore ultimately some influence on the sea ice conditions in the Beaufort Sea.

III.1.4 Long-Term Teleconnection Analysis

Although it has been shown on a local scale that these atmospheric variables have some predictive ability, little is known about the larger scale drivers of these variables. To improve forecasts, it is important to understand which teleconnection patterns may be influencing the conditions of these predictive variables. In the Arctic, the role of the AO/NAO have been studied extensively. Studies have found that sea ice extent does exhibit a relationship with the phase of the AO/NAO (Parkinson 2008, Rigor et al. 2002). Along with the AO and NAO, the PNA pattern has also been shown to have a relationship with sea ice extent (L'Heureux et al. 2008). It then follows that each of the predictive variables will also have a relationship with these same teleconnection patterns. It is possible that certain teleconnection patterns influence specific predictor

variables, and that better insight into the specific large scale drivers of each predictor variable will allow for more accurate predictions of sea ice extent to be made.

III.2 Study Region

For Chapter III, the study region is defined as a larger domain than for Chapter II. This is because the predictor variables show a large degree of spatial variability throughout the region and the conditions of the predictor variables in the area immediately adjacent to the study area used for Chapter II are important in understanding how and why the minimum ice extent is reached each year. For Chapter III, the northern edge of the study area is defined as 82.5°N, while the southern edge is defined as 62.5°N. The western edge is defined as 170°W, and the eastern edge is defined as 110°W (Figure 1).

III.3 Data

III.3.1 National Snow and Ice Data Center (NSIDC) Sea Ice Data

Monthly average sea ice concentration data were obtained from the NSIDC Sea Ice Concentrations from Nimbus-7 Scanning Multichannel Microwave Radiometer (SMMR) and Defense Meteorological Satellite Program (DMSP) -F8, -F11 and -F13 Special Sensor Microwave/Imagers (SSM/Is), and the DMSP-F17 Special Sensor Microwave Imager/Sounder (SSMIS) Passive Microwave Dataset for 1979 through 2012 (Cavalieri et al. 1996). The SMMR was operational every other day for the period of 1979 through 1987. Starting in July of 1987, the two satellites (SSMR and SSM/I) are merged and provide daily sea ice concentrations. Concentration data are provided on a 25 km by 25 km grid as the percentage of each grid cell covered by ice. Because this

dataset is only available beginning in 1979, the time period for this analysis is restricted to the period from 1979 through 2012. This source provides the data for the TI predictor variable. The TI is the monthly mean percentage of each grid cell that is covered by sea ice and this value ranges from 0% to 100%.

III.3.2 Multiyear Ice Data

The multiyear ice dataset is obtained from personal communication with Drs. James Maslanik and Mark Tschudi. This dataset utilizes sea ice concentration data from NSIDC (detailed above) as well as gridded satellite-derived motion fields from the International Arctic Buoy Program buoy position data (Maslanik et al. 2011). The age of the ice in a particular grid cell is estimated using these motion fields by transporting a parcel of ice at weekly time steps (Maslanik et al. 2011). In cases where ice of multiple ages is present in one grid cell, the cell is assigned the older age (Maslanik et al. 2011). The NSIDC data are used to determine whether a parcel of ice has lasted through the melt season, i.e. if the ice in that grid cell remains at 15% or higher concentration throughout the year (Maslanik et al. 2011). When a parcel of ice lasts throughout the melt season, its age is increased by one year (Maslanik et al. 2011). This dataset is utilized from 1979 through 2012 and provides the basis for the MYI predictor variable, which represents the monthly mean ice age at each grid cell, ranging from 0–4+ years.

III.3.3 National Centers for Environmental Prediction (NCEP)/Department of Energy (DOE) Reanalysis 2

The NCEP/DOE Reanalysis 2 dataset represents an advanced data assimilation effort that utilizes data from 1979 to the present to provide atmospheric variables with

global coverage (Kistler et al. 2001). This version 2 dataset was created to correct known errors in the National Centers for Environmental Prediction/National Center for Atmospheric Research (NCAR) Reanalysis 1 product, including updates such as a new boundary layer scheme and a fix in the cloud-top cooling radiation budget (Kistler et al. 2001). In this study, the NCEP/DOE Reanalysis 2 dataset was selected because of its coverage of the desired study area and its state-of-the-art analysis system that represents one of the most accurate reanalysis datasets available (Kistler et al. 2001). The atmospheric variables utilized from this dataset include monthly average air temperatures at 850 hPa, 700 hPa, 500 hPa, and 300 hPa, daily and monthly average air temperatures at 2 meters, geopotential heights at 850 hPa, 700 hPa, 500 hPa, and 300 hPa, sea level pressure, monthly mean u- and v-direction wind.

From these raw variables, some additional atmospheric predictor variables are calculated. FDDs are calculated using mean daily 2-m surface temperature values, where every degree Celsius below zero on each day is counted as a FDD and summed into a monthly FDD value (Polar Science Center 2010). For example, a daily temperature of −5°C will count as 5 FDDs toward the monthly total. TDDs are computed the same way, except only temperatures above 0°C are used toward the total (Polar Science Center 2010). Thus, using both FDD and TDD will provide a measure of the magnitude and duration of temperatures both below and above freezing, which corresponds to formation and melting of sea ice. The wind speed and wind direction are derived from the u and v components of wind provided in the reanalysis dataset.

III.3.4 Teleconnections

Teleconnection data are obtained from the NWS CPC (http://www.cpc.ncep.noaa.gov/data/teledoc/telecontents.shtml). AO data are obtained from the AO-index data provided by David J. W. Thompson (http://jisao.washington.edu/data/annularmodes/Data/ao_index.html). Monthly values are obtained for each teleconnection index for January 1978 through December 2012. The teleconnection indices used for this study include the AO, the NAO, the PNA, the EA pattern, the EAWR pattern, the EPNP pattern, the PE pattern, the WP pattern, the SOI, and Niño3.4. The AO is defined as the leading mode of variability in the empirical orthogonal function (EOF) analysis of monthly mean 100 hPa heights north of 20° latitude (Wallace and Gutzler 1981). The NAO is defined as the SLP difference between the Azores High and the Icelandic Low, with a positive phase indicating below normal heights and pressure in the region (Wallace and Gutzler 1981). While the AO and NAO have similar values and are highly correlated, they represent fundamentally different things and are therefore both included in this analysis. The PNA represents a quadripole pattern of 500 hPa height anomalies, with similar anomalies found south of the Aleutian Islands and over the southeastern United States and an opposite sign anomalies found near Hawaii and central Canada (Wallace and Gutzler 1981). The EA pattern is the second mode of SLP variability over the North Atlantic and is structurally similar to the NAO, with anomaly centers that are displaced southeastward from the NAO centers (Barnston and Livezey 1987). The EAWR is defined by four main anomaly centers: a positive phase associated with positive anomalies over Europe and northern China and a

negative phase with negative anomalies over the central North Atlantic and north of the Caspian Sea (Barnston and Livezey 1987). The EPNP pattern has three main anomaly centers located over Alaska, the central North Pacific, and eastern North America (Barnston and Livezey 1987). The PE pattern is represented by negative height anomalies over the polar region and positive anomalies over northern China and Mongolia in its positive phase (Overland et al. 1998). The WP pattern provides information about the location of the Pacific (East Asian) jet stream, with a strong positive phase representing pronounced zonal variation in the jet and a strong negative phase representing a pronounced meridional variation (Wallace and Gutzler 1981). The SOI and Niño3.4 both represent the phase of ENSO, but in different ways. The SOI represents the differences in the SST anomalies between Tahiti, French Polynesia and Darwin, Australia (Chen 1982). The Niño3.4 index represents the SST anomalies in the region from 5°S to 5°N and from 170°W to 120°W (NWS CPC).

III.4 Methods

III.4.1 Part 1: Composite Analysis

Using the five light ice years and five heavy ice years determined in Chapter II, composite maps were created for each predictor variable for each month of the year. The value of each variable during the five light ice or five heavy ice years was averaged to examine the most common pattern of variability for each variable throughout the study region throughout the year prior to the minimum sea ice extent, reached during September. Values from the five light ice years (2007, 2008, 2010, 2011, and 2012) and the five heavy ice years (1980, 1983, 1985, 1991, and 1996) were used for the months of

January through September, while values from the previous years (2006, 2007, 2009, 2010, and 2011 for the light ice years and 1979, 1983, 1985, 1990, and 1995 for the heavy ice years) were used for the months of October through December. The characteristics of each predictor variable were thus examined throughout the year leading up to the minimum ice extent.

The values of the composite groups for each variable were then compared to the dataset averages (1979–2012) for each variable. The anomalies were calculated and mapped for the light ice composite and the heavy ice composite by subtracting the 1979–2012average from each of these composite values for each predictor variable in each month.

To quantify how representative the composites are of average conditions, the standard deviation was also calculated and mapped for the five light ice years and the five heavy ice years at every grid cell in every month. The purpose of these maps is to identify regions in the study area that exhibit large deviations between the five years in each group. Larger deviations suggest that the composite is likely not representative of a consistent pattern for that variable in the years preceding extreme ice events, and therefore that variable may not have any predictive skill in a forecast model.

Lastly, maps of the differences between the light ice composite value and the heavy ice composite value at each grid cell were created by subtracting the value of the light ice years from the value of the heavy ice years. Statistical significance was assessed using Student's T-tests between means of the five light ice and five heavy ice years for each grid cell. First, an F-test was performed to determine whether the two groups had

equal variances. The results of this F-test were then used to determine the type of T-test to be used at each grid cell. At the grid cells where the variances were equal, a two-tailed T-test for independent samples was used. At the grid cells where the variances were not equal, a two-tailed Welch's T-test for independent samples was used.

III.4.2 Part 2: Teleconnections

Many of the surface and upper atmospheric predictor variables may be related to and the result of synoptic-scale atmospheric variability related to various teleconnections patterns affecting the Arctic. This will be of particular importance in Chapter IV, where multicollinearity between the predictors may produce variance inflation factors, thereby biasing the multiple regression and CART models. To assess the relative influence of each teleconnection index on each predictor variable, correlation analysis is performed between each of the 10 teleconnection indices and each of the 16 monthly predictor variables at each grid cell. Only correlations that are significant at the 95% confidence interval will be considered for analysis. Maps showing the significant correlations are created during each month. These will provide information regarding the potential large scale drivers of each of the 16 atmospheric predictor variables and information regarding multicollinearity among input variables.

III.4.3 Part 3: Long-Term Teleconnection Relationships

In addition to looking at the relationship between each teleconnection index and each predictor variable at the monthly time scale (Section 3.4.1), the overall long-term relationships are also important. Correlations between the 1979–2012 time series of each predictor variable and each teleconnection index are calculated at concurrent and lagged

(up to 12 months) timesteps. For example, the 2-month lag correlation would provide information on the relationship between the pattern of each predictor variable two months after a certain pattern of each teleconnection index.

Each predictor variable is standardized at the monthly and yearly time scales over 1979–2012 at each grid cell. First, the monthly values of each variable are standardized to remove the seasonal cycle. For example, the mean and standard deviation values for January surface air temperatures are calculated for the 34-year time period at each grid cell. For each year, the mean is subtracted from the data value and then divided by the standard deviation. Once monthly standardization is performed, the same standardization is performed for the overall time series (408 total time steps) at each grid cell. This overall standardization is used to pre-process the data for subsequent principal component analyses (PCA).

Next, PCA is performed on each predictor variable. PCA is used as a data reduction technique in which a new set of orthogonal variables is created from the main variability in the input predictor variables (North et al. 1982, Abdi and Williams 2010). For spatial data, PCA is used to reduce the spatial pattern of a single variable into a smaller number of principal component (PC) variables, which represent the leading modes of spatial variability in the data. In this analysis, PCA is performed on each predictor variable over the entire time series (408 time steps). The loadings represent the spatial pattern of each PC and the scores provide the value for each PC at each time step. In this analysis, the first few PCs will be used because these likely represent the leading

modes of variability within the dataset. The higher-order PCs account for very little variability and will not be included in the analysis.

Lastly, correlation analysis is performed between each teleconnection pattern and the scores of the dominant PCs for each predictor variable. Correlations that are significant at the 95% confidence level are considered for analysis. To test the time lag influence of each teleconnection, one-month time lag correlations are performed up to 12 months. For example, the values of the loadings of the predictor variables are lagged in one month intervals so that the influence of the previous month's teleconnection pattern on that variable can be assessed.

III.5 Results

III.5.1 Part 1: Composite Analysis

III.5.1.1 Upper Air Temperatures

Mean Patterns. The upper atmospheric temperature profile over the Beaufort Sea region is depicted by mean monthly temperature data at four pressure levels: 850 hPa, 700 hPa, 500 hPa, and 300 hPa. Throughout the troposphere, air temperatures decrease with height and the highest air temperatures among these levels are thus observed at 850 hPa and the lowest air temperatures at 300 hPa (not shown). At all four pressure levels, the highest temperatures during each month are observed in the southern portion of the study region and the lowest temperatures are observed in the northern and northeastern portions. The observed distributions generally follow a latitudinal pattern for most months of the year.

Differences. Throughout the four pressure levels, no significant differences were observed between the light and heavy ice composites for January, February, or March (Table 3). During these three winter months the air temperatures are extremely low

Table 3: Percentage of grid cells with significant differences at the 95% confidence level. Grey cells indicate that the specific measure is not applicable for that month.

	Jan	Feb	Mar	Apr	May	Jun	Jul	Aug	Sep	Oct	Nov	Dec
Total Ice	-	-	-	-	3	85	80	70	86	80	55	57
Multiyear Ice	6	6	7	6	5	6	8	7	21	9	16	11
FDD	-	-	-	28	5				51	34	-	21
TDD						8	2	32				
Surface Temp	3	-	2	35	9	13	22	41	53	61	30	32
Temp 850hPa	-	-	-	28	8	17	4	56	59	33	23	24
Temp 700hPa	-	-	-	29	8	18	-	63	5	-	-	35
Temp 500hPa	-	-	-	34	23	20	0	63	-	-	-	44
Temp 300hPa	-	-	-	-	2	-	3	10	-	-	-	21
SLP	15	-	-	0	-	49	37	20	-	-	-	-
Gph 850hPa	9	-	-	-	-	33	8	35	-	-	-	-
Gph 700hPa	2	-	-	-	-	35	-	43	4	-	-	5
Gph 500hPa	-	-	-	-	-	31	0	48	-	-	-	18
Gph 300hPa	-	-	-	4	2	32	-	55	-	-	-	25
Wind Speed	22	-	3	2	14	4	2	16	2	5	6	13
Wind Direction	10	1	4	3	2	17	26	4	2	6	2	4

because of a lack of incoming solar radiation. During April, May, and June, significant differences are observed at the 850 hPa, 700 hPa, and 500 hPa pressure levels, while significant differences are only observed for the 300 hPa level during May (Table 3). For the three pressure levels closer to the surface, the differences maps show the expected negative pattern indicating that the air temperatures were higher preceding the light ice years (Figure 7). During May, significant differences are only observed at very few of

the grid cells (Table 3). Throughout the remaining months (July through December) the expected negative patterns of temperature differences are observed for the 850 hPa, 700 hPa, and 500 hPa pressure levels. Unexpected patterns of both positive and negative

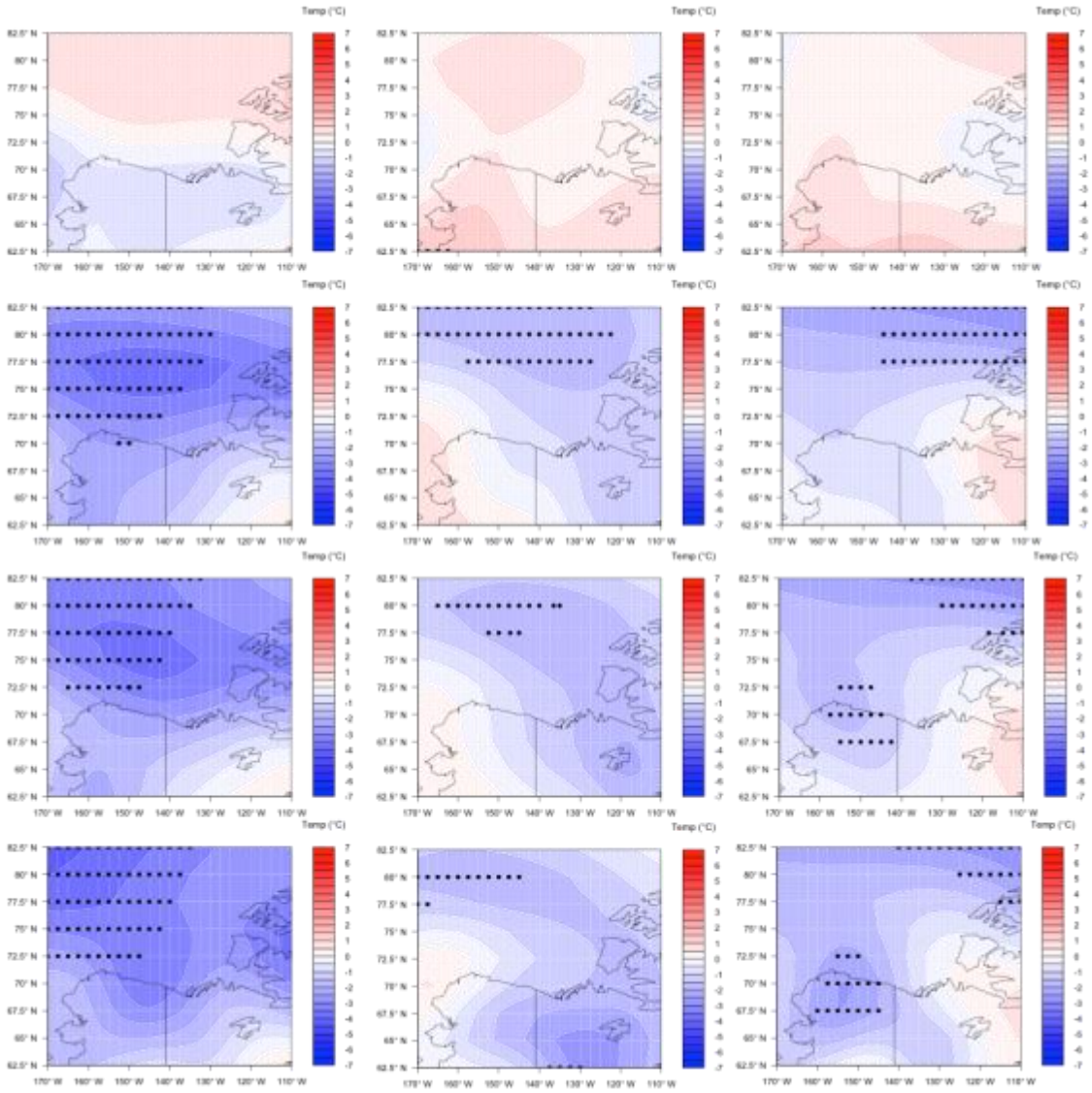

Figure 7: Air temperature difference maps during April (left column), May (middle column), and June (right column) at four pressure levels (from top to bottom: 300 hPa, 500 hPa, 700 hPa, 850 hPa). Black dots represent the center point of grid cells with significant differences.

differences are observed at the 300 hPa pressure level for all months. This may indicate that the 300 hPa pressure level is not representative of the mean upper atmospheric conditions, or that this pressure level is too far from the surface to have an effect on the conditions of the sea ice. Overall, the 850 hPa level shows the most significant differences throughout the largest number of months (Table 3). Generally, as the pressure level decreases (increasing elevation), the number of significant differences decreases and the number of months showing any significant differences also decreases. This agrees with Serreze and Barry (2011) regarding Arctic amplification, which is predominantly a surface-based phenomenon with evidence of enhanced Arctic warming only observed in the lower troposphere (Serreze and Barry 2011). For the 850 hPa, 700 hPa, and 500 hPa pressure levels, the largest numbers of significant differences are observed during August, with large differences also observed during December (Table 3). For the 300 hPa pressure level, the largest number of significant differences is observed during December (Table 3).

Anomalies. It is expected that for the heavy ice years, negative temperature anomalies would be observed. This would indicate that temperatures during the five heavy ice years were below average for each month. For the light ice years, positive anomalies are expected, indicating that the temperatures during these five years were above average. During January, February, and March for all four pressure levels, unexpected positive and negative differences are observed. For the 850, 700, and 500 hPa pressure levels the expected pattern of predominately negative anomalies for the heavy ice composites, and positive anomalies for the light ice composites are observed

from April through October (Figure 8). This indicates that the temperatures at these pressure levels are noticeably different in the months preceding these extreme ice events. During November, the expected patterns of extreme negative anomalies are observed for the heavy ice years at all four pressure levels, while unexpected negative anomalies are observed for the light ice years. December shows a return to the expected patterns for all three levels. Overall, the magnitude of the anomalies is greater for the heavy ice group as compared to the light ice group. This may indicate that the upper atmospheric air temperature conditions preceding the five heavy ice years were particularly anomalous when compared to the mean. The air temperatures preceding the light ice years are not as drastically different from average. Throughout the year, the weakest anomalies are observed during the spring and summer months of May, June, and July while the strongest anomalies are observed during the late summer, fall, and winter months of August, September, October, and December. At 300 hPa, unexpected patterns of both positive and negative anomalies are evident throughout the year. The expected anomaly pattern is only observed during December. It is important to note that this is also the month that showed the largest number of significant differences between the light and heavy ice composites at this pressure level.

Standard Deviations. Overall, the largest standard deviations are observed during January, February, and March for all four pressure levels (Figure 9). As the months progress into the late spring and summer, the standard deviations decrease for both the heavy and light ice groups at all four pressure levels (Figure 9). Starting in November the standard deviations begin to increase again at all pressure levels (Figure

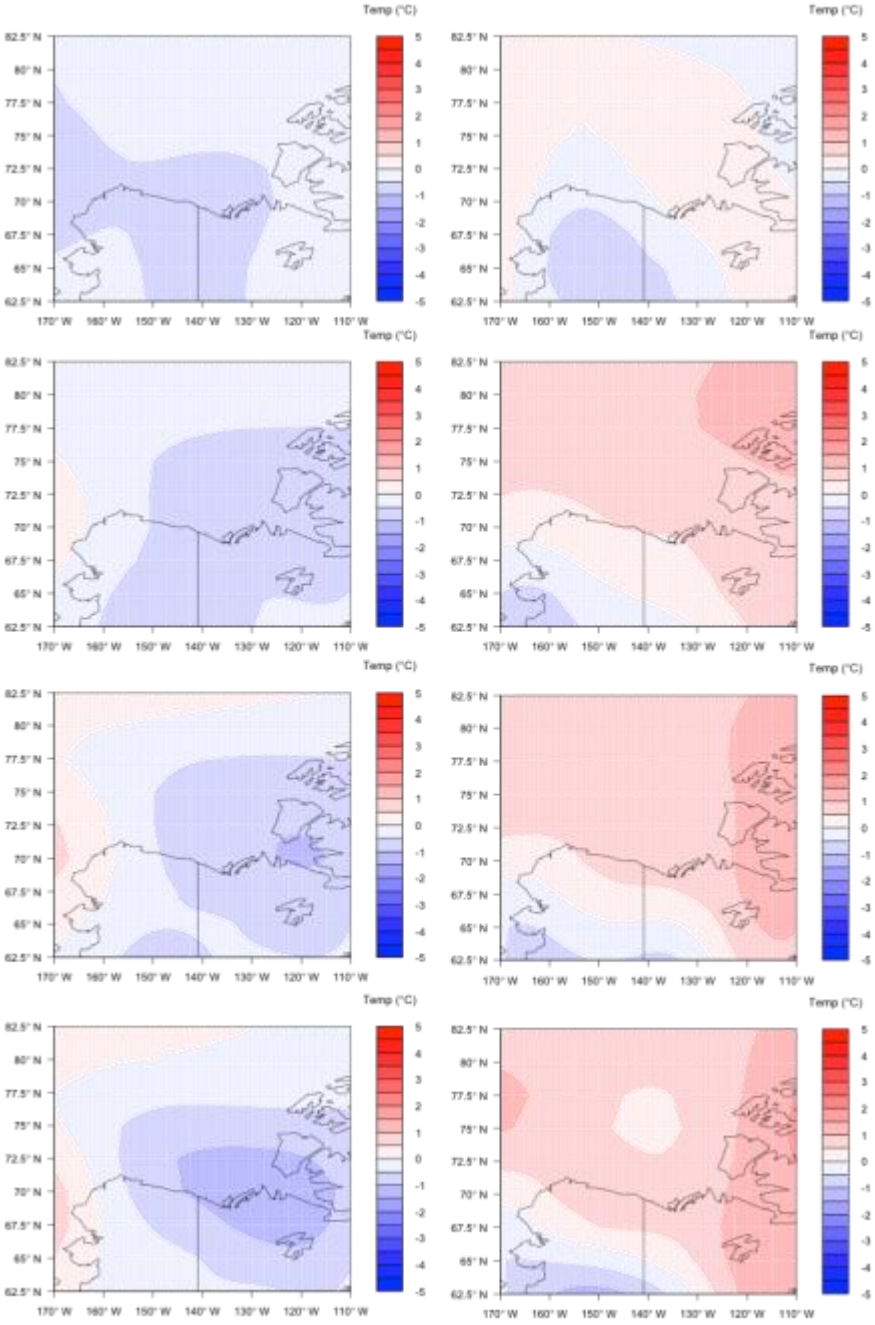

Figure 8: Air temperature anomaly maps during July for the heavy ice years (left column) and the light ice years (right column) at four pressure levels (from top to bottom: 300 hPa, 500 hPa, 700 hPa, 850 hPa).

9). In general, the magnitude of the standard deviations is the same or similar for the heavy and light ice groups during each months.

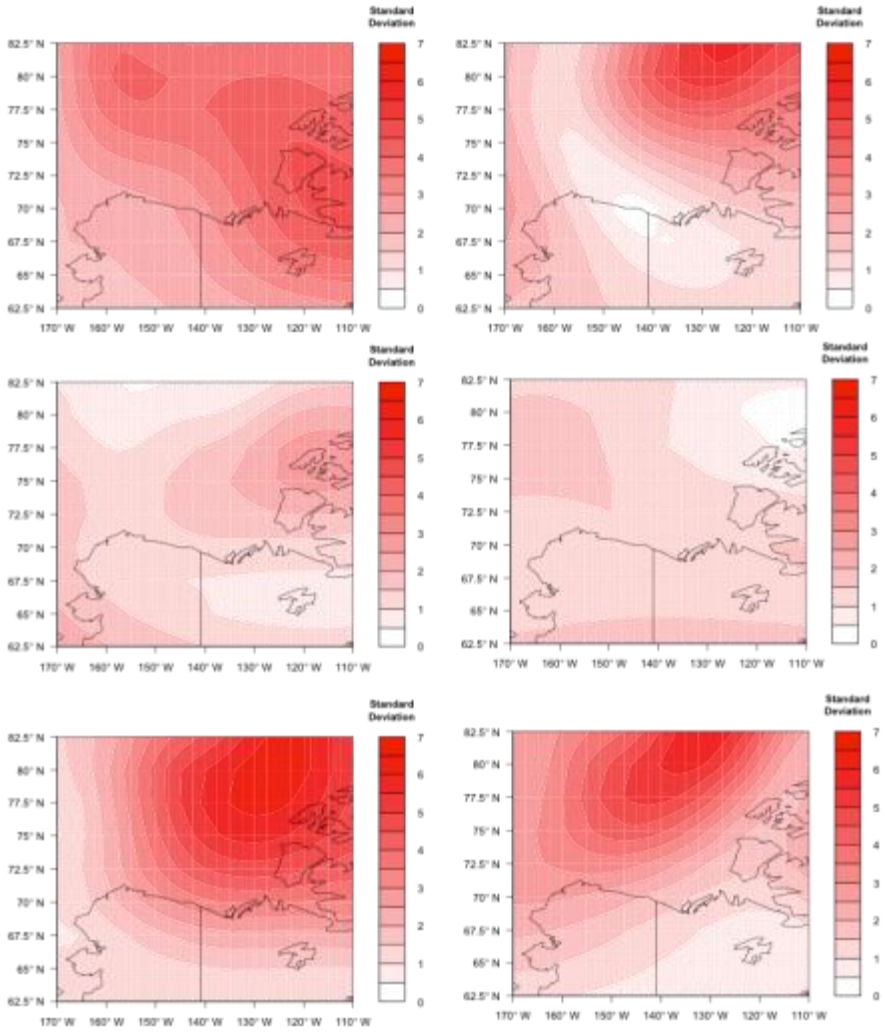

Figure 9: Air temperature standard deviation maps for the heavy ice years (left column) and the light ice years (right column) at 500 hPa during February (top row), July (middle row), and November (bottom row).

Discussion. Overall, this assessment of the upper atmospheric air temperature characteristics has shown that the largest and most significant differences between the heavy ice and light ice composites is observed at the 850 hPa pressure level, with the magnitude and number of significant differences decreasing with increasing height in the atmosphere. The pressure levels of 850 hPa, 700 hPa, and 500 hPa show similar patterns of temperature differences and anomalies throughout the year, while the 300 hPa level does not show the expected pattern throughout most of the year. This indicates that this pressure level may not be useful in forecasting surface conditions. Looking at each pressure level, it is clear that the months of January, February, and March are not useful in forecasting because of the lack of significant differences between the light and heavy composites and the unexpected patterns of anomalies observed. Because the remaining months of the year show the expected patterns of differences and anomalies with small standard deviations, the air temperature conditions during months are expected to have some utility in forecasting sea ice conditions.

III.5.1.2 Geopotential Heights

Mean Patterns. Upper atmospheric variability in the Beaufort Sea region is further provided by geopotential height data at 850 hPa, 700 hPa, 500 hPa, and 300 hPa. Geopotential height is defined as the height in the atmosphere needed to reach a certain pressure level, and is therefore linked to air temperature. For the composite maps of the five heavy ice and five light ice years, a general latitudinal pattern of geopotential height is observed during all months at all four pressure levels. This corresponds to the latitudinal pattern observed with the upper atmosphere air temperatures, where the lower

latitudes have generally higher geopotential heights and the higher latitudes (specifically the northeastern portion of the study region) have lower geopotential heights.

Differences. It is expected that heavier ice years will have overall lower geopotential heights. This would correspond to lower air temperatures during these years. This means that the difference maps are expected to show predominately negative height differences. At all four pressure levels during January, an unexpected pattern of strong positive differences is found. Only a small percentage of these differences are significant at the 850 hPa and 700 hPa pressure levels, with no significant differences at the two highest pressure levels (Table 3). No significant differences are observed during February and March (Table 3). Beginning in April, the expected negative differences are found at all four pressure levels. This predominately negative pattern is observed in all months until November (Figure 10). Differences are significant beginning in April, with larger percentages of significant differences during June, July, and August for all pressure levels (Table 3). During some months, a small region of positive differences is evident in the southern portion of the study region (June, July, October) (Figure 10). These positive differences are significant at some pressure levels and are consistent among the four pressure levels (Table 3, Figure 10). They are therefore likely physically significant and not an artifact of the analysis. December shows strong negative differences in the eastern portion of the study region and strong positive differences in the western portion (Figure 10). Overall, the spring and summer months exhibit the largest percentages of significant differences for all pressure levels with the expected

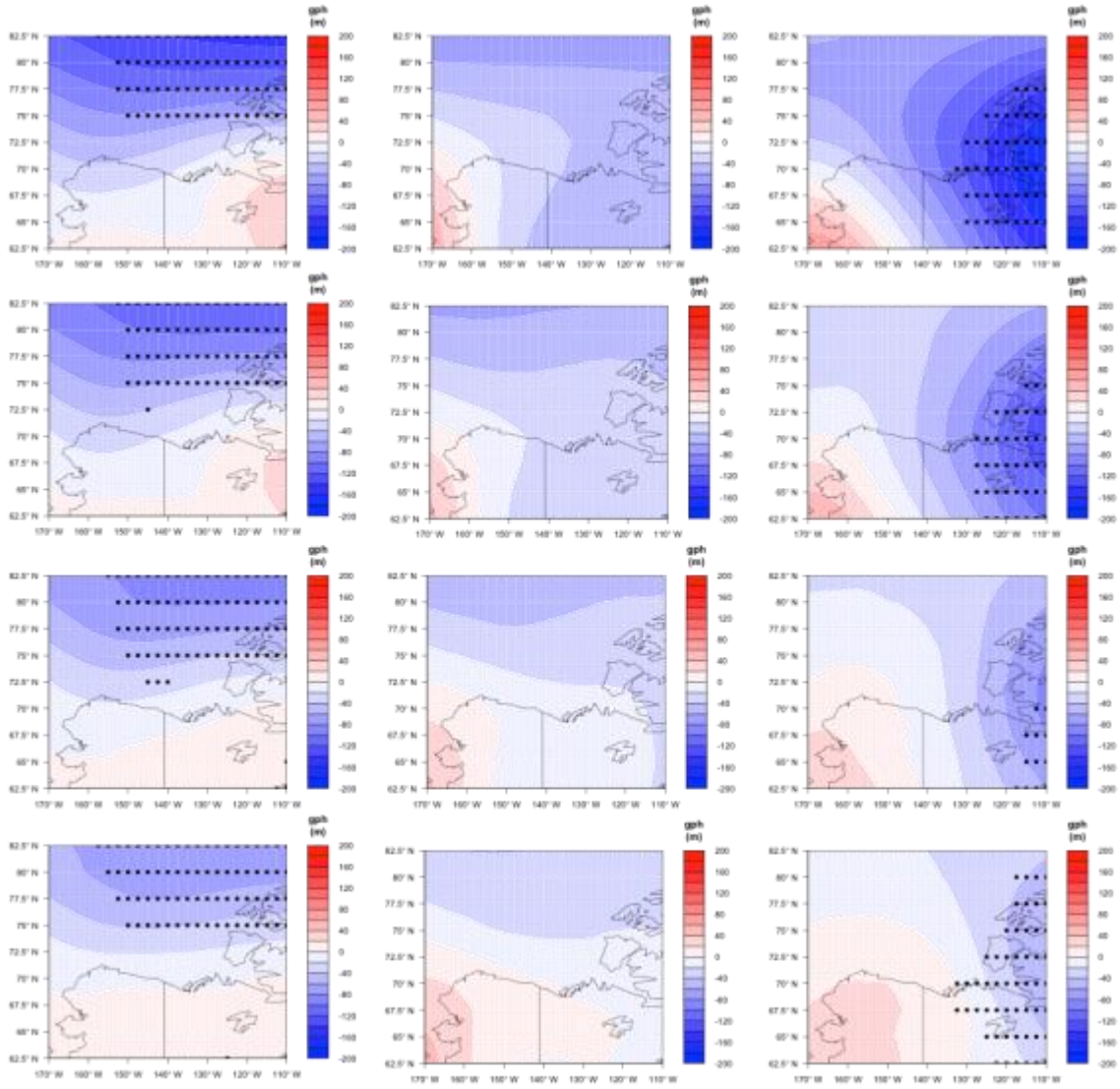

Figure 10: Geopotential height difference maps during June (left column), October (middle column), and December (right column) at four pressure levels (from top to bottom: 300 hPa, 500 hPa, 700 hPa, 850 hPa). Black dots represent the center point of grid cells with significant differences.

pattern of differences (Table 3). When lower temperatures are observed in the region, unexpected and weak differences are evident. This includes the months from November through March. There does not appear to be any consistent pattern in the percentage of significant differences observed at each pressure level. For example, during June the largest percentage of significant differences is observed at the 700 hPa pressure level (Table 3). During July, the largest percentage is observed at the 850 hPa pressure level and during August the largest percentage is observed at the 300 hPa pressure level (Table 3). This may suggest that the differences in the geopotential heights are not consistent at each pressure level throughout the year.

Anomalies. When comparing the heavy ice years to the average, a pattern of negative anomalies is expected. This would indicate that the geopotential heights during the five heavy ice years are lower than average. A pattern of positive anomalies is expected for the light ice anomalies. Overall, the anomaly maps are consistent for each month at all four pressure levels (i.e. the same patterns are observed at all four pressure levels for each month), but the patterns do not persist throughout the year (Figure 11); each month has very different anomalies. This variability in the anomalies and lack of expected patterns suggests that the geopotential heights during the heavy and light ice years are not very indicative of differences from the normal conditions. Because they show no consistent differences from the average conditions, these variables may not be useful in forecasting sea ice conditions in the region.

Standard Deviations. Overall, the standard deviations for both the light ice and the heavy ice groups are large for all months at all pressure levels. The largest standard

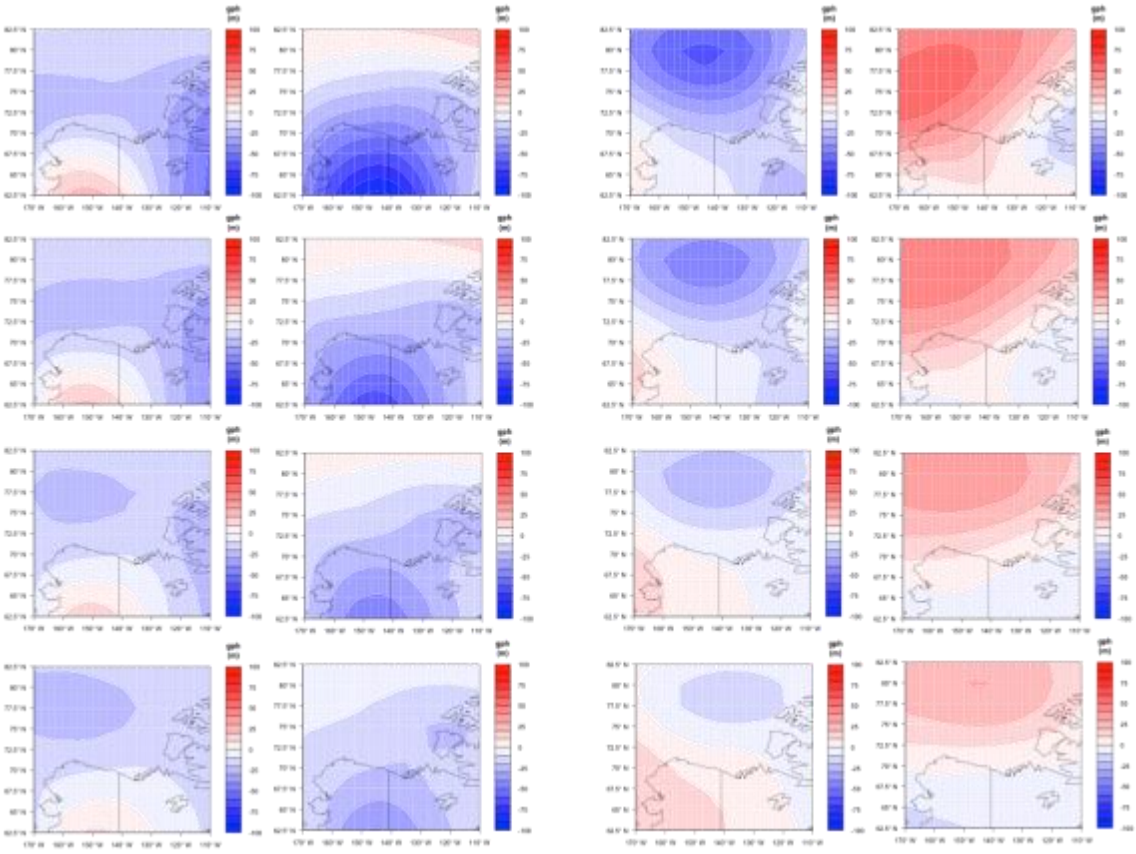

Figure 11: Geopotential height anomaly maps during March (left group) and during September (right group). The right column of each group represents the light ice anomalies and the right column represents the heavy ice anomalies. Maps are displayed for four pressure levels (from top to bottom: 300 hPa, 500 hPa, 700 hPa, 850 hPa).

deviations are observed during the months from November through March for all pressure levels. This corresponds with the months where the least amount of significant differences are observed. The smallest standard deviations are observed during June, but these standard deviations are still large. The smallest values observed during these

months are still approximately 5 standard deviations. Because such large differences are observed throughout the year at all pressure levels, this suggests that there is a large amount of discrepancy between the geopotential heights in the years preceding heavy and light ice events.

Discussion. Overall, the geopotential height patterns do not show any consistency throughout the year. The differences and anomalies do not fit the expected patterns and change drastically from month to month. Coupled with large standard deviations, this suggests that geopotential heights are most likely not useful in forecasting sea ice conditions. It is possible that the geopotential height conditions are too variable throughout the years to provide a consistent pattern that would be useful for making predictions.

III.5.1.3 Surface Temperature Conditions

Mean Patterns. The surface temperatures in the Beaufort Sea region are depicted by three variables: 2-meter monthly average air temperatures, FDD, and TDD. Of these variables, the mean monthly temperatures are used to provide an overall picture of the temperature variability throughout the year. The FDD and TDD will provide information about the duration and magnitude of temperature variability.

The three air temperature variables depict a consistent latitudinal pattern during all months. This corresponds to the upper air temperature patterns and the geopotential heights. For the monthly mean temperatures, the highest values are observed in the southern portion of the study region, while the lowest temperatures are in the northeastern portion. Higher FDDs indicate more persistent lower daily air temperatures.

The expected pattern of larger FDD values in the northern portion of the study region and smaller FDD values in the southern portion is evident. It is important to note that FDDs during the late spring and summer months are zero because there are no daily air temperatures below 0°C. For the TDD, larger values indicate more persistent high temperatures. The expected pattern of larger values in the southern portion of the study region and smaller values in the northern portion is found. TDDs from late fall to early spring are zero because no temperature values above zero are recorded.

Differences. It is expected that mean differences for the three temperature variables will be consistent throughout the year. For the monthly mean temperatures, a predominately negative difference pattern is expected, suggesting that the air temperatures preceding heavy ice years are lower than those preceding light ice years. For FDD, positive differences are expected. This would indicate a longer and/or more severe freezing season preceding the heavy ice years than before light ice years. FDD will not be considered for analysis during the late spring and summer because all values are zero. For the TDD, a negative pattern is expected. This would suggest a longer and/or more intense melt season preceding light ice years. TDD will not be considered for analysis during late fall through early spring because all values are zero. During January, February, and March unexpected differences are observed for both the monthly mean temperatures and the FDD. During April, many statistically significant differences of the expected negative sign for the monthly temperatures and positive sign for the FDD are observed. From May through August, the monthly temperatures show large areas of unexpected positive differences (Figure 12). In these months, some differences

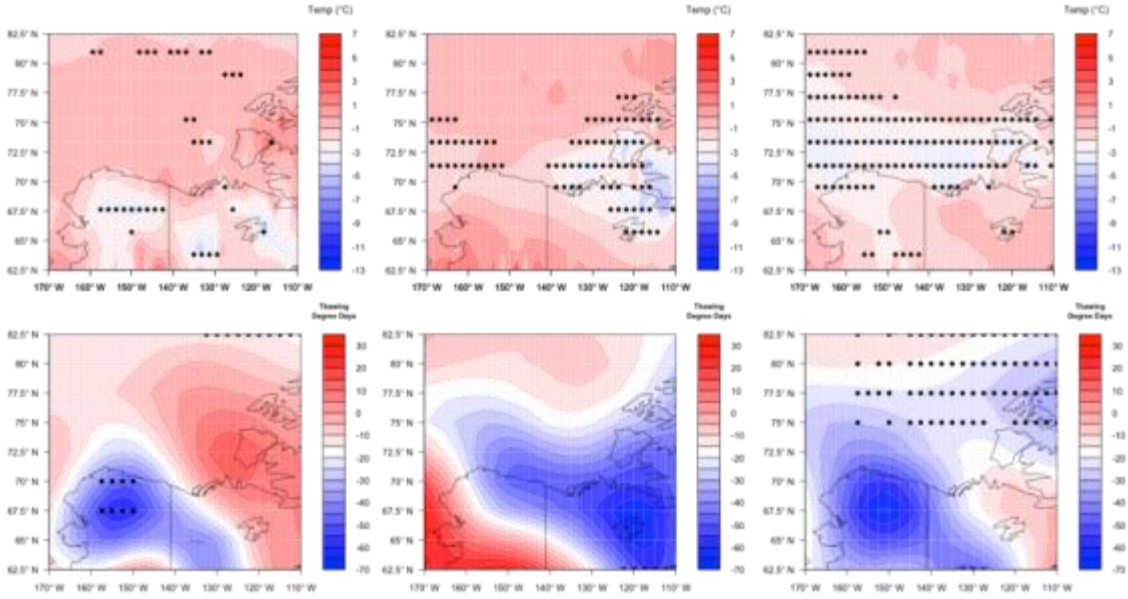

Figure 12: Difference maps for surface air temperatures (top row) and TDD (bottom row) during June, July, August (from left to right). Black dots represent the center point of grid cells with significant differences.

are significant, but these differences are confined to areas where the expected negative differences occur (Table 3, Figure 12). During June, July, and August, significant differences of the expected negative sign occur (Figure 12). For these three months, the negative pattern becomes most prominent during August (Figure 12). This is also when the largest percentage of significant differences is observed (Table 3). Beginning in September, the expected negative differences are found for the monthly temperatures and these patterns hold through November. Large percentages of significant differences occur during these months (Table 3). During September and October, expected positive differences (with many being significant) are observed for the FDD. Overall, the FDD

and TDD conditions confirm the monthly mean temperatures. When monthly mean temperatures exhibit the expected differences, the expected pattern is also found for the FDD or TDD. In general, the months from December through March seem to have unexpected patterns. These variables may not be as useful during these months where the temperatures are extremely low.

Anomalies. For the monthly mean temperatures and the TDD, negative anomalies are expected for the heavy ice years and a positive anomalies for the heavy ice years. For FDD, the heavy ice years should have positive anomalies while the light ice years should be negative. For all three variables, this would indicate that the temperatures during the heavy ice years are below average. As with the difference maps, unexpected anomalies occur during January, February, and March for the monthly temperatures and FDD (Figure 13). Beginning in April, expected anomalies are observed for the monthly temperatures, which persist through December (Figure 13). During June, July, and August the light ice years show some positive anomalies, but negative anomalies are also observed (Figure 13). For the TDD the expected anomalies occur during all months (June, July, and August) (Figure 13). Expected FDD anomalies are found from September through December (Figure 13). Throughout the year, the expected patterns are observed for all three variables during all months excluding winter and early spring. This indicates that these variables may have some forecasting utility.

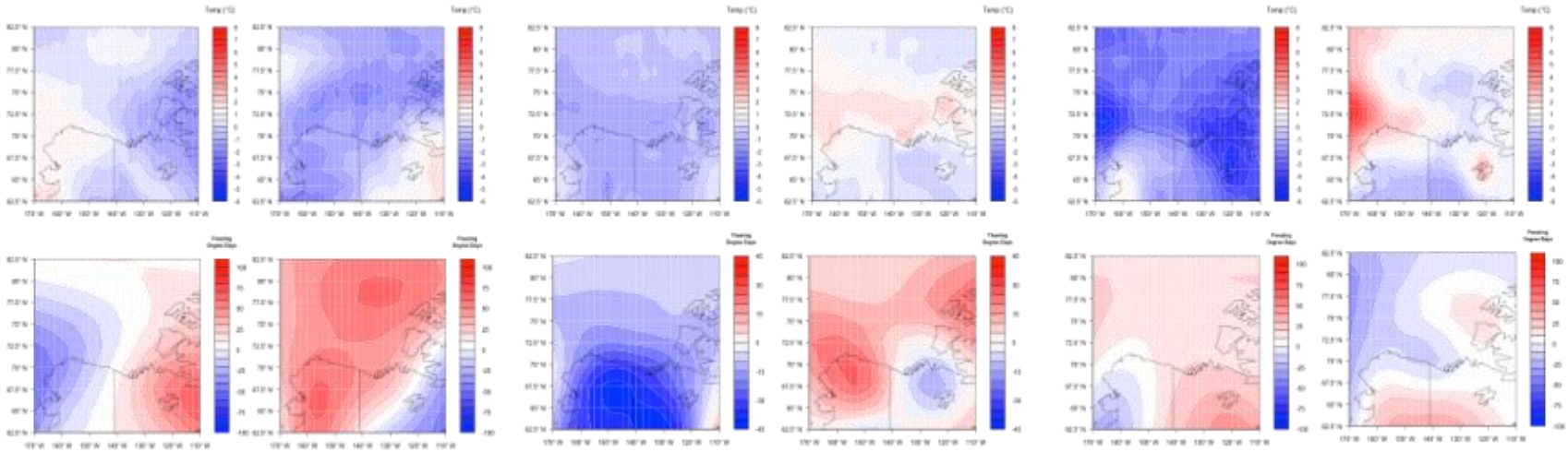

Figure 13: Anomaly maps during January (left group), August (middle group), and October (right group) for SAT (top row) and FDD (for January and October) or TDD (August) (bottom row). Light ice anomalies are shown in the left column of each group and heavy ice anomalies are shown in the right column.

Standard Deviations. Monthly mean temperatures exhibit low standard deviations throughout the year. The lowest values occur during the summer months while the highest values are during winter. This corresponds to the overall pattern observed in the significant differences. For TDD, the same-magnitude standard deviations are observed for all three months. The largest FDD standard deviations are typically found during the light ice years for each month. There does not appear to be much change in the standard deviations throughout the year.

Discussion. Overall, the three temperature variables exhibit consistent variability, with FDD and TDD patterns following similar monthly mean temperature patterns. The consistency throughout the year for these variables suggests that they will prove useful in forecasting sea ice extent because distinct patterns are evident for the extreme heavy ice and light ice years.

III.5.1.4 Other Surface Variables

Mean Patterns. The remaining surface variables include SLP, 2-meter monthly mean wind speed and 2-meter monthly mean wind direction. For SLP, a generally latitudinal pattern (following the observed pattern for all other variables) is observed, although this latitudinal pattern is not as distinct or consistent as for the other variables. This indicates that SLP may exhibit more subtle variability, potentially corresponding to the transient movement of high and low pressure systems. For both wind speed and wind direction, no distinct patterns occur for heavy ice and light ice composites for any month.

Differences. Regions of both positive and negative differences are observed throughout the year. The strongest and most significant differences occur during June, July, and August (Table 3). During these months, there are large significant negative differences in the northern portion of the study region and large significant positive differences in the south (Figure 14). The SLP patterns during these summer months are the most consistent when compared with the rest of the year. During the remaining months, the differences change on a month-to-month basis and very few, if any, significant differences occur (Table 3, Figure 14). These three summer months correspond with the monthly mean temperatures, which also had the most significant

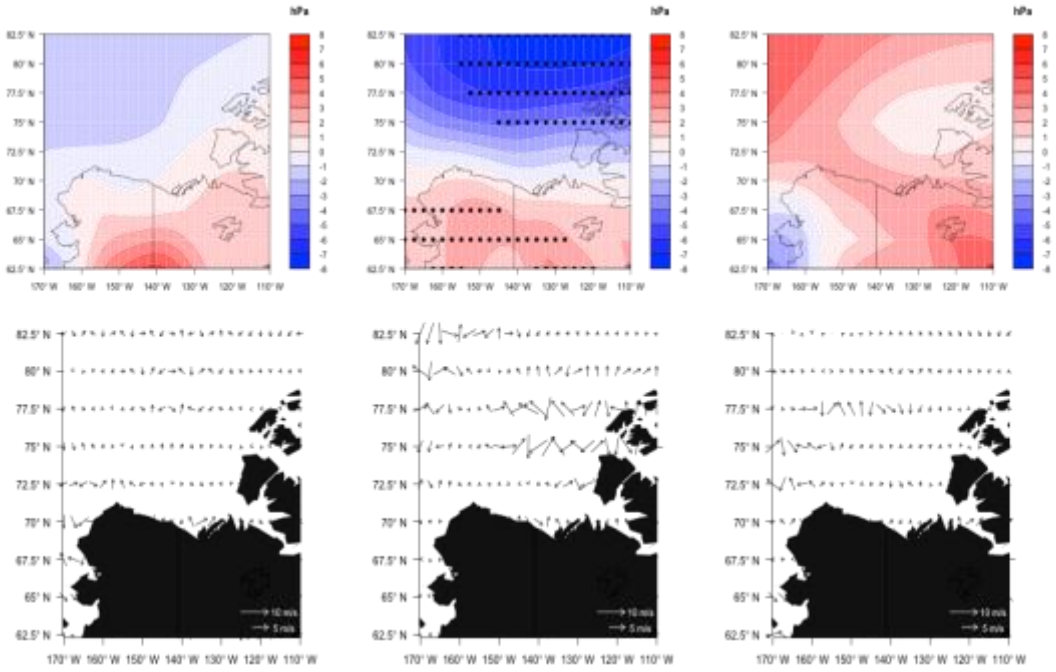

Figure 14: Difference maps for SLP (top row) and surface wind (bottom row) during March, June, and November (from left to right). Black dots represent the center point of grid cells with significant differences.

differences during this time of the year. For the wind speed and wind direction, some significant differences occur in almost all months (excluding February wind speed), but the percentage of significant differences is always small (Table 3). The difference maps for these two variables do not show any consistent patterns and the locations of the significant differences change from month to month with no apparent consistency (Figure 14). Because these differences are so sporadic, it suggests that the wind speed and direction in the year preceding extreme ice events may be too variable in the composites.

Anomalies. No consistent SLP anomalies occurred from January through May (Figure 15). Starting in June, a consistent pattern for both the heavy and light ice anomalies is evident through November (Figure 15). For the heavy ice anomalies, generally negative anomalies occur in the northern portion of the study region and positive anomalies in the south, although the strength of the anomalies changes from month to month (Figure 15). For the light ice anomalies, generally positive anomalies are evident in the northern portion of the study region, with negative anomalies in the south (Figure 15). The persistence of these patterns suggests that SLP may have some forecasting utility from June–November. The December anomalies do not follow this same pattern. Wind speed and direction again do not exhibit any consistent anomaly patterns throughout the year (Figure 15)

Standard Deviations. The greatest SLP standard deviations are observed from November through April. Beginning in May, standard deviations begin to decrease, with the smallest standard deviations during June, July, and August. The same magnitude

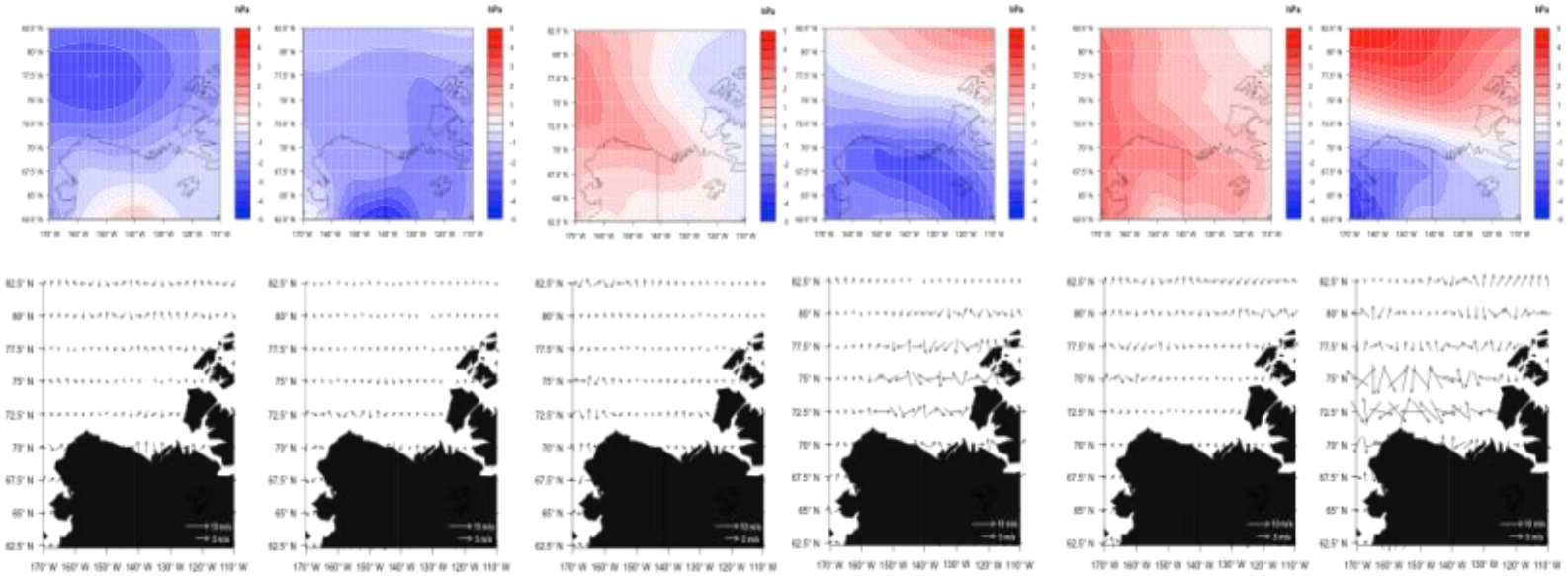

Figure 15: Anomaly maps during March (left group), July (middle group), and October (right group) for SLP (top row) and surface wind (bottom row). The left column of each group represents light ice anomalies and the right column represents heavy ice anomalies.

of standard deviations occur for both the heavy ice and light ice groups. For wind speed and wind direction, large standard deviations are observed throughout the study region for every month. There appears to be no pattern in the changes of the standard deviations throughout the year.

Discussion. SLP also appears to follow the same general pattern as many of the other predictor variables, with the strongest and most significant differences occurring during the summer months. Although wind speed and direction are expected to have an influence on sea ice (Ogi and Wallace 2012, Ballinger and Sheridan 2013, Wood et al. 2013), it is possible that the patterns for these two variables do not have enough yearly persistence to show a distinct pattern in the composite analysis. The wind conditions preceding the five heavy ice (or five light ice) years may not be the same for each extreme ice event, but that does not mean that it is not important.

III.5.1.5 Antecedent Ice Conditions

Mean Patterns. The characteristics of the sea ice itself throughout the year have been shown to have a direct relationship with the September minimum ice extent, and two measures of the antecedent ice conditions are therefore used in this study: TI and MYI. The composite maps of the five heavy ice and five light ice years reveal obvious differences. For TI from July through October, differences in the ice concentration can be observed for each month (Figure 16). In all cases, the heavy ice composites show higher concentrations of ice in the months leading up to and following the minimum ice extent in September (Figure 16). During the remaining months of the year, from November through June, the composite maps are very similar for the two groups (Figure

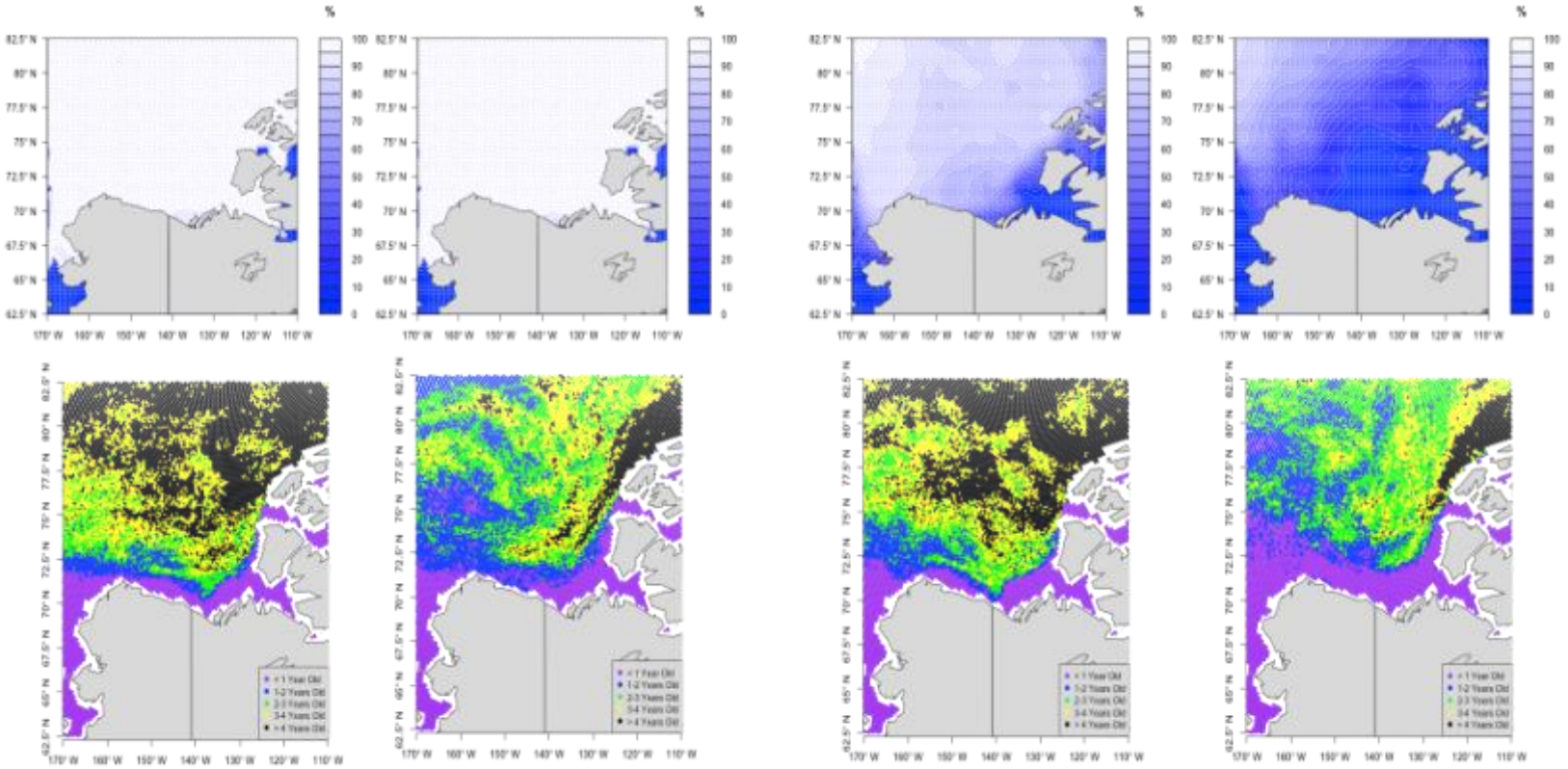

Figure 16: TI (top row) and MYI (bottom row) for February (left group) and August (right group) during heavy ice (left column) and light ice (right column) years.

16). During these months, the sea ice cover expands to the coast of Alaska and therefore no differences are evident. For the MYI, differences between the heavy ice and light ice composites are also obvious throughout all months (Figure 16). The heavy ice composites have more older ice, specifically in the northern part of the study region (Figure 16). In contrast, the light ice composites have more younger ice, with the oldest ice types only appearing in the northeastern portion of the study region (Figure 16).

Differences. No significant TI differences are observed from January through April. Beginning in May, significant differences occur during all months until December (Figure 17). The largest percentage of significant differences are observed during the summer and early fall, from June through October (Table 3). In these months, over 70% of the area exhibits significant differences between the heavy and light ice composites (Table 3). Where significant differences occur, they are positive, indicating that the heavy ice years have significantly higher ice concentrations than the light ice years (Figure 17). For the MYI, predominately positive differences are observed during all months (Figure 17, Table 3). These positive differences indicate that the heavy ice years exhibit older ice ages than the light ice years. All months have some grid cells with significant differences, although this is generally a small percentage (Table 3). The largest percentage of significant differences are in September, when the minimum ice extent is reached.

Anomalies. TI anomalies for the heavy ice composites are expected to be positive, which would indicate that the ice concentration is greater during these heavy years. The light ice composites are expected to have negative TI anomalies. During the

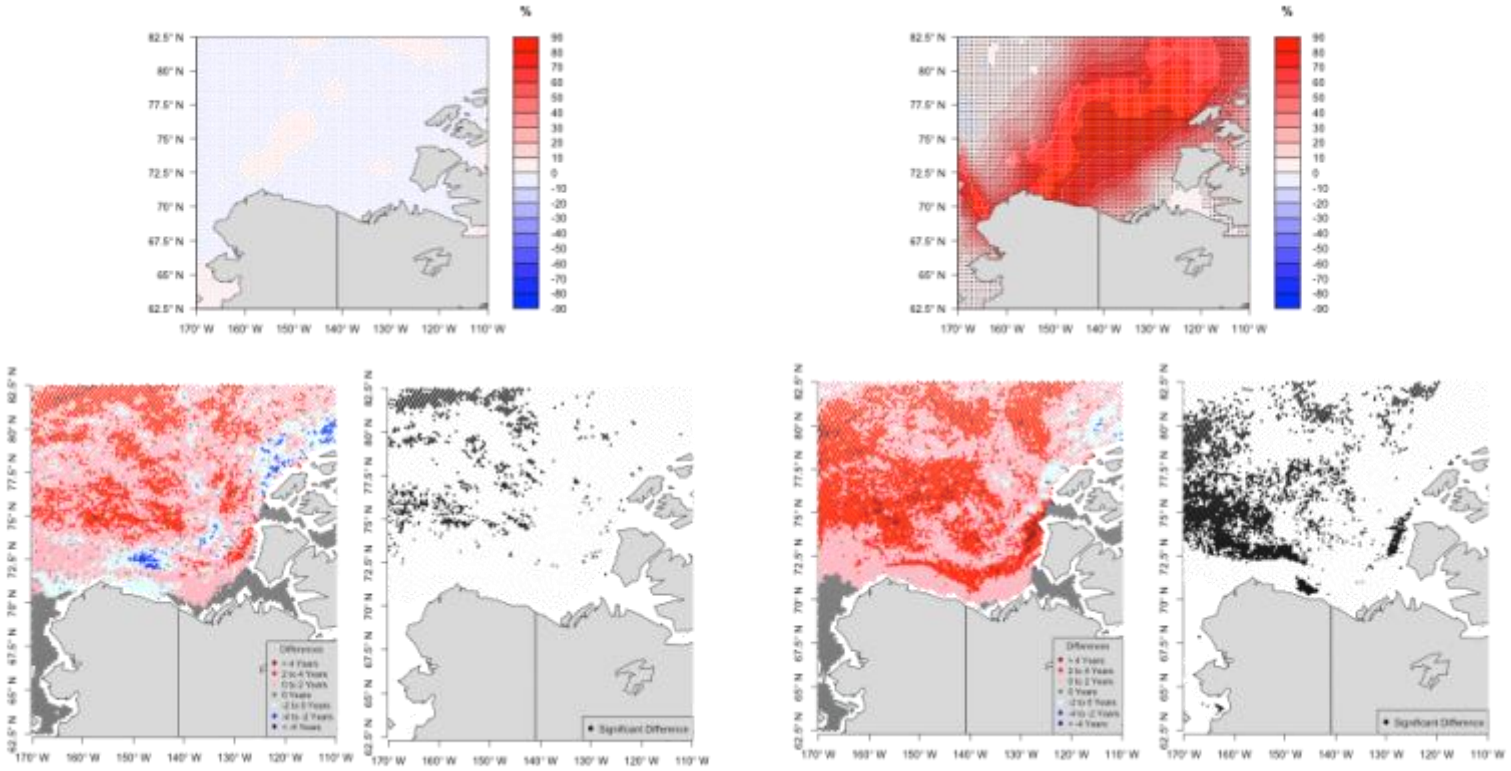

Figure 17: Difference maps for TI (top row) and MYI (bottom row) during March (left) and September (right). Black dots represent the center point of each grid cell with significant differences.

winter and spring months (from November through May), very weak anomalies are observed for both the heavy ice and light ice groups. Beginning in June, the magnitude of the anomalies begins to increase, with the largest anomalies during September. This confirms the idea that the September ice conditions deviate the most from the patterns observed in the past. For the MYI, predominately positive anomalies occur during the heavy ice years in all months. This indicates that the heavy ice years have generally older ice types than the 1979–2012 average. During light ice years, predominately negative anomalies are evident. These patterns hold throughout the year for both the heavy ice and light ice anomalies, with the strongest and most consistent patterns observed during September.

Standard Deviations. Larger TI standard deviations are found for the light ice group (when compared to the heavy ice group) from January through June. Beginning in July, the heavy and light ice composites show regions of both large and small standard deviations. The locations of these regions of large standard deviations change from month to month. Both November and December show very small standard deviations throughout the study region for both the heavy ice and the light ice groups. For the MYI, all grid cells during all months for both the heavy ice and light ice groups had standard deviations less than one. This indicates that there is a large amount of agreement between the patterns of ice age for the five heavy and five light ice years. This adds more validity to the use of this measure.

Discussion. Overall, the TI and MYI confirm expected changes in the sea ice in the Beaufort Sea region. Both TI and MYI have the largest anomalies and number of

significant differences during September, which corresponds to the minimum ice extent. Because these measures represent the conditions of the ice throughout the year, they can be useful in forecasting the minimum ice extent.

III.5.2 Part 2: Predictor Variable Correlations with Teleconnections

III.5.2.1 Upper Air Temperatures

The upper atmospheric temperature variables (850, 700, 500, and 300 hPa monthly mean air temperatures) show consistent correlations with the ten teleconnection indices. The AO correlates predominately negatively with temperature throughout the year, with the strongest and most extensive correlations during winter when the AO signature is the strongest (Figure 18). This pattern is observed at all four pressure levels (Figure 18). In general, negative correlations are observed in the northern and northeastern portion of the study region, with no correlations present in the southern portion for many months (Figure 18). Negative correlations indicate that higher air temperatures are associated with the negative AO phase—higher pressure in the Arctic and lower pressure in the midlatitudes (Wallace and Gutzler 1981). A small region of positive correlations is present during July for the 300 hPa, 500 hPa, and 700 hPa pressure levels and during August at all four pressure levels. For the NAO, similar correlation patterns are observed, with strong negative correlations during the winter months for all four pressure levels. Again these correlations generally occur in the northern portion of the study region, with no significant correlations present in the south for most months. These negative correlations similarly mean that higher air temperatures are associated with the negative phase of the NAO, which brings higher temperatures to

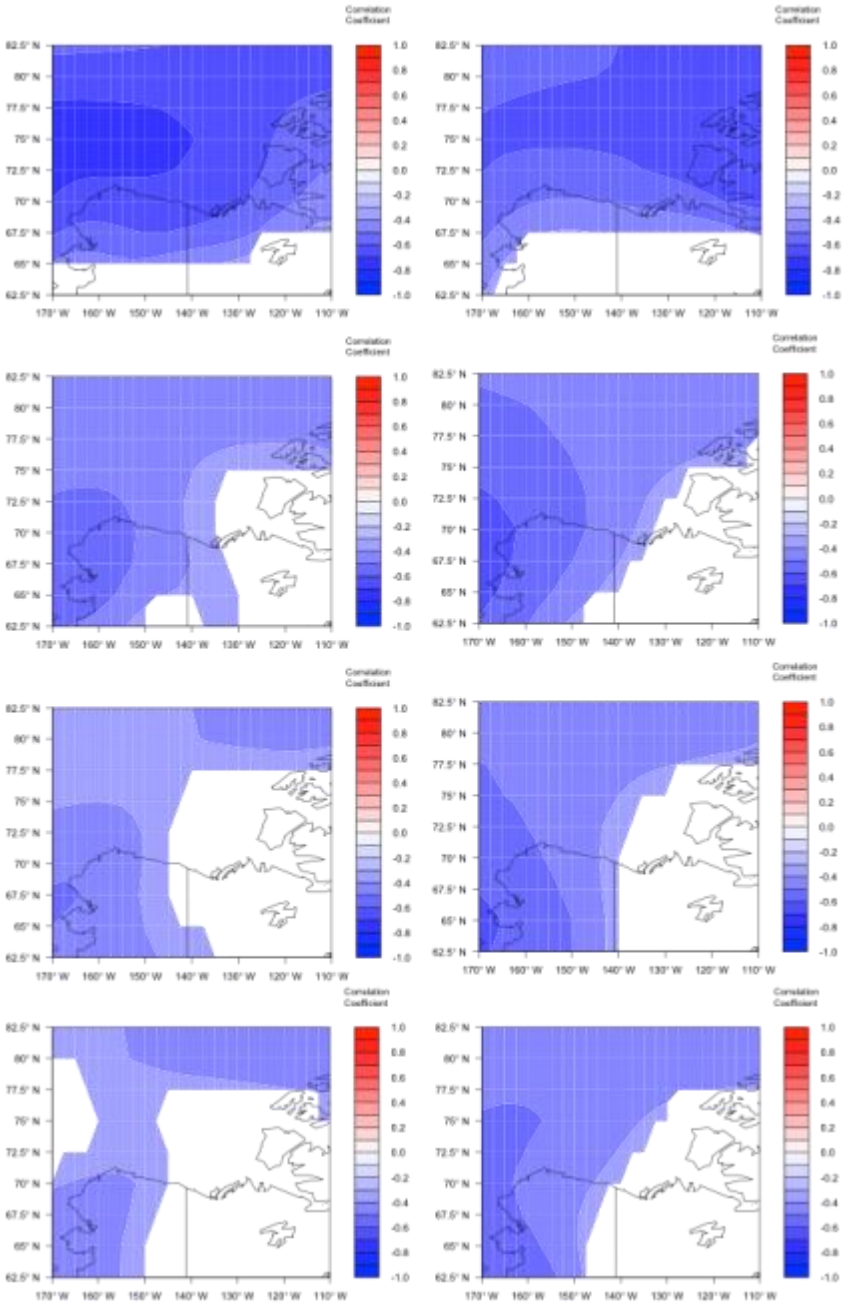

Figure 18: Air temperature correlation maps with AO during December (left) and January (right) at four pressure levels (from top to bottom: 300 hPa, 500 hPa, 700 hPa, 850 hPa). Cells with correlations significant at the 95% confidence level are plotted.

the Canadian Arctic Archipelago and lower temperatures to Europe (Wallace and Gutzler 1981). As with the AO, some small regions of significant positive correlations are observed during summer and early fall (July for all four pressure levels, August for 300 hPa, and September for the 500, 700, and 850 hPa levels). The patterns of correlations observed are fairly consistent between all four levels.

PNA is correlated predominately positively with temperature at all pressure levels throughout the year. From January through April these significant positive correlations occur in the southeastern portion of the study region for 850, 700, and 500 hPa (Figure 19). The strength of the correlations decreases with height during these months (Figure 19). At the 300 hPa pressure level positive correlations are found during January, and instead some negative correlations from February through April (Figure 19). Positive correlations with the PNA suggest that increased air temperatures are associated with ridging over the western United States, which moves warmer air into parts of the Arctic (Wallace and Gutzler 1981). Beginning in May, no large regions of significant correlations are observed at any pressure level until July. From July through December regions of positive correlations occur with temperature at the 850, 700, and 500 hPa levels for all months (Figure 19). The patterns of these correlations are consistent for these three pressure levels. At 300 hPa, both positive and negative correlations are found (Figure 19).

For the SOI and Niño 3.4 index, only very small regions of significant correlations appear throughout the year for each pressure level. Significant correlations with SOI were only observed with temperature at 300 hPa. These correlations were both

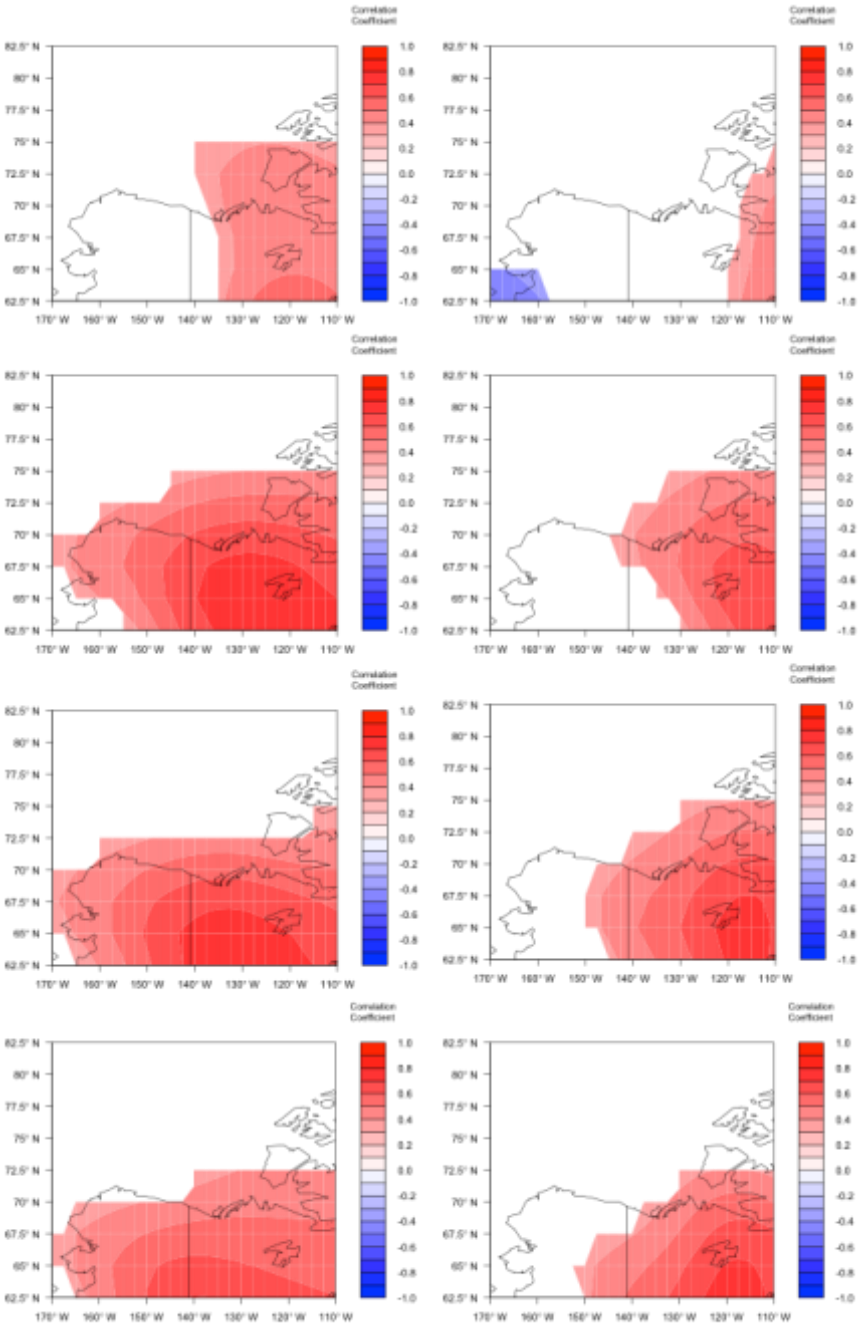

Figure 19: Air temperature correlation maps with PNA during January (left) and October (right) at four pressure levels (from top to bottom: 300 hPa, 500 hPa, 700 hPa, 850 hPa). Cells with correlations significant at the 95% confidence level are plotted.

positive and negative and no spatially consistent patterns are observed. The Niño 3.4 index showed some significant correlations at all pressure levels, although these regions are very small and generally not consistent for the four pressure levels.

Temperature at all four pressure levels exhibits significant negative correlations with the EAWR teleconnection index. For 300 hPa, the fewest significant correlations are observed throughout the year. At this level, large regions of significant negative correlations occur only during November and December (Figure 20). At the three lower pressure levels, regions of significant negative correlations are evident throughout the year, although the patterns of these correlations are not consistent between pressure levels. For example, large regions of strong negative correlations occur with temperature at 500 and 700 hPa during May, but a smaller area of significant negative correlations is evident at the 850hPa level (Figure 20). Significant positive correlations are also found during February and December for temperatures at all three lower pressure levels (Figure 20).

For the EA teleconnection index, regions of both positive and negative correlations are evident throughout the year at all four pressure levels. Where significant correlations are observed, they are clustered into very small regions. During all months, most of the study region shows no significant correlations. The patterns of isolated significant correlations are very inconsistent throughout the year and between pressure levels and therefore the EA index may not have an appreciable physical influence on the upper atmospheric air temperature profile.

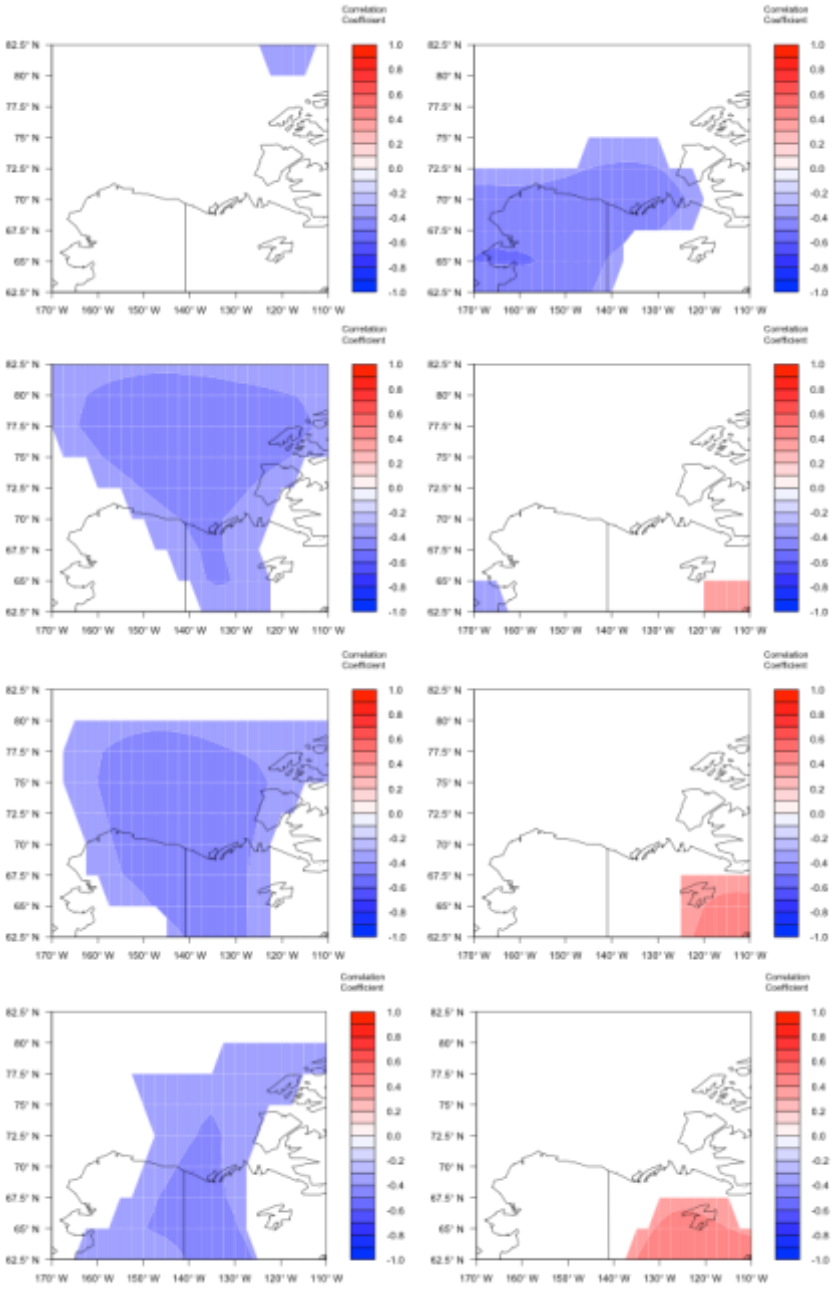

Figure 20: Air temperature correlation maps with EAWR during May (left) and December (right) at four pressure levels (from top to bottom: 300 hPa, 500 hPa, 700 hPa, 850 hPa). Cells with correlations significant at the 95% confidence level are plotted.

The EPNP teleconnection index has large areas of significant positive correlations throughout the year at all pressure levels. The most spatially extensive patterns of positive correlations occur from January through April for the three lowest pressure levels (Figure 21). Higher air temperatures are thus associated with the positive phase of the EPNP pattern, which includes positive height anomalies over Alaska and Western Canada and negative height anomalies over the central North Pacific (Barnston and Livezey 1987). For these three levels, negative correlations appear beginning in May and persist through August (Figure 21). The locations of these negative correlations are consistent for all three pressure levels. During October and November, large regions of positive correlations are evident (Figure 21). The 300 hPa pressure level does not follow the same correlation patterns throughout the year in terms of significant correlations of the same magnitude. For January and February some positive correlations are observed, which is similar to the three lower pressure levels. Beginning in March, no positive correlations occur and negative correlations begin to appear in April, which contradicts the pattern at the other pressure levels (Figure 21). The 300 hPa pattern deviates from the other pressure levels during all months until October and November, when large areas of positive correlations occur, in agreement with the other pressure levels (Figure 21).

Only very small regions of both positive and negative correlations are found between temperature and the PE index from January through August at all four pressure levels. Significant correlations occur only in very small clusters with little consistency between pressure levels. Starting in September, some consistency is observed between

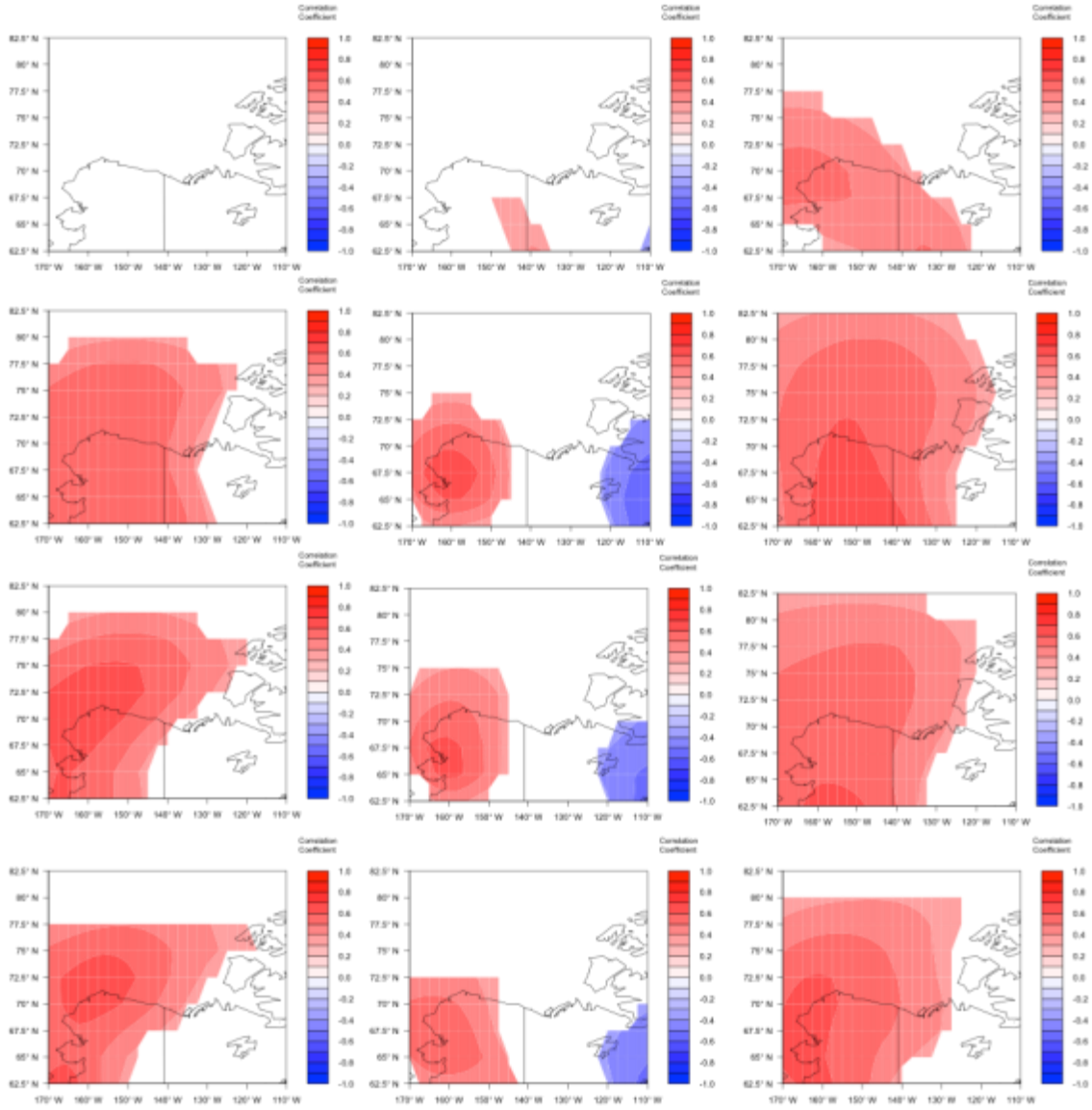

Figure 21: Air temperature correlation maps with EPNP during March (left), July (middle), and November (right) at four pressure levels (from top to bottom: 300 hPa, 500 hPa, 700 hPa, and 850 hPa). Cells with correlations significant at the 95% confidence level are plotted.

the three lowest pressure levels. In September, these three pressure levels indicate large regions of positive correlations. The 300 hPa pressure level does not show any extensive significant correlations. In October, large regions of negative correlations with temperature are found at all four levels. During November, no significant correlations are observed at the three lower levels. In December, negative correlations are evident at all four pressure levels. The lack of consistency between pressure levels and lack of significant correlations during most months suggests that this index is not useful in explaining the upper air temperature variability throughout the year.

Lastly, the WP teleconnection index shows some regions of positive correlations during many months throughout the year with temperature at all four pressure levels, although large regions of significant correlations are only found during July, August, and September for some pressure levels. When these large correlation areas are observed during July and August, they are not consistent between pressure levels. The 300 hPa pressure level shows the least consistency with the other levels. At this level, some regions of negative correlations also occur.

Discussion. Overall, the AO, NAO, PNA, and EPNP teleconnection indices appear to have the most potential utility in explaining and driving the upper atmospheric air temperatures over the Beaufort Sea region. These four indices exhibit extensive regions of significant correlations and these patterns are consistent between pressure levels and throughout the year. This suggests that these indices may be useful in accounting for the air temperature patterns observed throughout the year, which may help in understanding the large scale drivers of sea ice changes. In general, the largest

amount of consistency was observed between the three lowest pressure levels, while the 300 hPa level deviated from the common pattern. This follows the findings of the composite analysis: the 300 hPa pattern is different from the other three pressure levels and may be too far removed from the surface to provide any useful information regarding surface conditions. The other teleconnection indices studied do not appear useful in explaining the upper air temperature patterns because of a lack of significant correlations and a lack of consistency between pressure levels and throughout the year.

III.5.2.2 Geopotential Heights

The geopotential heights at 300, 500, 700, and 850 hPa show consistent significant correlations throughout the year for most of the teleconnection indices. For the AO, strong negative correlations are observed throughout the year at all four pressure levels. In most months, these significant correlations show nearly continuous spatial patterns, especially from October through January for all four pressure levels (Figure 22). Similar patterns are evident for the NAO, where strong negative correlations occur during nearly every month of the year for all four pressure levels (Figure 22). Unlike the AO, some small regions of positive correlations appear during July at the 300 hPa and 500 hPa pressure levels and during September at all four pressure levels (Figure 22). The most extensive patterns of significant correlations are observed during October and November at all four pressure levels (Figure 22), although large areas of significant negative correlations are found in nearly every month. Negative correlations between geopotential height and the AO/NAO indicate that increases in height over the Beaufort Sea are associated with the negative phase of the AO/NAO (Wallace and Gutzler 1981).

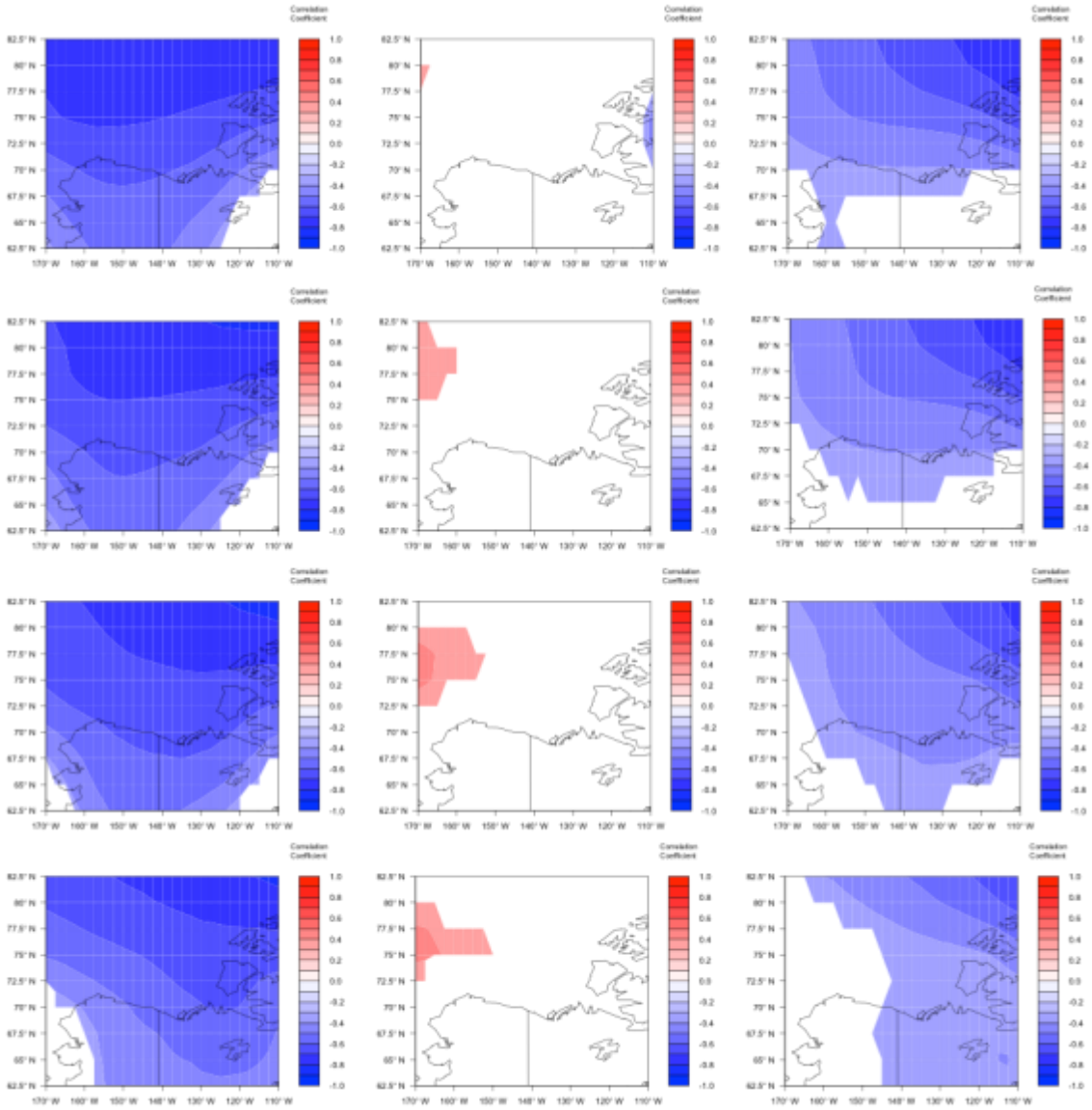

Figure 22: Geopotential height correlation maps with AO during October (left) and NAO during September (middle) and October (right) at four pressure levels (from top to bottom: 300 hPa, 500 hPa, 700 hPa, 850 hPa). Cells with correlations significant at the 95% confidence level are plotted.

The negative phase of the AO/NAO is typically associated with high pressure in the Arctic (Wallace and Gutzler 1981).

The PNA exhibits large regions of positive correlations, with some small regions of negative correlations appearing in some months. The most extensive correlations are observed during September for all four pressure levels, where significant positive correlations cover most of the study region (Figure 23). The positive correlations suggest that increased geopotential height corresponds to the positive phase of the PNA, where positive geopotential height anomalies are normally present over the western half of North America (Wallace and Gutzler 1981). In general, the amount of significant negative correlations increased as the pressure level increases (Figure 23). For example, the largest areas of negative correlations during the most months are at the 850 hPa pressure level, with the fewest negative correlations at the 300 hPa.

The SOI and the Niño 3.4 index show little to no grid cells with significant correlations. For the SOI, no significant correlations are observed throughout the year for the 300 hPa and 500 hPa pressure levels, while some very small regions of significant, albeit likely spurious, negative correlations occur during February, April, July, and September at the 700 hPa and 850 hPa pressure levels. Niño 3.4 shows only very small regions of significant positive correlations during July at the 300 and 500 hPa levels, and during February and July at the 700 and 850 hPa levels. Some small regions of negative correlations occur, but these regions are not consistent throughout the pressure levels.

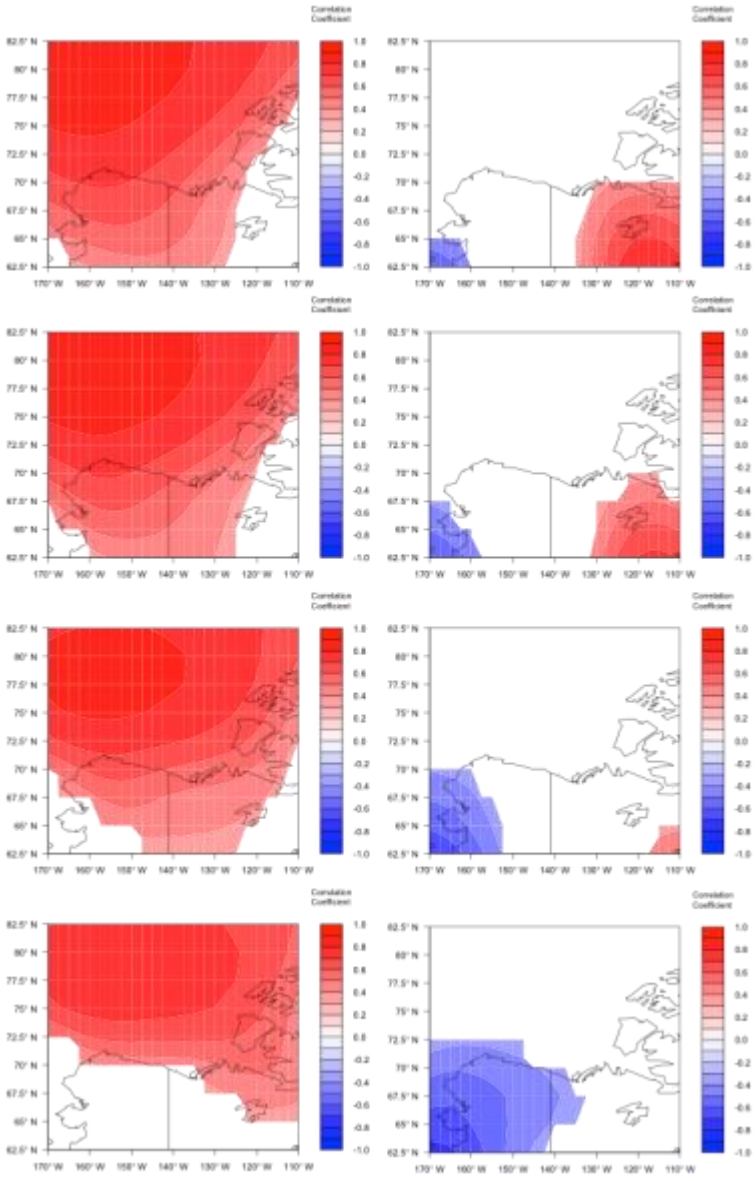

Figure 23: Geopotential height correlation maps with PNA during September (left) and December (right) at four pressure levels (from top to bottom: 300 hPa, 500 hPa, 700 hPa, 850 hPa). Cells with correlations significant at the 95% confidence level are plotted.

The EAWR teleconnection index shows strong negative correlations over large regions of throughout most months of the year at all four pressure levels. The negative correlations are the most extensive during November and December (Figure 24). Positive geopotential height anomalies are associated with the negative phase of the EAWR pattern, which is associated with positive heights over central North America (Barnston and Livezey 1987). Some positive correlations occur at all four pressure levels during February at the three highest pressure levels in July (Figure 24). During months where significant positive or negative correlations are observed, the locations of these correlations are generally consistent between all four pressure levels.

For the EA index, small regions of positive and negative correlations are observed throughout the year at all four pressure levels. The largest spatially consistent patterns of significant negative correlations are in July at all four pressure levels (Figure 25). Throughout the rest of the year, only very small regions of significant correlations are evident, and these regions are generally not consistent between pressure levels.

The EPNP teleconnection index has strong positive correlations that cover almost the entire study area throughout the year at all four pressure levels. For all months, the locations and spatial extent of these positive correlations is consistent between all four atmospheric levels (Figure 25). These positive correlations correspond to positive height anomalies with the positive phase of the EPNP pattern. The fewest significant correlations occur in August, when no significant correlations are observed at 300 hPa and 500 hPa and only a very small area of significant correlations at 700 and 850 hPa (Figure 25).

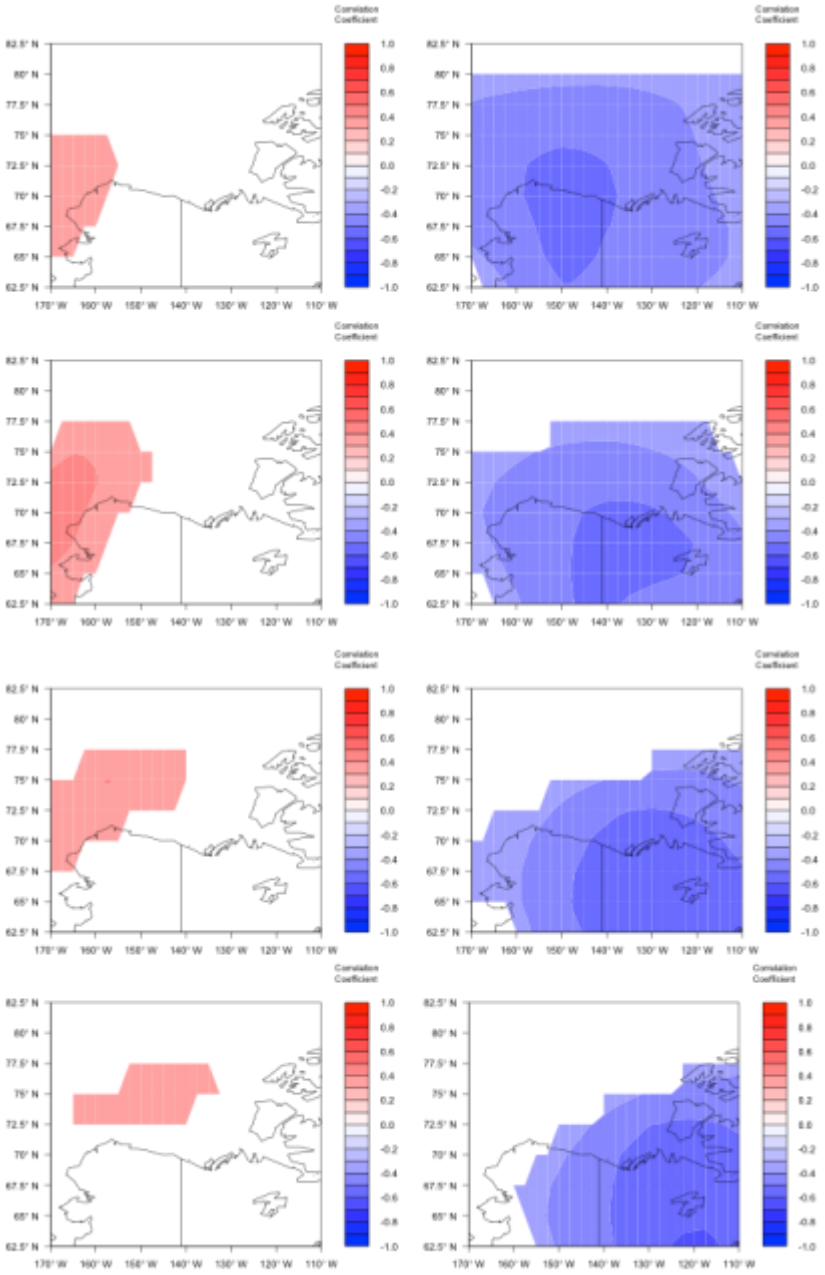

Figure 24: Geopotential height correlation maps with EAWR during February (left) and November (right) at four pressure levels (from top to bottom: 300 hPa, 500 hPa, 700 hPa, 850 hPa). Cells with correlations significant at the 95% confidence level are plotted.

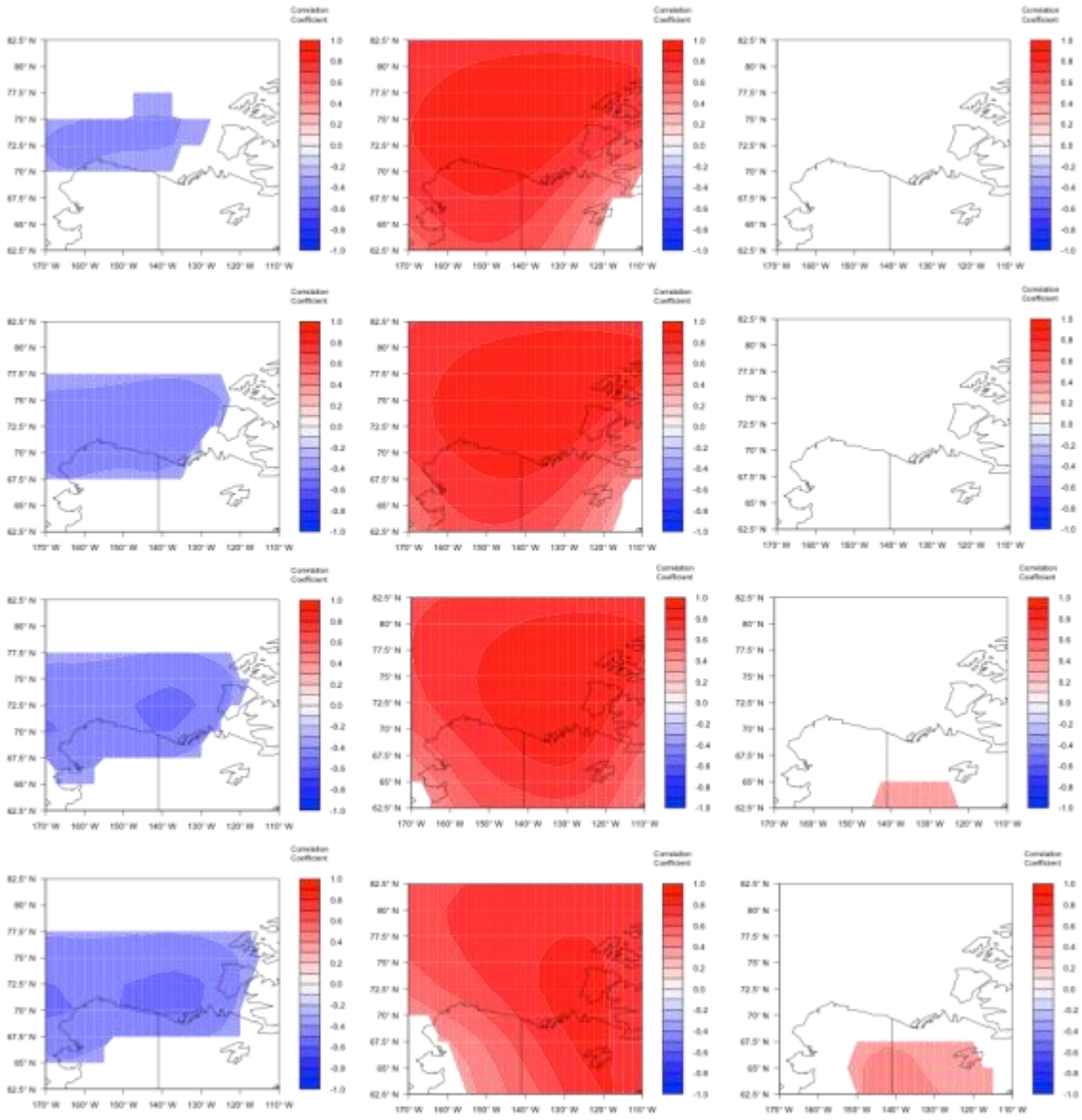

Figure 25: Geopotential height correlation maps with EA during July (left) and EPNP during January (middle) and August (right) at four pressure levels (from top to bottom: 300 hPa, 500 hPa, 700 hPa, 850 hPa). Cells with correlations significant at the 95% confidence level are plotted.

For the PE teleconnection, regions of both positive and negative correlations are evident throughout the year, consistent between the pressure levels. During January, August, and September, predominately positive correlations occur, and predominately negative correlations during March, April, May, October, November, and December. Throughout the remaining months, few to no significant correlations are observed. The most extensive correlation patterns occur during October at all pressure levels, November at the 500, 700, and 850 hPa pressure levels, and December for the 300hPa level.

The WP index is negatively correlated with height, although large regions of significant positive correlations do occur in August at all four pressure levels. In general, the spatial extent of the significant correlations decreases with increasing pressure level. For example, the largest spatial patterns of significant correlations are at the 850 hPa pressure level, with the smallest spatial patterns at 300hPa. Overall, the most extensive correlations are in October, November, and December, especially at the higher pressure levels.

Discussion. In general, the AO, NAO, PNA, EAWR, and EPNP indices have the strongest relationships with geopotential heights over the Beaufort Sea. The PE and WP indices both show some relationship during specific months of the year (October through December), which indicates that these teleconnections may also provide some use in explaining the driving forces behind the geopotential height patterns observed in the region. The teleconnections with the strongest relationships with geopotential heights

generally follow the results from the upper air temperatures, indicating that these indices could be driving the upper atmospheric conditions of the region.

III.5.2.3 Surface Temperature

For the three surface temperature variables (SAT, FDD, and TDD), it is expected that similar spatial correlation patterns will be observed, with some differences in magnitude. The AO and NAO have negative correlations with surface air temperatures while large areas of positive correlations occur with FDD (Figure 26). This opposite pattern is expected because large FDD values indicate lower daily air temperatures. For AO, a large region of significant correlations is only evident during October for the

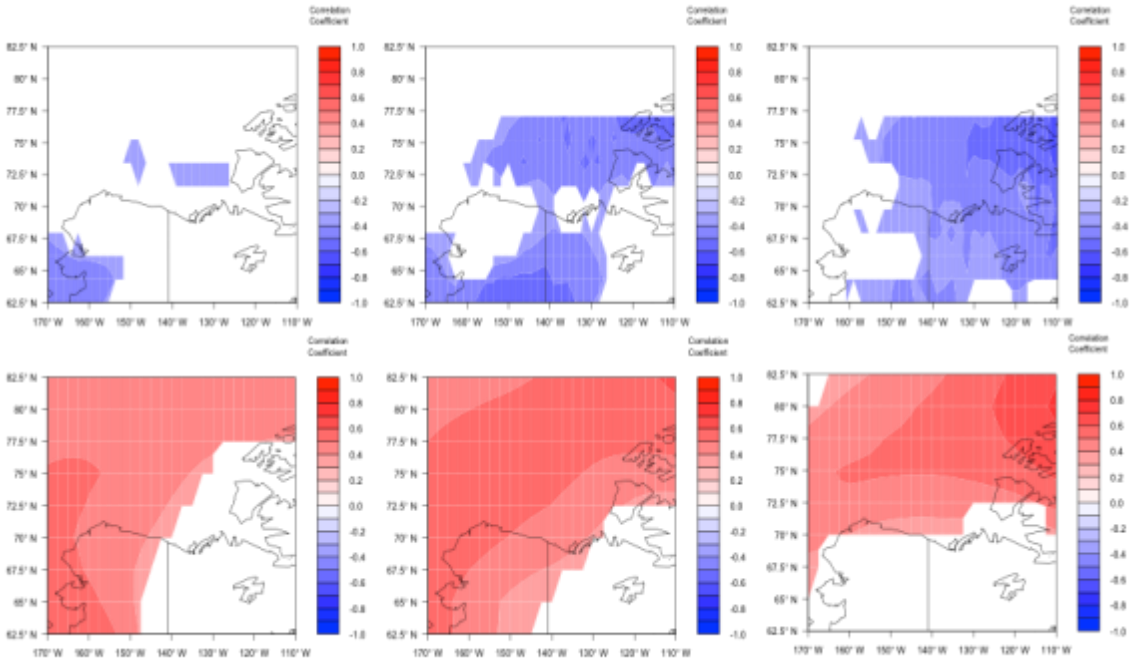

Figure 26: Correlation maps with AO during January (left) and October (middle), and with NAO during October (right) for SAT (top row) and FDD (bottom row). Cells with correlations significant at the 95% confidence level are plotted.

surface air temperatures, with smaller regions during the remainder of the year (Figure 26). For the NAO, a large region of negative correlations with surface temperature is observed during October (Figure 26). FDD has extensive regions of positive correlations during January, May, October, and December with the AO, and May and November for the NAO (Figure 26). The TDD, only used from June through August when air temperatures are above freezing, do not show many significant correlations. During the positive phase of the AO/NAO, lower air temperatures are present in the Canadian Arctic Archipelago and the Beaufort Sea region (Wallace and Gutzler 1981), which corresponds to the correlation patterns observed for SAT, FDD, and TDD.

The PNA has both positive and negative correlations throughout the year with surface air temperatures, although the positive correlations are more extensive, especially during August and September (Figure 27). For the FDD, strong and spatially consistent patterns of negative correlations are found throughout the year (excluding the summer months when FDD values are zero). The negative FDD correlations agree with the positive temperature correlations observed during August and September (Figure 27). The TDD are only significantly correlated during August, when a large region of positive correlations occurs in the northwest portion of the study region and a small region of negative correlations in the southeast (Figure 27). These positive TDD correlations correspond to the positive temperature and the negative FDD correlations. These correlation patterns suggest that positive PNA brings increases in air temperatures to the Beaufort Sea region. This potentially corresponds to the ridging that is typically

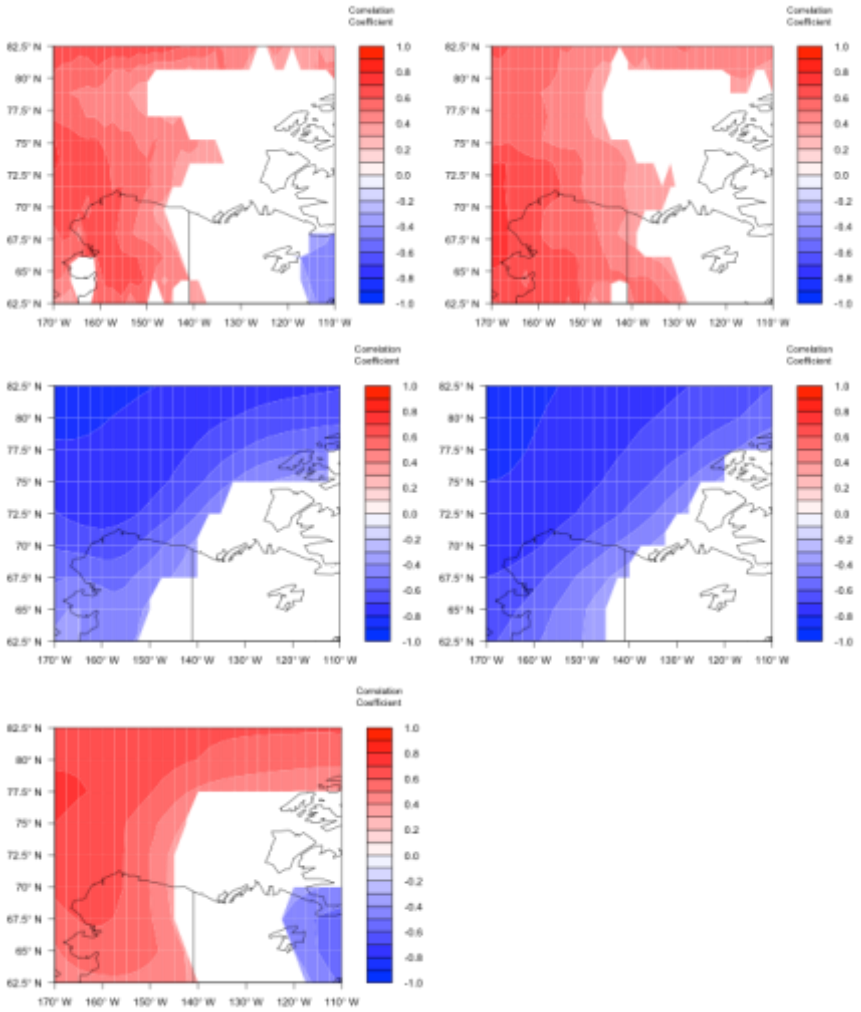

Figure 27: Correlation maps with PNA during August (left) and September (right) for SAT (top), FDD (middle), and TDD (bottom). Cells with correlations significant at the 95% confidence level are plotted.

present over the western United States during the positive phase (Wallace and Gutzler 1981).

SOI and Niño 3.4 are again not significantly correlated with any of the three surface air temperature variables. For the EAWR teleconnection index, some regions of

negative correlations are found throughout the year for the surface air temperatures, although the locations of these regions are not consistent throughout the year. FDD shows both positive and negative correlations throughout the year with no discernible pattern. The location and timing of these correlations does not correspond with the surface air temperatures. The TDD show some negative correlations, although they do not correspond with the FDD or surface air temperatures. For the EA teleconnection index, only small regions of significant positive and negative correlations occur for the three surface temperature variables throughout the year. Where significant correlations are present for one variable, they are absent for the other variables and there appears to be no consistent pattern for the locations of the significant correlations.

For the EPNP index, strong positive correlations are evident for surface air temperatures from January through March and during November (Figure 28). These correspond with strong negative correlations for FDD during these same months (Figure 28). Increases in air temperatures correspond to the positive phase of the EPNP pattern, where positive height anomalies are observed over Alaska (Barnston and Livezey 1987). Strong negative correlations are also found in October for the FDD, although no significant correlations occur based on surface air temperatures during this month. The TDD shows a strong and spatially consistent pattern of positive correlations during June, although no corresponding correlations are observed for the surface air temperatures.

The PE and WP teleconnection indices both indicate inconsistent patterns of significant correlations throughout the year. For these indices, correlations of both signs occur for all three variables throughout the year, and there appears to be no consistent

spatial pattern for the significant correlations. There is also no correspondence between the three variables in terms of the locations of these significant correlations.

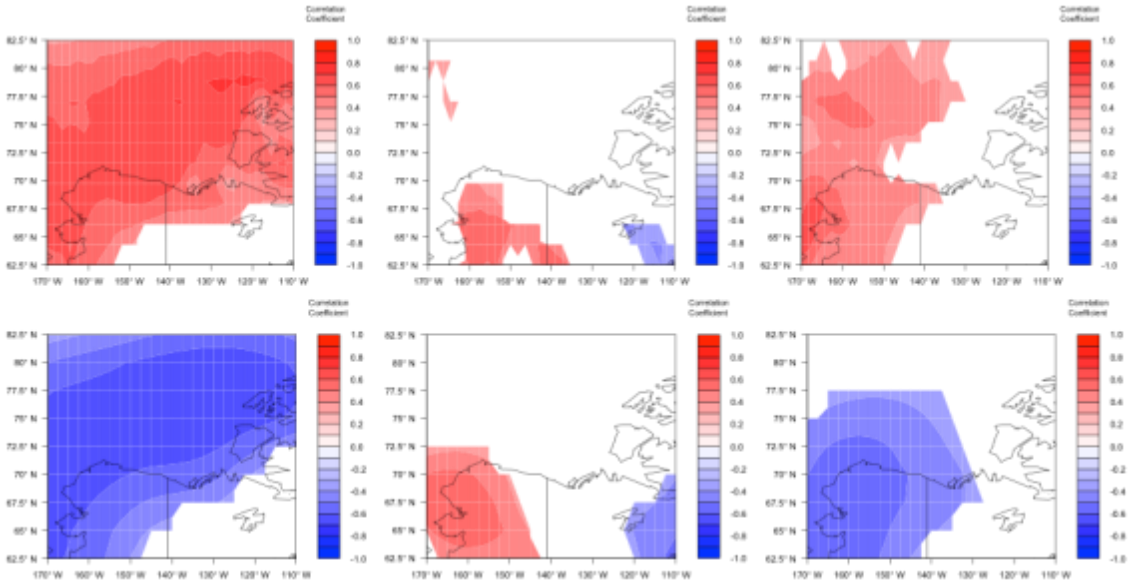

Figure 28: Correlation maps with EPNP during February (left), July (middle), and November (right) for SAT (top) and FDD (for February and November) and TDD (for July) (bottom). Cells with correlations significant at the 95% confidence level are plotted.

Discussion. Overall, the AO, NAO, PNA, and EPNP teleconnection indices have the most consistent and extensive patterns of significant correlations for all three temperature variables. These four teleconnection indices match with the most significant indices for both the upper atmospheric air temperatures and the geopotential heights. The inconsistent patterns observed for the remaining indices indicate that these teleconnections may not have an influence on the regional scale surface conditions in the Beaufort Sea region.

III.5.2.4 Other surface variables

The remaining surface variables include SLP, wind speed, and wind direction. For the AO and NAO, a consistent pattern of predominately negative correlations is observed for SLP (Figure 29). The significant correlations are located in the north and northeastern portions of the study region for all months. Overall, the pattern of significant correlations is larger for the AO versus the NAO (Figure 29). Negative correlations indicate that positive SLP anomalies are associated with the negative phase

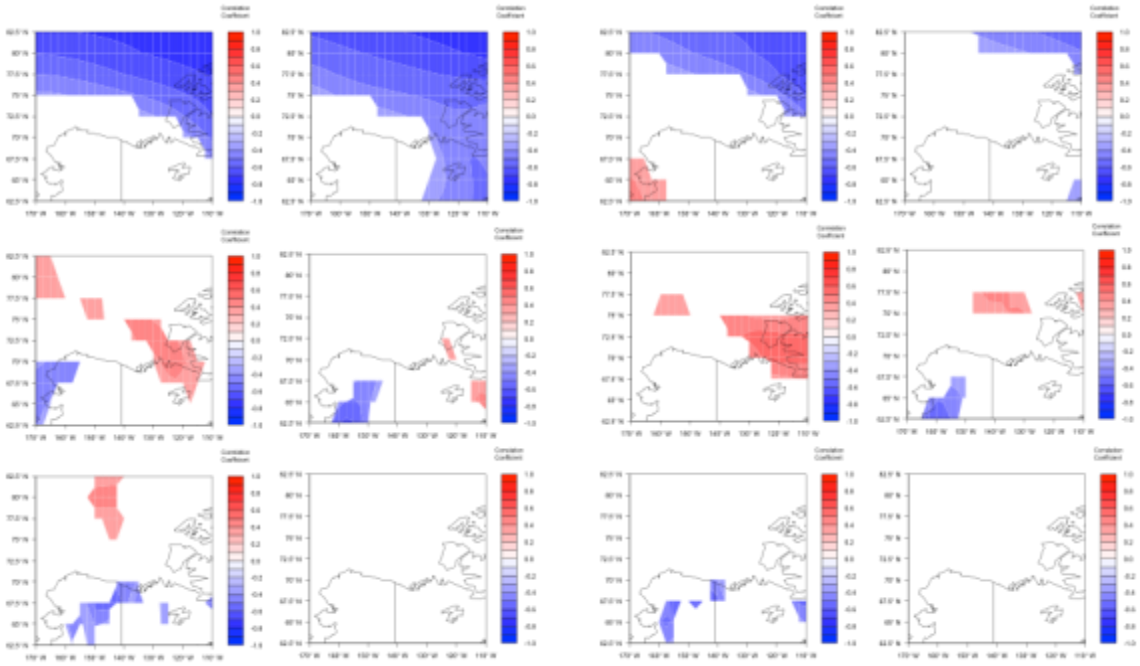

Figure 29: Correlation maps for AO (left group) and NAO (right group) during March (left) and October (right) for SLP (top), wind speed (middle), and wind direction (bottom). Cells with correlations significant at the 95% confidence level are plotted.

of the AO/NAO, where high pressure is typically observed in the Arctic (Wallace and Gutzler 1981). For wind speed, both positive and negative correlations occur throughout the year for AO and NAO (Figure 29). Generally, when positive correlations occur they are in the northeastern portion of the study region, while negative correlations are generally found in the southwestern portion. Wind direction shows little to no significant correlations throughout the year for either the AO or the NAO, and when significant correlations occur they are not consistent throughout the year (Figure 29).

For the PNA, negative SLP correlations are found in the southern portion of the study region and positive correlations in the north for most months (Figure 30). Except for during May, June, and July, these patterns are consistent over extensive regions (Figure 30). Wind speed and direction again only have small regions of both positive and negative correlations throughout the year, although these correlations are not consistent (Figure 30).

The SOI and Niño 3.4 teleconnection indices do show some significant correlations with SLP, wind speed, and direction throughout the year. But these correlations are in very small areas and are seemingly randomly distributed throughout the study region. For the EAWR and EA teleconnection indices, no consistent patterns of correlations are found for SLP, wind speed, or direction. SLP has a large area of significant correlations during December for the EAWR index, and during July for the EA index. Throughout the rest of the year almost no significant correlations are observed. Wind speed and direction produce no large areas with significant correlations.

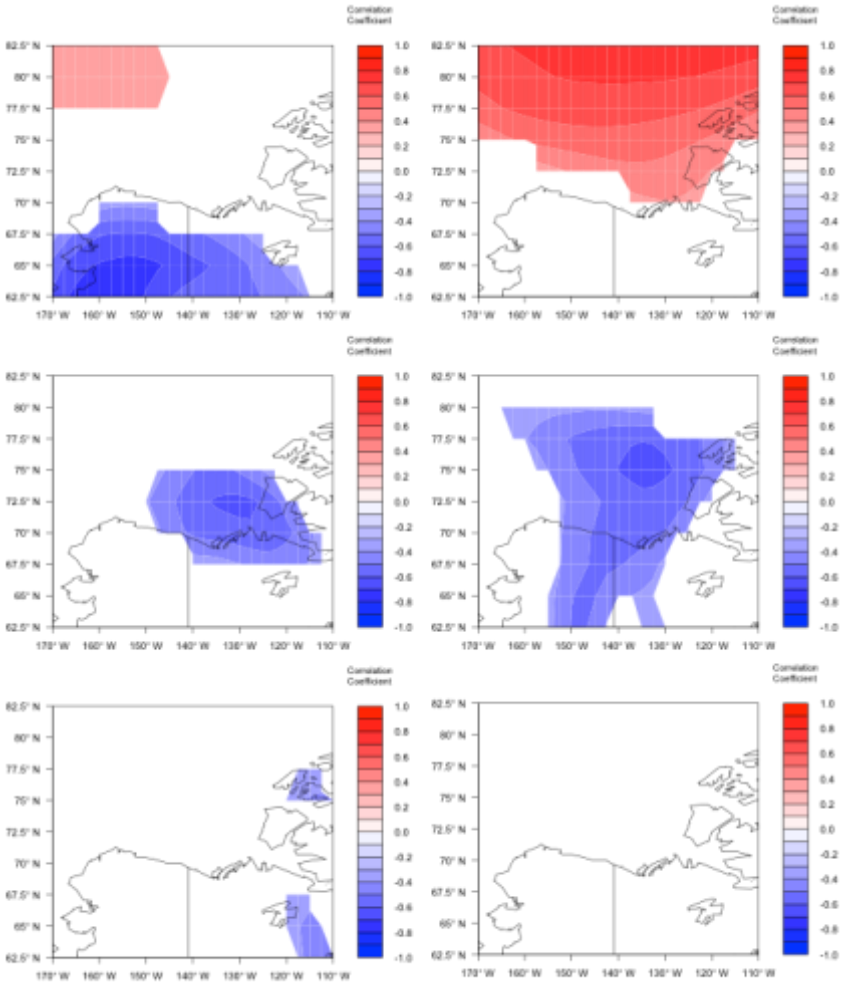

Figure 30: Correlation maps with PNA during February (left) and August (right) for SLP (top), wind speed (middle), and wind direction (bottom). Cells with correlations significant at the 95% confidence level are plotted.

The EPNP teleconnection index shows large regions of significant positive correlations throughout the year for SLP (Figure 31). Increases in SLP occur during the positive phase of the EPNP pattern, which is typically associated with positive height

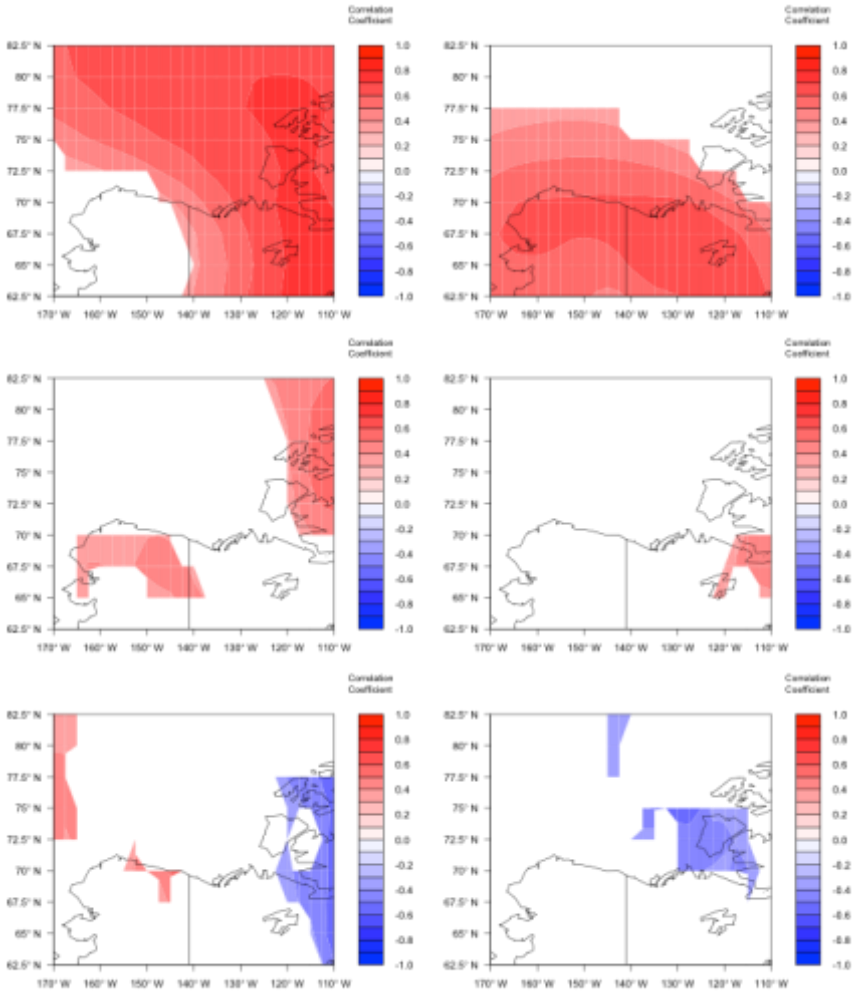

Figure 31: Correlation maps with EPNP during January (left) and July (right) for SLP (top), wind speed (middle), and wind direction (bottom). Cells with correlations significant at the 95% confidence level are plotted.

anomalies over Western Canada (Barnston and Livezey 1987). For wind speed and direction, both positive and negative spurious correlations are again observed throughout the year with no consistency to their locations (Figure 31).

The PE and WP teleconnection indices show similar correlation patterns for SLP. From January through May, significant negative correlations are observed. Beginning in June, positive correlations occur until August, and negative correlations from September through December. The most spatially consistent SLP correlation patterns are during the winter when both indices are negatively correlated. For wind speed, small regions of both positive and negative correlations occur throughout the year for both indices, and these correlations are again not consistent in their location or sign throughout the year. Wind direction has predominately positive correlations throughout the year with both indices, although these correlations are not very extensive.

Discussion. Overall, the AO, NAO, PNA, and EPNP teleconnection indices have the most consistent correlation patterns with SLP. The PE and WP patterns also show some consistent patterns, although these correlations are not as extensive. Correlations with AO, NAO, PNA, and EPNP agree with the results for the upper atmospheric temperature variables, geopotential heights, and surface temperature variables. No consistent correlation patterns occur with wind speed and direction. This can be attributed to the fact that these two variables also showed no consistent patterns throughout the study region in the composite analysis.

III.5.2.5 Antecedent Ice Conditions

AO and NAO have similar correlation patterns with TI and MYI. For both variables, predominately positive correlations are observed throughout most of the year with the AO (Figure 32). Positive correlations indicate that the positive phase of the AO/NAO may be associated with increases in sea ice concentration and sea ice age. The

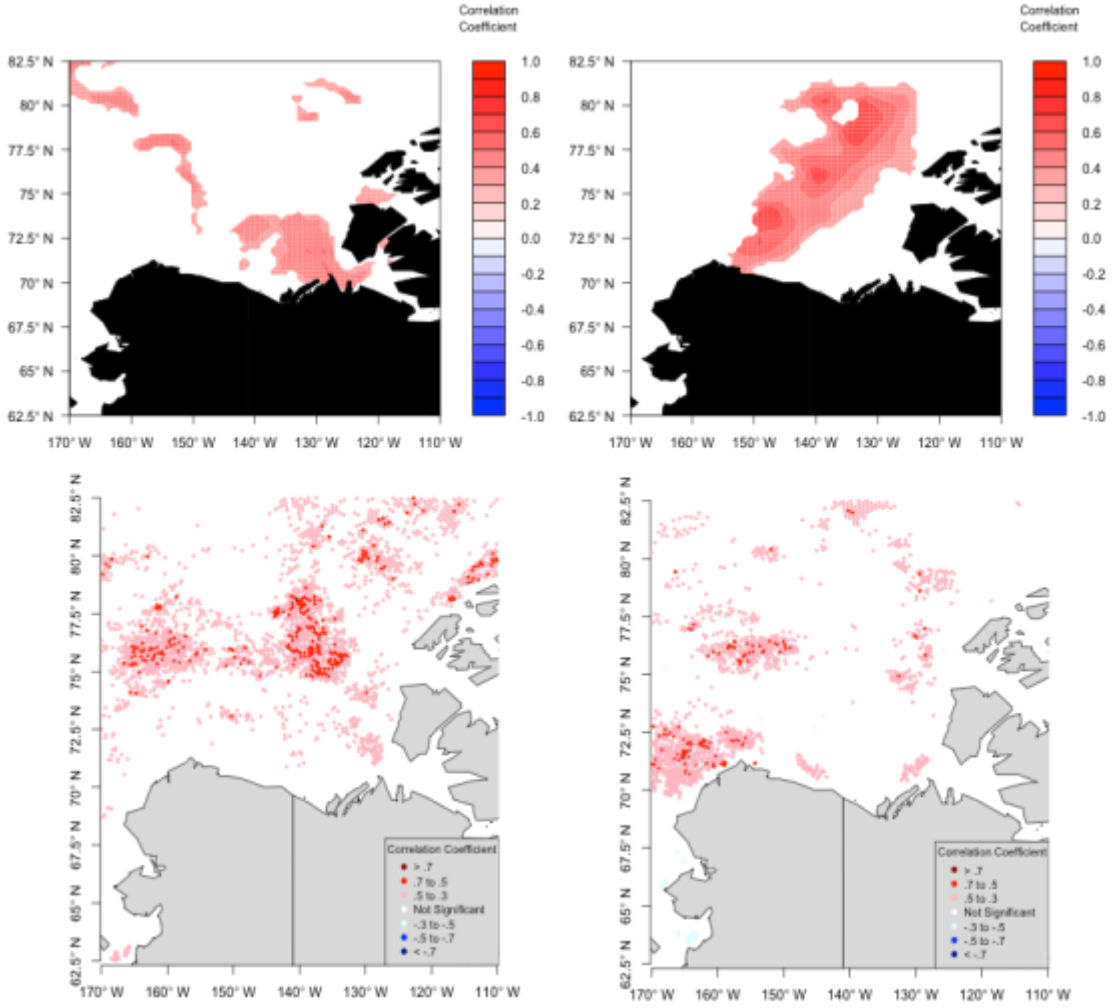

Figure 32: Correlation maps with AO during January (left) and August (right) for TI (top) and MYI (bottom). Cells with correlations significant at the 95% confidence level are plotted.

positive phase generally brings lower air temperatures to the high latitudes (Walace and Gutzler 1981). The most spatially consistent correlation patterns are found during January and August for both variables (Figure 32, 33). For the NAO, the most spatially consistent patterns of significant positive correlations occur during July and August for

both variables (Figure 33). Significant negative correlations are also found in September for both variables, which suggests a reversal of the relationship with the NAO during this month (Figure 33).

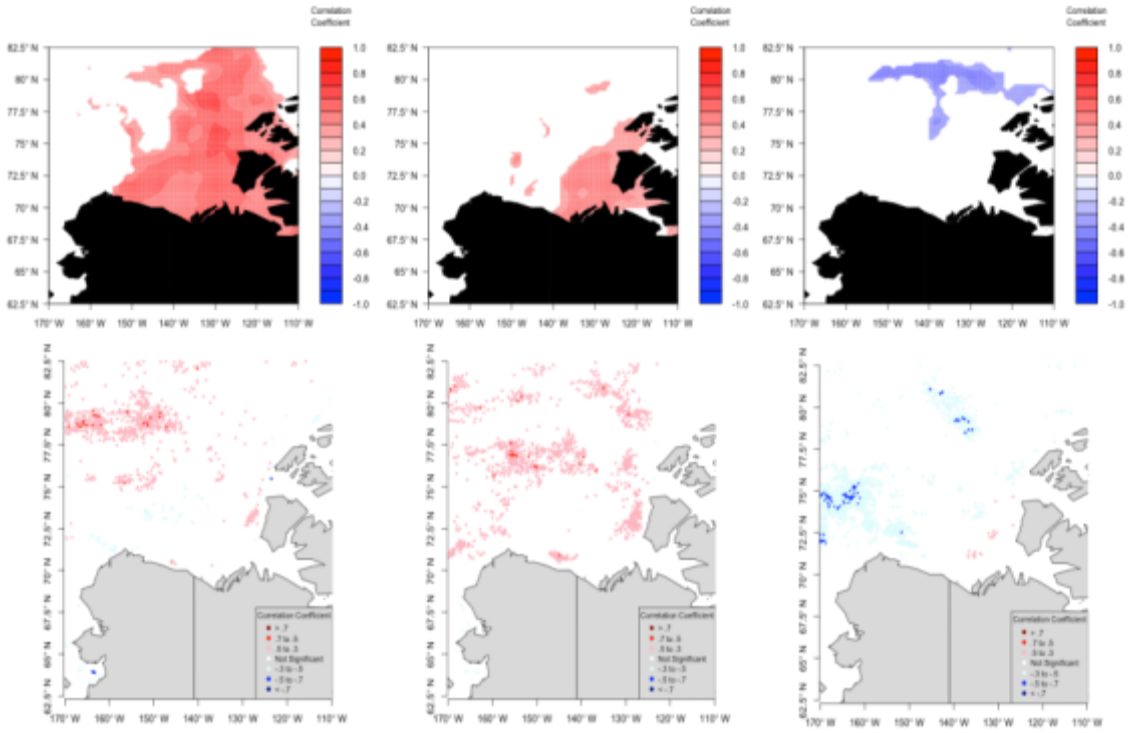

Figure 33: Correlation maps with NAO during July (left), August (middle), and December (right) for TI (top) and MYI (bottom). Cells with correlations significant at the 95% confidence level are plotted.

The PNA has positive and negative correlations with both ice variables, and more spatially consistent patterns of significant differences observed for TI (Figure 34). For TI, extensive positive correlations are found during June and large areas of significant negative correlations in August and September (Figure 34). MYI has few significant

correlations, except in September when a large area of significant negative correlations occurs (Figure 34). Negative correlations during September with both TI and MYI suggests that the PNA does have some relationship with sea ice conditions, especially when the minimum ice extent is reached.

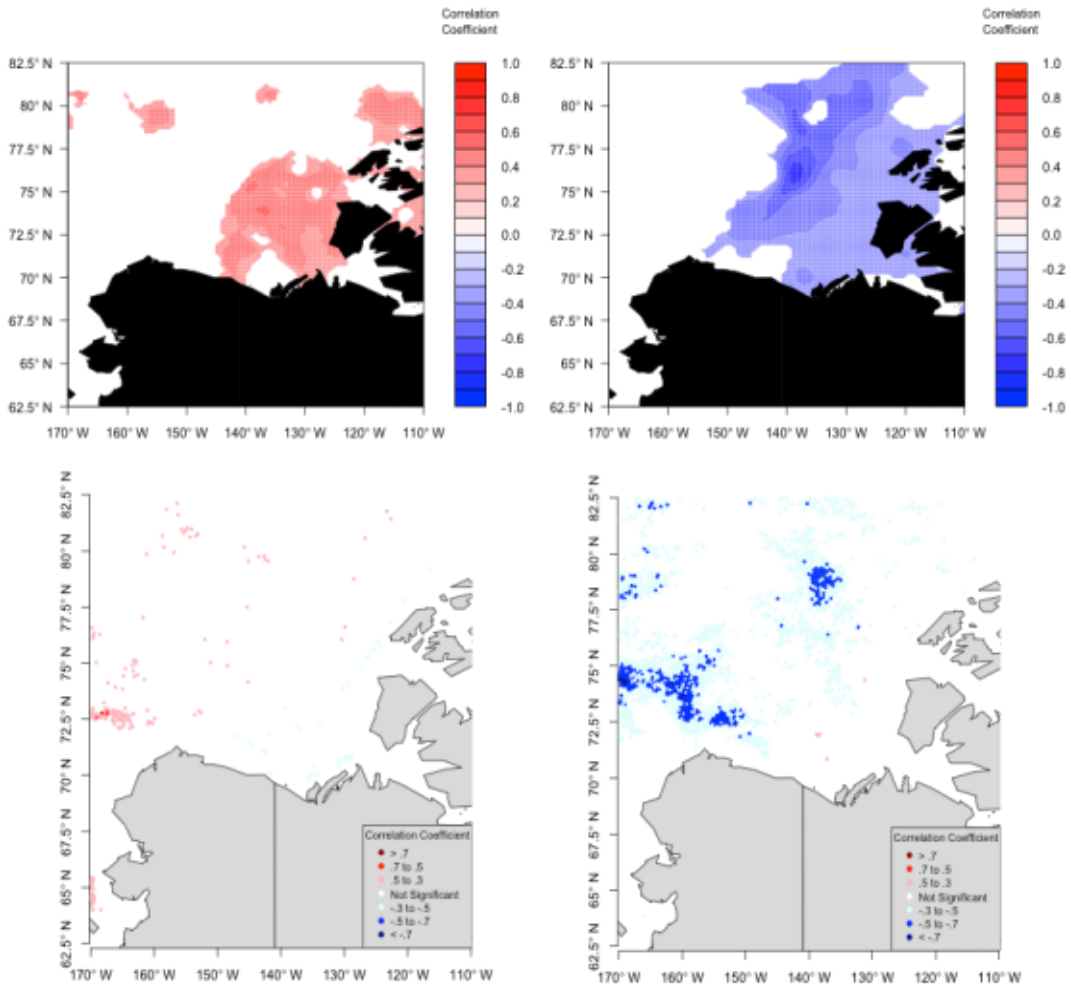

Figure 34: Correlation maps with PNA during January (left) and September (right) for TI (top) and MYI (bottom). Cells with correlations significant at the 95% confidence level are plotted.

The SOI and Niño 3.4 again produce very few significant correlations throughout the year for both TI and MYI. For the SOI, some significant negative correlations are evident, but with no consistent spatial patterns for either variable. Niño 3.4 similarly only has spurious positive correlations with the two ice variables.

The EAWR teleconnection pattern shows small areas of significant positive correlations with TI and MYI throughout the year. The most spatially consistent pattern of significant correlations is in August for TI, and in December for MYI. Throughout the rest of the year, only small areas of significant correlations occur.

For the EA teleconnection index, extensive negative correlations are evident during July and August for TI. This suggests that some relationship might exist between the EA and TI during these months, but no overall relationship emerges. For MYI, no spatially consistent pattern of correlations occurs.

The EPNP pattern shows consistent patterns of significant negative correlations with TI during January, and significant positive correlations during August and September. For MYI, significant correlations are observed during all months, although no spatially coherent pattern emerges.

The PE and WP teleconnections are significantly correlated with TI and MYI throughout the year, although these are not extensive patterns. The month with the largest spatial pattern of significant correlations is October for both TI and MYI. WP has no months with large correlations.

Discussion. Overall, the AO, NAO, and PNA show extensive patterns of significant correlations with the most persistence throughout the year. Similar correlation

patterns are found for both TI and MYI, with many of the strongest patterns observed during September when the minimum ice extent is reached. Because these strong and spatially consistent correlations exist during September, it indicates that these teleconnection indices may have some relationship with the minimum sea ice extent in the Beaufort Sea region. This means that these teleconnections can be expected to have some utility in forecasting the minimum sea ice extent.

III.5.3 Part 3: Long-Term Teleconnection Relationships

III.5.3.1 Principal Component Analysis

PCA is performed on each of the standardized predictor variables to identify the leading modes of variability of each variable over the entire study region. The proportion of variance explained by the first five PCs for each variable is displayed in Table 4. For the upper atmospheric temperature variables (air temperatures at 300, 500, 700, and 850 hPa), the geopotential heights (300, 500, 700, and 850 hPa), SLP, and FDD, the first PC explains over 50% of the variance in the respective original dataset (Table 4). For TDD and SAT, over 40% of the variance is explained by the first PC (Table 4). The presence of a dominant first PC suggests that these variables have a prevailing pattern of variability that can be utilized to represent the overall spatial distribution of the data over the study region. For the remaining variables (TI, MYI, wind speed, and wind direction), the first PC explains less than 35% of the variance in the dataset (Table 4), although the first PC can still be considered a dominant mode because the variance explained by the higher order PCs is substantially less.

Table 4: The proportion of variance explained by the first five PCs for each predictor variable.

Proportion of Variance Explained by each Principle Component					
	PC1	**PC2**	**PC3**	**PC4**	**PC5**
Total Ice	0.325	0.120	0.073	0.047	0.036
Multiyear Ice	0.229	0.054	0.052	0.028	0.020
FDD	0.563	0.167	0.123	0.039	0.028
TDD	0.480	0.136	0.122	0.047	0.042
Surface Temp	0.466	0.152	0.109	0.061	0.038
Temp 850hPa	0.571	0.188	0.121	0.039	0.025
Temp 700hPa	0.575	0.186	0.125	0.036	0.026
Temp 500hPa	0.590	0.173	0.130	0.035	0.025
Temp 300hPa	0.635	0.146	0.092	0.037	0.026
SLP	0.593	0.252	0.063	0.032	0.024
Gph 850hPa	0.610	0.222	0.081	0.029	0.026
Gph 700hPa	0.613	0.184	0.112	0.031	0.026
Gph 500hPa	0.608	0.168	0.133	0.032	0.025
Gph 300hPa	0.621	0.158	0.138	0.029	0.023
Wind Speed	0.308	0.143	0.115	0.075	0.063
Wind Direction	0.222	0.144	0.115	0.059	0.053

In this study, the first three PCs will be utilized in the correlation analysis. As observed in Table 4, after the third PC less than 10% of the total variance is explained by each PC (starting with PC 4). This means that these higher-order PCs do not represent any appreciable amount of variability in the dataset and therefore would likely not provide any useful information regarding the large-scale drivers of each of these predictor variables. Because the first three PCs represent an appreciable amount of variance in the data, they will be applied in the subsequent correlation analyses.

III.5.2.3 Correlation Analysis

Correlations were performed between the first three PCs for each predictor variable and each teleconnection index to further investigate the degree to which the individual teleconnections may drive the observed surface and atmospheric variability. These correlations were performed for the concurrent relationship and for monthly lags up to one year, with the teleconnections always leading.

The results for the concurrent correlations are provided in Tables 5, 6, and 7. Only results which are significant at the 95% confidence level are considered for analysis. For PCs 1 of the predictor variables, the teleconnection pattern showing significant correlations is the EAWR pattern (Table 5). Overall, only a small number of significant correlations are observed between the first PC and the teleconnection indices. When significant correlations are observed, these correlation values are very small (Table 5). Almost no significant correlations are observed between the teleconnection indices and PCs 2 for each variable (Table 6). Only three significant correlations are observed, and these occur between the EA index and SLP, the EA index and TI, and the PE index and 300hPa geopotential height (Table 6). Although these three correlations are significant at the 95% confidence level, their magnitudes are extremely small (Table 6). It is likely that these significant correlations are not physically meaningful. For the correlations between the teleconnection patterns and PC 3 for each variable, only five significant correlations are observed (Table 7). These occur between the AO and MYI, the NAO and SAT, the NAO and MYI, the PE and 850hPa air temperatures, and the PE and wind direction (Table 7). In these cases, the correlations are again very small.

Table 5: Concurrent correlations between the teleconnection patterns and PC1. Shaded areas indicate correlations that were not significant at the 95% confidence level.

	AO		NAO		PNA		EAWR		EA		EANP		PE	
	p-value	r	p-value	r	p-value	r	p-value	r	p-value	r	p-value	r	p-value	r
850hPa Air Temp							0.003	0.147						
700hPa Air Temp							0.002	0.152						
500hPa Air Temp							0.002	-0.155	0.022	0.114				
300hPa Air Temp									0.022	-0.114				
850hPa GPH													0.015	-0.121
700hPa GPH													0.011	0.126
500hPa GPH							0.091	-0.084					0.018	-0.117
300hPa GPH							0.026	-0.110	0.042	0.101			0.033	-0.106
SLP													0.032	-0.106
Wind Speed									0.011	-0.126				
Wind Direction														
FDD							0.020	-0.116						
TDD							0.049	0.098						
SAT							0.014	0.121						
Total Ice							0.016	0.119						
Multiyear Ice	0.004	0.143	0.010	0.129			0.001	0.164					0.004	0.142

Table 6: Concurrent correlations between the teleconnection patterns and PC2. Shaded areas indicate correlations that were not significant at the 95% confidence level.

	AO		NAO		PNA		EAWR		EA		EANP		PE	
	p-value	r	p-value	r	p-value	r	p-value	r	p-value	r	p-value	r	p-value	r
850hPa Air Temp														
700hPa Air Temp														
500hPa Air Temp														
300hPa Air Temp														
850hPa GPH														
700hPa GPH														
500hPa GPH														
300hPa GPH														
SLP													0.009	-0.130
Wind Speed									0.021	-0.115				
Wind Direction														
FDD														
TDD														
SAT														
Total Ice									0.048	0.098				
Multiyear Ice														

Table 7: Concurrent correlations between the teleconnection patterns and PC3. Shaded areas indicate correlations that were not significant at the 95% confidence level.

	AO		NAO		PNA		EAWR		EA		EANP		PE	
	p-value	r	p-value	r	p-value	r	p-value	r	p-value	r	p-value	r	p-value	r
850hPa Air Temp														
700hPa Air Temp														
500hPa Air Temp														
300hPa Air Temp														
850hPa GPH													0.042	-0.101
700hPa GPH														
500hPa GPH														
300hPa GPH														
SLP														
Wind Speed														
Wind Direction													0.001	0.162
FDD														
TDD														
SAT			0.003	-0.150										
Total Ice														
Multiyear Ice	0.045	0.101	0.001	0.160										

III.5.3.2.1 Lag Correlations for PC 1

The significant lag correlations for select months for PCs 1 are provided in Table 8. For PC1, large numbers of significant correlations are observed for the 1 and 2 month lags. For the 1-month lag, the largest number of significant correlations is observed for the EAWR, although these correlations are very small. The largest number of significant correlations occurs at the 2-month lag. For this lag, the significant correlations are found between many predictor variables and each of the teleconnections (excluding the EANP index), and these correlations are stronger than for any other lags. Significant correlations are evident between the NAO and every predictor, and these correlations are the strongest of all the lags. Many significant correlations are also observed between the

Table 8: Significant correlations for PC1 during the 1-month and 2-month lags.

1 Month Lag	p-value	r	2 Month Lag	p-value	r
AO and MYI	0.004	0.146	AO and MYI	0.003	0.150
NAO and TI	0.003	0.147	NAO and 850hPa Air Temp	0.000	0.260
NAO and MYI	0.000	0.173	NAO and 700hPa Air Temp	0.000	0.244
EAWR and 850hPa Air Temp	0.003	0.147	NAO and 500hPa Air Temp	0.000	-0.257
EAWR and 700hPa Air Temp	0.002	0.152	NAO and 300hPa Air Temp	0.000	0.225
EAWR and 500hPa Air Temp	0.002	-0.155	NAO and 850hPa GPH	0.000	-0.331
EAWR and Wind Speed	0.026	-0.110	NAO and 700hPa GPH	0.000	0.351
EAWR and FDD	0.020	-0.116	NAO and 500hPa GPH	0.000	-0.344
EAWR and TDD	0.049	0.098	NAO and 300hPa GPH	0.000	-0.343
EAWR and SAT	0.014	0.121	NAO and SLP	0.000	-0.267
EAWR and TI	0.016	0.119	NAO and Wind Speed	0.000	0.266
EAWR and MYI	0.001	0.164	NAO and Wind Direction	0.001	-0.169
EA and 500hPa Air Temp	0.022	0.114	NAO and FDD	0.000	-0.248
EA and 300hPa Air Temp	0.022	-0.114	NAO and TDD	0.009	0.130
EA and 300Pa GPH	0.042	0.101	NAO and SAT	0.000	0.224
EA and Wind Speed	0.011	-0.126	NAO and Total Ice	0.000	0.230
PE and 850hPa GPH	0.015	-0.121	NAO and Multiyear Ice	0.000	0.186
PE and 700hPa GPH	0.011	0.126	PNA and 850hPa Air Temp	0.000	-0.365
PE and 500hPa GPH	0.018	-0.117	PNA and 700hPa Air Temp	0.000	-0.396
PE and 300hPa GPH	0.033	-0.106	PNA and 500hPa Air Temp	0.000	0.335
PE and SLP	0.032	-0.106	PNA and 300hPa Air Temp	0.021	-0.114
			PNA and 850hPa GPH	0.005	0.138
			PNA and 700hPa GPH	0.000	-0.243
			PNA and 500hPa GPH	0.000	0.305
			PNA and 300hPa GPH	0.000	0.314
			PNA and Wind Speed	0.039	-0.102
			PNA and FDD	0.000	0.367
			PNA and TDD	0.000	-0.201
			PNA and SAT	0.000	-0.214
			EAWR and 850hPa Air Temp	0.000	0.210
			EAWR and 700hPa Air Temp	0.000	0.193
			EAWR and 500hPa Air Temp	0.000	-0.190
			EAWR and 300hPa Air Temp	0.002	0.156
			EAWR and 850hPa GPH	0.000	-0.212
			EAWR and 700hPa GPH	0.000	0.236
			EAWR and 500hPa GPH	0.000	-0.234
			EAWR and 300hPa GPH	0.000	-0.229
			EAWR and SLP	0.006	-0.135
			EAWR and FDD	0.000	-0.179
			EAWR and TDD	0.004	0.141
			EAWR and SAT	0.000	0.215
			EAWR and Total Ice	0.002	0.153
			EAWR and Multiyear Ice	0.000	0.177
			PE and 300hPa Air Temp	0.021	0.114
			PE and 850hPa GPH	0.005	-0.139
			PE and 700hPa GPH	0.021	0.114
			PE and 500hPa GPH	0.045	-0.099
			PE and 300hPa GPH	0.035	-0.105
			PE and SLP	0.000	-0.179
			PE and Wind Direction	0.000	0.346
			PE and MYI	0.014	0.122

PNA and many of the predictor variables, and these correlations are again strongest at this 2-month lag. The same is true for the EAWR teleconnection pattern, which shows the strongest significant correlations with nearly all of the predictor variables during the 2-month lag. The PE teleconnection pattern has the most significant correlations (when compared to the other lags), but does not show as many significant correlations as the NAO, PNA, or EAWR.

Beginning with the 3-month lag, only few significant correlations occur and they are very weak. Generally, if correlations are significant, they only appear for one or two predictor variables and are not consistent between the lags. For example, a significant correlation may be observed between the PE pattern and wind speed at the 3-month lag, but not at any other lag. This indicates that these significant correlations are most likely spurious and do not have a physical relationship. One exception may be MYI, which is significantly correlated with the AO, NAO, and EAWR teleconnection patterns at many of the lags (Table 9). This suggests that MYI may be linked to these teleconnection indices.

The 12-month lag has many significant correlations between the AO and the predictor PCs and the correlations are generally strong (Table 10). This indicates that although strong significant correlations are not evident for the AO at the other lags, the AO may have an influence on the predictor variables at longer lag times. This follows the expected relationship between the AO and sea ice that has been discovered previously, where the wintertime AO pattern was significantly correlated with SAT and sea ice concentration throughout the following year (Parkinson 2008, Rigor et al. 2002).

Table 9: Significant correlations for MYI between PC1 and AO, NAO, and EAWR. Shaded areas indicate correlations that are not significant at the 95% confidence level.

	AO		NAO		EAWR	
	p-value	r	p-value	r	p-value	r
1 Month	0.004	0.146	0.000	0.173	0.001	0.164
2 Month	0.003	0.150	0.000	0.186	0.000	0.177
3 Month	0.002	0.157	0.000	0.202	0.000	0.181
4 Month	0.002	0.152	0.000	0.194	0.000	0.172
5 Month	0.002	0.156	0.000	0.182	0.002	0.154
6 Month	0.002	0.153	0.000	0.184	0.004	0.142
7 Month	0.003	0.150	0.001	0.170	0.006	0.135
8 Month	0.002	0.157	0.002	0.154	0.032	0.106
9 Month	0.001	0.166	0.011	0.126		
10 Month	0.001	0.160	0.015	0.120		
11 Month	0.000	0.172	0.012	0.125		
12 Month	0.000	0.176	0.010	0.128		

Table 10: Significant correlations between the teleconnection indices and PC1 for the 12-month lag.

12 Month Lag	p-value	r
AO and 850hPa Air Temp	0.000	0.260
AO and 700hPa Air Temp	0.000	0.270
AO and 500hPa Air Temp	0.000	-0.294
AO and 300hPa Air Temp	0.000	0.342
AO and 850hPa GPH	0.000	-0.495
AO and 700hPa GPH	0.000	0.495
AO and 500hPa GPH	0.000	-0.467
AO and 300hPa GPH	0.000	-0.459
AO and SLP	0.000	-0.471
AO and Wind Speed	0.000	0.203
AO and Wind Direction	0.042	0.101
AO and FDD	0.000	-0.247
AO and TDD	0.011	0.126
AO and SAT	0.007	0.132
AO and Total Ice	0.004	0.143
AO and Multiyear Ice	0.000	0.176
NAO and TI	0.030	0.107
NAO and MYI	0.010	0.128
PNA and TI	0.019	-0.116
PE and 850hPa GPH	0.024	-0.112
PE and SLP	0.010	-0.127

III.5.3.2.2 Lag Correlations for PC 2

As with PC 1, the largest number of significant correlations is observed at the 2-month lag (Table 11). At this lag, the correlations are also strongest, although not as strong as for PC 1 (Table 8). Additionally, fewer significant correlations are observed for PCs 2 when compared to PCs 1. Among the lags there appears to be no consistency to the significant correlations. This means that the same correlations are not observed at multiple lags. Unlike PC 1, no consistent significant correlations with MYI are observed at different lags.

Because the second PC represents an appreciably smaller amount of the total variance in each of the predictor variables (Table 4), it is expected that fewer significant correlations are observed. The lack of consistency and fewer correlations indicates that PC 2 may not be useful for identifying the large-scale patterns influencing each of the predictor variables.

III.5.3.2.3 Lag Correlations for PC 3

The significant lag correlations between the teleconnection patterns and PC 3 for each variable for the first two lags are displayed in Table 12. For PCs 3, only a very small number of significant correlations occur at each lag, and none at the 9-month lag. Unlike PC 1 and PC 2, the largest number of significant correlations is not observed during the 2-month lag, but at 6 months. The significant correlations are very weak (Table 12) with no consistency across multiple lags. Because these correlations are so weak and inconsistent, they likely do not explain any physical relationships.

Table 11: Significant correlations for PC2 during the 1-month and 2-month lags.

1 Month Lag	p-value	r	2 Month Lag	p-value	r
NAO and 700hPa GPH	0.003	0.149	AO and Wind Speed	0.045	0.101
NAO and 500hPaGPH	0.004	0.141	NAO and 300hPa Air Temp	0.077	-0.088
NAO and 300hPa GPH	0.036	0.104	NAO and 850hPa GPH	0.000	0.212
NAO and SLP	0.002	-0.150	NAO and 700hPa GPH	0.000	0.172
EA and Wind Speed	0.021	-0.115	NAO and 500hPa GPH	0.035	0.104
EA and TI	0.048	0.098	NAO and SLP	0.000	-0.241
PE and SLP	0.009	-0.130	PNA and 850hPa Air Temp	0.000	0.220
			PNA and 700hPa Air Temp	0.000	-0.240
			PNA and 500hPa Air Temp	0.000	0.252
			PNA and 850hPa GPH	0.000	-0.293
			PNA and 700hPa GPH	0.009	-0.129
			PNA and 300hPa GPH	0.001	-0.162
			PNA and SLP	0.000	0.392
			PNA and FDD	0.002	-0.154
			PNA and SAT	0.000	0.309
			EA and 300hPa Air Temp	0.021	0.115
			EA and FDD	0.006	-0.136
			EA and TI	0.049	0.098
			PE and 850hPa Air Temp	0.007	0.133
			PE and 700hPa Air Temp	0.009	-0.129
			PE and 500hPa Air Temp	0.014	0.122
			PE and 300hPa Air Temp	0.020	-0.115
			PE and 850hPa GPH	0.000	0.238
			PE and 700hPa GPH	0.000	0.272
			PE and 500hPa GPH	0.000	0.279
			PE and 300hPa GPH	0.000	-0.258
			PE and SLP	0.000	-0.194
			PE and Wind Direction	0.000	-0.206
			PE and FDD	0.009	-0.129

Table 12: Significant correlations for PC3 during the 1-month and 2-month lags.

1 Month Lag	p-value	r	2 Month Lag	p-value	r
NAO and 500hPa GPh	0.029	-0.108	NAO and 500hPa Air Temp	0.003	0.148
NAO and 300hPa GPH	0.004	-0.142	NAO and 850hPa GPH	0.000	-0.240
NAO and Wind Speed	0.012	0.125	NAO and 700hPa GPH	0.000	-0.209
PNA and FDD	0.037	0.104	NAO and 500hPa GPH	0.000	-0.223
PNA and TI	0.047	0.099	NAO and 300hPa GPH	0.000	-0.254
PE and 850hPa GPH	0.042	-0.101	NAO and SLP	0.000	-0.246
PE and Wind Direction	0.001	0.162	NAO and Wind Speed	0.000	0.257
			NAO and TI	0.046	0.099
			EAWR and 850hPa GPH	0.012	-0.125
			EAWR and SLP	0.022	-0.113
			PE and 850hPa GPH	0.000	0.243
			PE and 700hPa GPH	0.002	0.151
			PE and SLP	0.000	0.258

Overall, the third PC only represents a very small proportion of the total variance in each of the predictor variables, so it is not surprising that only a few weak correlations are found. As for PC 2, the lack of strong significant correlations suggests that these PCs are not useful in characterizing the possible influence of the teleconnection patterns on the predictor variables.

III.5.3.3 Discussion

This analysis has shown that PCA can be used to represent the dominant patterns of variability for each of the predictor variables and that the information is useful in identifying the overall large-scale relationships for each of these variables. The main conclusions are detailed below:

1. Because PC 1 represents the dominant pattern of variability in each of the predictor variables, this PC is the most useful in identifying the teleconnection

patterns that may be driving the spatial distributions of each variable. PCs 2 and 3 represent only a small amount of the total variance in the predictor variables and therefore do not provide any useful information regarding the large-scale relationships to the teleconnection patterns.

2. Few significant correlations are observed at the concurrent lag. This suggests that if any relationship is present between the predictor variables and the teleconnection patterns, there is some amount of lag time present. The characteristics of the teleconnection patterns thus take some amount of time to exert any appreciable influence on the variables in the Beaufort Sea region.
3. Of the lagged correlations, the 2-month lag had the most and the strongest significant correlations. At this lag, many significant correlations are observed for the NAO, PNA, and EAWR teleconnection patterns. Because of the many strong significant correlations, this 2-month lag is useful and important in identifying important teleconnection relationships.
4. In addition to the 2-month lag, strong significant correlations between the AO and each of the predictor variables are observed at the 12-month lag. This suggests that there may be a relationship between the AO and the predictor variables, but that the variables take a longer time to express a response to the AO. The strong correlations at the 12-month lag suggest that there may be some predictive information a year in advance.

5. No significant correlations are observed for the EANP teleconnection pattern, which indicates that this pattern does not have an influence on the Beaufort Sea region.
6. Of the predictor variables, only MYI has a consistent relationship with the teleconnection indices at many of the lags. MYI is significantly correlated with the AO, NAO, and EAWR at the concurrent and almost every other lag. This suggests that these three teleconnections do have some relationship with MYI and could be driving the changes observed in ice ages in the Beaufort Sea region.

For the AO, a negative phase, characterized by high pressure in the Arctic and low pressure in the midlatitudes, typically brings warm conditions to the high latitudes (Wallace and Gutzler 1981). The positive phase, on the other hand, is typically associated with the northern movement of storm tracks, which contributes to wetter conditions in Alaska, Scotland, and Scandinavia and drier conditions in the western United States and the Mediterranean (Wallace and Gutzler 1981). The positive phase is also associated with lower air temperatures in the Arctic (Wallace and Gutzler 1981). It is possible that because significant correlations between the predictor variables and the AO during the 12-month lag are present, the conditions and phase of the AO may be driving temperature changes in the Beaufort Sea region. The positive phase of the AO would be associated with colder air in the Arctic, and therefore would lead to more expansive sea ice in the Beaufort Sea.

The phase of the NAO is associated with changes in the intensity and location of the North Atlantic jet steam and storm track, and therefore could provide important

information about available moisture and air temperatures in the Arctic (Wallace and Gutzler 1981). The positive phase of the NAO brings lower air temperatures to the Canadian Arctic Archipelago, while bringing warmer and wetter air to Europe (Wallace and Gutzler 1981). The negative phase is associated with the opposite temperature pattern. The presence of significant correlations with the NAO at the 2-month lag indicates that the phase of the NAO could be useful in predicting the atmospheric conditions in the Beaufort Sea two months in advance. When the positive phase of the NAO is present, it is expected that colder air could be advected into the Beaufort Sea region. This would ultimately allow for more sea ice growth in the region.

The EAWR pattern is one of the main teleconnection patterns that influences the air temperature and precipitation patterns over Eurasia. During its positive phase, above-average temperatures are observed over eastern Asia and below-average temperatures are observed over western Russia (Barnston and Livezey 1987). Associated with this is above-average precipitation in eastern China and below-average precipitation in central Europe (Barnston and Livezey 1987). It is possible that during its positive phase, the warm air located over eastern Asia is advected into the Arctic and specifically the Beaufort Sea region, causing the enhanced melt of sea ice.

The positive phase of the PNA is associated with positive geopotential height anomalies over the western United States and negative geopotential height anomalies over the eastern United States (Wallace and Gutzler 1981). This results in the southward movement of cold air from the Arctic into the midlatitudes, ultimately creating below normal air temperatures in the eastern United States and above normal temperatures in

the western United States (Wallace and Gutzler 1981). The negative phase is associated with troughing over the western United States, which causes below average temperatures in the west and above average temperatures in the east (Wallace and Gutzler 1981). During the negative phase, if the ridge over the western United States extends far enough northward, above average air temperatures would be expected in the Beaufort Sea region. This would be associated with a smaller sea ice extent.

Overall, the teleconnection patterns that show the largest number of significant correlations and therefore have the largest influence on the predictor variables are the NAO, PNA, and EAWR teleconnection patterns at a 2-month lag and the AO at a 12-month lag. It is likely that each of the teleconnections has some influence on the predictor variables and the overall characteristics of the atmospheric patterns observed in the Beaufort Sea. This analysis suggests that these teleconnection patterns most likely interact to influence the predictor variables and that no one pattern can be identified as driving any specific predictor variables.

III.6 Conclusions

III.6.1 Part 1: Composite Analysis

Of the 16 predictor variables, the upper atmospheric air temperatures, surface air temperatures (monthly means, FDD, and TDD), SLP, TI, and MYI all appear to show consistent and significant differences between the heavy ice and light ice years based on the monthly analysis. This indicates that these variables will most likely have the most utility in predicting the summer minimum sea ice conditions in the Beaufort Sea. For the upper atmospheric air temperatures, the magnitude and number of grid cells with

significant differences decreased with height, with the most significant differences occurring at the 850 hPa pressure level. The three pressure levels closest to the surface (850, 700, and 500 hPa) showed consistent, significant differences throughout the year. Differences at the 300 hPa pressure level showed a different pattern with fewer significantly different grid cells, which may indicate that this pressure level is too far from the surface to have an appreciable predictive ability. The surface temperature variables, including monthly mean air temperatures, FDD, and TDD, all showed significant differences between the light ice and heavy ice years and these differences were consistent throughout the year. For SLP, the expected pattern of differences was observed throughout the year, with the largest and most significant differences during the summer months. This follows the patterns of the surface temperature variables. Lastly, TI and MYI experienced significant differences throughout the year with the most differences occurring during September when the minimum sea ice extent is reached. Because all of these variables show significant differences throughout the year preceding heavy ice and light ice events, they will most likely have the greatest contributions to more accurate sea ice forecasts.

The remaining predictor variables—including the four levels' geopotential heights, wind speed, and wind direction—do not exhibit consistent patterns throughout the year and do not have many significant differences between the heavy ice and light ice years. For the geopotential heights, it is possible that the patterns preceding heavy ice and light ice years occur at a larger scales and therefore cannot be observed for this small study region. The wind speed and direction are known to drive sea ice transport in

the Beaufort Sea region, but it is likely that the wind conditions from year to year are too different and even though the wind characteristics are important, no typical mean pattern can be used for statistical forecasts. A case study approach would most likely show that the wind patterns do have some influence on sea ice extent.

III.6.2 Part 2: Teleconnections

The monthly relationships indicate that the most important teleconnection patterns influencing the predictor variables in the Beaufort Sea region are the AO, NAO, PNA, and EPNP patterns. These four indices showed strong, significant correlations throughout the year for nearly every predictor variable (excluding wind speed and direction). This indicates that these teleconnection patterns have some relationship with the atmospheric and surface conditions in the Beaufort Sea region and therefore will most likely have some predictive ability. The EAWR teleconnection pattern did show large spatial patterns of significant correlations with the geopotential height variables, which indicates that this teleconnection may also have some predictive ability, at least in informing the geopotential height characteristics in the region.

For the antecedent ice conditions (TI and MYI), only the AO, NAO, and PNA showed large areas of significant correlations throughout the year. Because these two variables represent the conditions of the sea ice itself, it is possible that these three teleconnection indices are the most important for understanding the conditions of the sea ice and for predicting the minimum sea ice extent.

The remaining teleconnection indices, including the SOI, Niño 3.4, EA, PE, and WP, do not show any consistent patterns of significant correlations for any of the

predictor variables. This indicates that these teleconnection patterns most likely do not have any direct relationship with the Beaufort Sea region and therefore will not provide any useful information for improving statistical forecasts of sea ice in the region.

III.6.3 Part 3: Long-Term Teleconnection Relationships

The purpose of section 3.5.3 was to further identify the large-scale atmospheric teleconnection patterns that have the strongest influence on each of the predictor variables in the Beaufort Sea region. A better understanding of the large-scale drivers of these predictor variables will provide more accurate forecasts of sea ice conditions in the region. Of the teleconnection patterns investigated, the NAO, PNA, EAWR, and AO all show some relationship to each of the predictor variables. The NAO, PNA, and EAWR have the strongest correlations and are therefore the most influential at the 2-month lag, while the AO has the strongest relationship at the 12-month lag. The only variable that has a relationship with the teleconnections at most lags is MYI, which correlates significantly with the AO, NAO, and EAWR teleconnection patterns. Although the EPNP pattern appeared as a possible significant teleconnection in the analysis from section 3.5.2, it does not show up in section 3.5.3. The EPNP pattern is very weak during December, when it is no longer the leading mode of variability. Because it is so weak during this month, perhaps including December in the analysis diminished the correlations based on the yearly relationships. It is possible that the EPNP pattern does have a strong relationship with the predictor variables during many months of the year (as shown in section 3.5.2), but does not have an overall relationship with the variables over the entire time series (as shown in section 3.5.3).

Overall, these teleconnection patterns are expected to interact to drive the overall atmospheric and surface conditions in the Beaufort Sea region. Teasing out the influence of one single teleconnection pattern for each predictor variable is therefore difficult.

III.6.4 Final Conclusions

Generally, it is clear that some of the predictor variables will have predictive ability in the statistical forecast models. These variables include upper atmospheric air temperatures at 850 hPa, 700 hPa, and 500 hPa, monthly mean surface air temperatures, FDD, TDD, SLP, TI, and MYI. Wind speed, wind direction, and the geopotential heights may not provide any useful predictive information. Of the teleconnections, the AO, NAO, and PNA have the strongest relationships with the predictor variables and therefore will most likely have the greatest contributions to the forecast models. The EAWR and EPNP patterns do have some significant relationships with the predictor variables, and may also have some predictive ability, at least during select months.

CHAPTER IV

PREDICTING SEPTEMBER SEA ICE EXTENT

IV.1 Introduction

Statistical forecast models predicting the minimum sea ice extent in the Beaufort Sea have varying levels of precision, with better predictions at shorter lead time before the September minimum ice extent is reached. While more accurate predictions can be made using data from the previous spring and summer, fairly accurate predictions are possible up to a year in advance, using data from the previous October (Barnett 1980, Walsh 1980, Drobot and Maslanik 2003, Drobot 2003, Drobot 2007, Lindsay et al. 2008, Drobot et al. 2009). These previous studies, in general, have utilized multiple linear regression (MLR) to create forecast models using information about the atmosphere and the conditions of the sea ice itself as inputs.

Drobot and Maslanik (2003) used MLR, starting in October and going through July, to predict summer sea ice conditions using the Barnett Severity Index (BSI). In all months, at least three predictors are utilized in the final forecast models, with useful variables from the previous months carried over for subsequent models. For example, if MYI was retained as a useful predictor in the October model, this variable was retained for the November model. Of these models, the least exact forecasts came from the October model ($R^2 = 0.74$), with the fit of the models increasing every month through July ($R^2 = 0.92$). For the October model, TI, MYI, and the EA are retained. In the subsequent models, both October TI and October EA remain in every model, while MYI

is replaced by the MYI data for each individual month. During March, the NAO is added as a predictor, while FDD is added for the July model.

Drobot (2007) applied MLR to predict the minimum sea ice extent in the Beaufort Sea using seasonally averaged input data for spring and summer. The final regression equations included one to three input predictors. As with the previous study (Drobot and Maslanik 2003), the variables from the spring model were carried over as inputs into the summer model. During spring, MYI was the only predictor in the model, with an R^2 value of 0.52. Better predictive ability is observed for the summer model (R^2 = 0.80), which included spring MYI, summer surface albedo, and summer TI. When compared to climatology, the spring model provides a 33% increase in predictive ability, while the summer model provides a 55% increase.

Lindsay et al. (2008) create monthly statistical models using MLR to predict the Arctic-wide minimum sea ice extent. Once again, they find that the most truthful predictions are based on spring and summer data, while predictions made using data from fall and winter are slightly less precise. For each forecast model, two input variables are retained. The least correct predictions are made during October (R^2 = 0.81), which are based on ocean temperature data and the NAO. From November through March, ocean temperature and the AO are retained. April includes ocean temperature data as well as the Pacific Decadal Oscillation (PDO), while May and June retain ocean temperature data and ice fraction. The models created for July, August, and September are based on ice concentration and either the NAO (July and August) or the PDO

(September). The most precise model is created for August, which has an R^2 value of 0.95.

Drobot et al. (2009) construct forecast models predicting the opening date of the Prudhoe Bay shipping season. Based on ordinal regression, they predict whether the opening date will be early, normal, or late. Ultimately, Drobot et al. (2009) create a statistical model using the mean sea ice concentration in the Bering Sea during April, the average accumulated FDD, and the frequency of the occurrence of self-organizing map (SOM) patterns depicting the SLP characteristics of the region. Their final model retains sea ice concentration and FDD, with a correct prediction of either an early, normal, or late opening date 60 percent of the time.

Overall, these previous models have found that the summer sea ice conditions in the Beaufort Sea can be forecast with some truth using both atmospheric data and sea ice concentration data. These previous models, however, are limited by their choices of input data (such as including only a few predictive variables to input) as well as their decisions on how to represent this input data (such as averaging the conditions of a variable over the entire study region or using data from only one grid cell to represent the conditions over the region) (Drobot and Maslanik 2003, Drobot 2007, Lindsay et al. 2008, Drobot et al. 2009). These choices can act to either inflate or lessen the fit of the model results.

IV.1.1 Limitations of Statistical Forecasts of Sea Ice Extent

Although linear forecast models of sea ice extent in the Arctic are useful in understanding the yearly conditions of Arctic sea ice, there are some uncertainties that

limit their forecasting ability. First, the fit of these models is dependent on our understanding of the complex interactions between sea ice and many atmospheric processes at differing scales (National Research Council 2012, Lemke et al. 2007). Although our knowledge of the drivers of changes in sea ice has progressed in recent years, there is still a large amount of uncertainty. Without a complete understanding of the complex interactions between sea ice, the ocean, and the atmosphere, seasonal forecast models cannot be entirely accurate (National Research Council 2012, Stroeve et al. 2011, Maslanik et al. 2007b).

Second, a regime shift in the character of sea ice in the Arctic may change the known relationships between sea ice conditions and atmospheric predictor variables. In recent years, the proportion of thinner first year ice present in the spring has increased, from 38% in the early and mid-1980s, to 52% by the spring of 1996 (Fowler et al. 2004, Maslanik et al. 2007b, Stroeve et al. 2011). This increase in first year ice is accompanied by a decrease in the proportion of thicker and more stable multiyear ice. This regime shift from predominately multiyear ice to predominately first year ice may limit the predictive ability of known climatic variables (National Research Council 2012, Maslanik et al. 2007b, Stroeve et al. 2007). It is likely that this thinner first year ice coverage will have different relationships with predictor variables than the relationships observed with the thicker multiyear ice.

Third, many positive feedback trends will become more important as the amount of sea ice present during the summer months continues to decrease. Of great importance is the ice-albedo feedback. As a smaller amount of sea ice is present in the summer,

more dark ocean water is exposed. This water absorbs a large amount of solar radiation, which heats the ocean surface and initiates further melt of sea ice. The observed downward trend of sea ice extent can be in part attributed to this ice–albedo feedback (Perovich et al. 2007, Lindsay and Zhang 2005). As the ice pack becomes thinner, this feedback mechanism will become even more important in accelerating sea ice loss (Stroeve et al. 2011).

Fourth, with large decreases in sea ice extent observed beginning in the 1990s, it is possible that a shift has occurred and that the sea ice dataset no longer shows a decreasing linear trend (Stroeve et al. 2011). The sea ice data before and after this shift exhibit differing linear patterns. Therefore, using the entire record of data (back to 1979) in creating a forecast model may limit the models' predictive ability. With observed changes in the character of the Arctic sea ice since the 1990s, it is possible that the statistical relationships between sea ice and the predictor variables are changing (Holland and Stroeve 2011). Both Maslanik et al. (2007b) and Holland and Stroeve (2011) suggests that the usefulness of the predictive relationship between AO and summer sea ice extent may be decreasing over time.

Lastly, processes associated with AA are relatively unknown. It is possible that more pronounced AA will have unknown impacts on the climate system. Our predictive ability relies on knowledge of the interactions between sea ice and predictor variables in our current climate system. If AA brings unexpected changes, our ability to accurately predict sea ice extent based on our current knowledge may decrease drastically (Serreze and Francis 2006, Serreze et al. 2011).

Although limitations to this forecasting approach do exist, a comprehensive study is needed to accurately reflect our knowledge of the existing relationships between sea ice and atmospheric predictor variables. This study aims to improve existing statistical forecast models by including a greater number of input parameters as well as representing these input variables in a less biased way using Principal Component Analysis (PCA). It will provide information regarding changes that have occurred in our predictive ability using the most up to date data available.

IV.2 Study Region

The extent of the Beaufort Sea is defined using the limits outlined by the IHO (1953). Details on the exact coordinates used can be found in the Study Area section of chapter II. These coordinates are used to calculate the extent of the Beaufort Sea minimum sea ice extent, which serves as the dependent variable for all statistical models created for this chapter.

The Arctic-wide extents of the 16 atmospheric predictor variables are utilized to represent the character of the entire Arctic. In this study, the Arctic is defined as the region above 60°N. This differs from the smaller study area used to explore these variables in Chapter III. In Chapter III, each variable was investigated over the smaller study region to explore the atmospheric conditions of the Beaufort Sea region and to inform decisions about variable selection for the subsequent statistical models. Because these predictor variables represent aspects of the climate system that interact and vary over large distances, it is important to include a larger study area in this chapter to incorporate these changes and their potential influences on the Beaufort Sea region.

Although there is no accepted definition of the Arctic, the region is typically defined as the region north of 66.5°N (north of the Arctic Circle) (Serreze and Barry 2005). For this study, interactions between the Arctic and the surrounding land area to the south are important for understanding the larger scale patterns that are driving changes in the Beaufort Sea minimum sea ice extent. For this reason, the study area utilized for this chapter is extended farther south, to 60°N.

IV.3 Data

The data used for Chapter IV comes from a combination of data assembled either in Chapter II or Chapter III. From Chapter II, the Beaufort Sea minimum ice extent (BS) will be utilized to quantify the September minimum sea ice conditions in the study region. This ice extent is calculated using daily sea ice concentration data from the NSIDC Sea Ice Concentrations from Nimbus-7 Scanning Multichannel Microwave Radiometer (SMMR) and Defense Meteorological Satellite Program (DMSP) -F8, -F11 and -F13 Special Sensor Microwave/Imagers (SSM/Is), and the DMSP-F17 Special Sensor Microwave Imager/Sounder (SSMIS) Passive Microwave Dataset for 1980 through 2012 (Cavalieri et al. 1996). See the data section of Chapter II for more details.

The 16 atmospheric predictor variables described in detail in Chapter III are also used here: 850, 700, 500, and 300 hPa air temperature and geopotential height, 2-meter SAT, SLP, wind speed, wind direction, FDD, and TDD, which are obtained or calculated from the NCEP/DOE Reanalysis 2 dataset. Of the two remaining predictor variables, TI is obtained from the NSIDC Sea Ice Concentration dataset, while the MYI dataset is

obtained through personal communication with Drs. James Maslanik and Mark Tschudi. See the data section of Chapter III for more details.

Along with the 16 atmospheric predictor variables, data for 10 teleconnection indices are also employed as predictors. These teleconnections include the AO, NAO, PNA, EA, EAWR, EPNP, PE, WP, the SOI, and the Niño 3.4 index. The AO index is obtained from the website maintained by Dr. David J. W. Thompson (http://jisao.washington.edu/data/annularmodes/Data/ao_index.html). Indices for the nine remaining teleconnections are obtained from the NOAA CPC (http://www.cpc.ncep.noaa.gov/data/teledoc/telecontents.shtml). See the data section of Chapter III for more detailed information regarding these datasets.

IV.4 Methods

IV.4.1 Part 1: Principal Component Analysis

To create statistical models, one value for each year is needed for each predictor variable as an input. Because each predictor variable includes data over a large spatial area, PCA is used as a data-reduction technique. Once PCA is performed for each predictor variable in each month (October through August), the spatial loading patterns of the most significant PCs are examined. The spatial pattern of each PC will be compared to the map analysis performed in Chapter III to determine which PC most accurately reflects the most important mode of variability for each predictor variable.

IV.4.2 Part 2: Stepwise Linear Regression

Stepwise linear regression (SLR) is used to assess the predictability of the Beaufort Sea September minimum sea ice extent over the study period from 1980 to

2012 for each predictor month (October through August). Both forward and backward selection methods of SLR are used. Forward selection involves starting with no variables in the model and then testing the addition of each variable by adding the variable that improves the model most until some critical threshold is reached. Backward elimination involves starting with all candidate variables and then testing the deletion of each variable. The results from these two methods are then compared for feasibility and model fit based on results from Chapter III.

To avoid over-fitting the linear regression models, input variables are tested for multicollinearity. Over-fitting can occur when too many variables are used as inputs, and the resulting models therefore do not accurately reflect the actual predictive ability of the variables. Multicollinearity occurs when two input variables are highly correlated with one another. When two collinear variables are used as model inputs, the resulting model could produce inflated results, where the model results appear better than the real predictive ability of the variables because two variables representing the same information are utilized. The collinearity of the input variables is tested using the variance inflation factor (VIF). This index provides information on how much the variance of the model parameters is influenced by collinearity in the retained variables. In general, a VIF value near or slightly above 1 suggests that multicollinearity is negligible, while a VIF value greater than five indicates that there is a large influence from multicollinearity (Drobot and Maslanik 2003). When the VIF of a variable retained in the models is large, this variable is removed and the model is recreated without this variable as an input. Over-fitting of the models can also be observed in the model

outputs, where adding variables to the model only improves the model performance incrementally. To reduce over-fitting the models, output variables are systematically removed and the resulting models are compared.

IV.4.3 Part 3: Classification and Regression Trees (CART)

In addition to the SLR models, CART models are created for each predictor month. A CART model partitions the input predictor variables into similar groups, and then makes a categorical prediction of sea ice extent using the terminal nodes of these groups (Breiman et al. 1984). The advantages of CART models are that multicollinearity is not an issue (Breiman et al. 1084). Additionally, CART models provide information about the relative importance of each predictor variable in predicting sea ice extent, which is difficult to ascertain with SLR models. For each forecast month, a regression tree is created. Each tree is pruned using the cross-validation method, where the number of splits in the final regression tree is chosen based on the cross-validation error associated with each split (Breiman et al. 1984, De'ath and Fabricius 2000). The tree containing splits that minimizes the cross-validation error is selected as the final regression tree for each month.

IV.5 Results

IV.5.1 Part 1: Principal Component Analysis

PCA was performed on each of the 16 atmospheric predictor variables for each predictor month and the loading patterns of the most significant PCs were examined to determine which PC most accurately reflected the most important mode of variability for each variable. If the eigenvalue for a PC was greater than one, then that PC was

considered. In most cases, the number of PCs selected using this method coincided with the number of PCs that would be selected using the scree plot for each variable.

The loading patterns for the first three PCs of the select predictor variables are depicted in Figure 35. For all 16 predictor variables, the loading pattern of the first PC showed a pattern similar to the distribution of sea ice in the Arctic, with the ice edge being represented by the observed changes in the loadings (Figure 35). The subsequent PCs each show a different spatial pattern of loadings. Because the loading pattern of the first PC appears to follow the average distribution of sea ice throughout the study period, this PC is selected for use as the model input for each predictor variable. The purpose of this research is to identify the influence of these predictor variables on sea ice extent, so this loading pattern represents the most ideal PC to use in creating the forecast models.

IV.5.2 Part 2: Stepwise Linear Regression

Both forward and backward selection methods of SLR are performed for each predictor month and the results of this analysis are provided in Tables 1 and 2. The fit of these models is assessed using R^2, the RMSE, and the MAE. For the coefficient of determination, a value closer to 1 indicates better agreement. For both the RMSE and the MAE, values closer to zero indicate better agreement. These two measures are dependent of the scale of the data, and are therefore presented in km^2. An assessment of the impact of multicollinearity in the models is provided using the VIF.

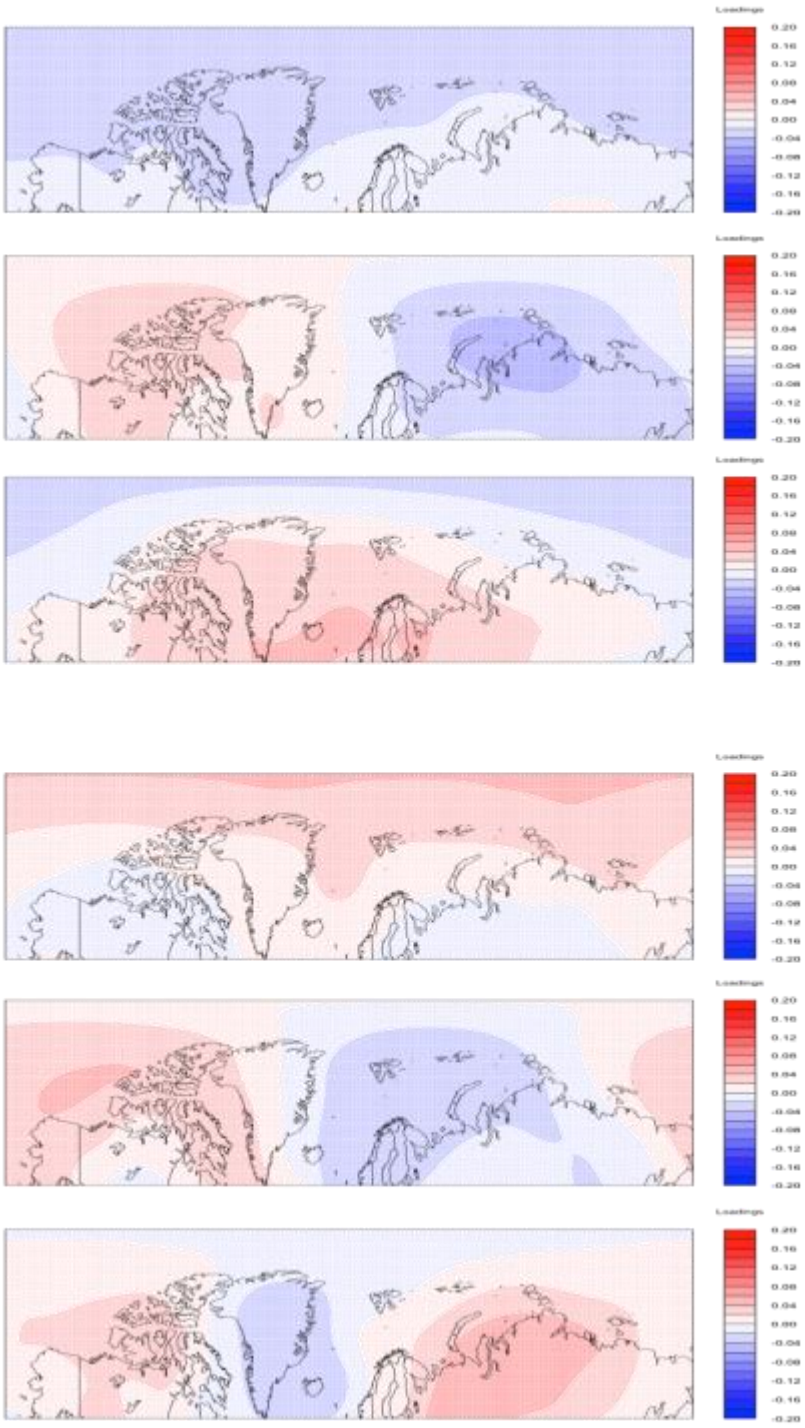

Figure 35: PC maps for PC1, PC2, and PC3 for 850 hPa geopotential height (top group) and 850 hPa air temperature (bottom group) during January.

For the forward method (Table 13), final models included between one and three predictor variables. In general, these models retained a combination of SAT, TI, and MYI, although EAWR, PNA, and 300 hPa air temperature do show up for some months. All models show VIFs close to 1, indicating that multicollinearity is not inflating the model results. Models for October, November, and December all include SAT, while models created for January, February, and March all include TI and MYI (Table 13). EAWR also appears in the final models for November and March. For April and May, only one variable is retained (Table 13). June includes three variables (SAT, TI, and PNA), while July only includes TI and 300 hPa air temperatures (Table 13). The final model, created for August, only includes TI (Table 13). Generally, the coefficient of determination increases as the lag time between the prediction month and the September minimum sea ice extent decreases. Only a few months (December and May) do not fit this general pattern (Table 13). These two months have significantly lower R^2 values, which can be attributed to the fact that they each retain only one predictor variable. Using the coefficient of determination, the most precise model is created in July (R^2 = 0.72). Overall, the RMSE values appear relatively steady (at around 90,000 km^2) until June (Table 13). Beginning in June, the RMSE values begin to decrease from 68,789 km^2 in June to 61,228 km^2 in August, indicating an increase in the fit of the model (Table 13). According to the RMSE, the most correct model is created in July, which has the lowest RMSE value of 59,482 km^2 (Table 13). The values of MAE show this same general pattern, with steady values in all models through May, and a decrease in values beginning in June (Table 13). As with the coefficient of determination and

Table 13: Results of the forward method SLR for each forecast month. RMSE and MAE percentage of minimum extent are the RMSE and MAE values for each month expressed as a percentage of the mean Beaufort Sea minimum sea ice extent of 254,231 km^2.

Month	Variables Retained	VIF	R^2	RMSE (km^2)	RMSE Percentage of Minimum Extent	MAE (km^2)	MAE Percentage of Minimum Extent
October	SAT	1.000	0.371	87,469	34	15,226	6
November	SAT	1.589	0.364	89,379	35	15,559	6
	EAWR	1.589					
December	SAT	1.000	0.190	99,277	39	17,282	7
January	TI	1.038	0.323	92,269	36	16,062	6
	MYI	1.038					
February	TI	0.988	0.302	93,689	37	16,309	6
	MYI	0.988					
March	EAWR	1.032	0.361	91,133	36	15,864	6
	TI	1.002					
	MYI	1.031					
April	SAT	1.000	0.334	90,011	35	15,669	6
May	MYI	1.000	0.134	102,634	40	17,866	7
June	SAT	1.276	0.636	68,789	27	11,975	5
	TI	1.475					
	PNA	1.277					
July	TI	1.002	0.719	59,482	23	10,355	4
	300hPa Air Temp	1.002					
August	TI	1.000	0.692	61,228	24	10,658	4

RMSE, the most precise model is created in July, which has a MAE value of 10,335 km^2 (Table 13).

The backward method models (Table 14) retain between one and six predictor variables. Generally, these variables match the forward models, although additional variables are included in the backward models for many of the forecast months. As with the forward models, SAT, TI, and MYI occur most frequently in the final models. Other variables present include FDD, 850 hPa air temperature, EAWR, WP, 300hPa air temperature, PE, EA, and 850 hPa geopotential height (Table 14). The variables retained in all forecast models have VIF values close to 1, which suggests that multicollinearity between the variables is not influencing the models (Table 14). Looking at the coefficient of determination for these models, there is less consistency than observed for the forward models. In general, the R^2 values increase as the predictor month approaches the September minimum ice extent, but there are a greater number of months that do not fit this pattern. For example, both November ($R^2 = 0.25$) and December ($R^2 = 0.19$) have R^2 values that are substantially lower than October ($R^2 = 0.37$). February and May also have R^2 values that are lower than expected (Table 14). According to the coefficient of determination, the most precise model is created during June ($R^2 = 0.76$). The RMSE and MAE also show the same patterns as the forward models (a fairly steady value until a drop in June), although larger ranges in these values are observed (Table 14). Both the RMSE and the MAE suggest that the most correct model is created in June (RMSE = 59,192 km^2 and MAE = 10,304 km^2) (Table 14).

Table 14: Results of the backward method SLR for each forecast month. RMSE and MAE percentage of minimum extent are the RMSE and MAE values for each month expressed as a percentage of the mean Beaufort Sea minimum sea ice extent of 254,231 km^2.

Month	Variables Retained	VIF	R^2	RMSE (km^2)	RMSE Percentage of Minimum Extent	MAE (km^2)	MAE Percentage of Minimum Extent
October	SAT	1.000	0.371	87,469	34	15,226	6
November	SAT	1.000	0.254	95,270	37	16,584	7
December	SAT	1.000	0.190	99,277	39	17,282	7
January	MYI	1.068	0.434	87,336	34	15,203	6
	TI	1.126					
	FDD	1.539					
	850hPa Air Temp	1.467					
February	MYI	1.033	0.377	89,977	35	15,663	6
	TI	1.013					
	EAWR	1.022					
March	WP	1.170	0.427	87,832	35	15,290	6
	EAWR	1.040					
	TI	1.120					
	MYI	1.068					
April	MYI	1.033	0.409	86,195	34	15,005	6
	SAT	1.033					
May	MYI	1.000	0.134	102,634	40	17,866	7
June	WP	1.234	0.758	59,192	23	10,304	4
	300hPa Air Temp	1.157					
	PE	1.238					
	EA	1.147					
	SAT	1.464					
	850hPa GPH	1.502					
July	TI	1.002	0.719	59,482	23	10,355	4
	300hPa Air Temp	1.002					
August	TI	1.000	0.692	61,228	24	10,658	4

These discrepancies in the values of R^2, RMSE, and MAE in the backward models from the expected patterns observed for the forward models indicate that the additional variables retained in the backward models do not improve model fit. The addition of these variables appears to complicate the observed results and does not add any appreciable predictive skill to the models. For this reason, the models created by the forward method are considered more precise and physically significant.

IV.5.3 Part 3: Classification and Regression Trees

The variables retained in the final regression trees for each forecast month are presented in Table 15, along with the number of years of record that are split into each terminal node. For each month, anywhere from zero to two splits are made. Four forecast months (January, February, March, and May) contain no splits in their final pruned regression trees. It is likely that during these months the differences observed in the predictor variables are not strong enough to allow for a split to be made using the cross-validation method of pruning. This means that although there are predictor variables that show more importance in forecasting, none of these variables has a strong enough relationship with the September minimum sea ice extent to validate a split using this pruning method. For all months in which a split does occur, the first split is made using either TI or SAT (Table 15). This indicates that for most months these are the two most important variables in predicting the minimum sea ice extent. There are only two months where a second split is made. For April, the second split is made using MYI and for June, the second split is made using PE (Table 15). The results of the final regression trees match with the results of the SLR models, discussed in section 4.5.2, where SAT,

TI, and MYI appeared most frequently. PE, which only appears as a split in the regression tree for June, also only appears in the backward SLR model for June. This indicates that although a pattern between sea ice extent and PE is not present year round,

Table 15: CART model results for each forecast month.

Month	Splitting Variable	Number of Years in Terminal Node
October	TI	12 21
November	SAT	12 21
December	SAT	12 21
January, February, March	(no splits)	
April	SAT MYI	12 10 11
May	(no splits)	
June	SAT PE	11 13 9
July	TI	18 15
August	TI	11 22

there may be some relationship between the two during June that can be utilized in forecasting.

While only a small number of splits are retained in the final regression trees, information about the importance of each predictor variable can still be obtained from the CART analysis. The order of importance of predictor variables indicates which input variables would have been used for further splits if a larger tree had met the cross-validation criteria. The three most important variables for each forecast month are provided in Table 16. The variable importance has been scaled so that the most important variable for each month has a variable importance value of 100. As seen in the final regression trees for each month (Table 15), TI and SAT appear as the most important variables for most forecast months. Only February and March have different variables as the most important predictors (WP and MYI, respectively). Overall, TI, SAT, and MYI appear most frequently in the top three rankings of variable importance (Table 16). This matches the results of the SLR models. In many cases, other air temperature variables, such as FDD and air temperatures at varying atmospheric pressure levels, appear as the second and third most important variables. This supports the conclusion that air temperature conditions throughout the Arctic are critical in understanding the sea ice response each year. A few other predictor variables, such as SLP, wind speed, and geopotential height, appear as important variables for a small number of months. In most cases, these are months, such as January, where no splits were retained in the final regression tree. This indicates that although these variables

appear important, their predictive ability is not strong enough to add any predictive ability to a forecast model.

Table 16: Ranked variable importance for each forecast month. Variable importance is scaled so that the most important variable for each month has an importance score of 100.

	Variable Importance		
	1st	**2nd**	**3rd**
October	TI	SAT	FDD
	100	75	50
November	SAT	FDD	EAWR
	100	58.1	41.9
December	SAT	300hPa Air Temp	500hPa GPH
	100	57.1	50
January	TI	SLP	Wind Speed
	100	70	70
February	WP	MYI	700hPa GPH
	100	69	27.6
March	MYI	700hPa GPH	AO
	100	93.3	73.3
April	SAT	500hPa Air Temp	PE
	100	57.1	52.4
May	SAT	500hPa Air Temp	TI
	100	65.4	65.4
June	SAT	850hPa Air Temp	300hPa GPH
	100	58.3	50
July	TI	SAT	MYI
	100	69	55.2
August	TI	SAT	300hPa GPH
	100	66.7	55.6

IV.6 Discussion and Conclusions

This study examined the predictive ability of atmospheric and sea ice data in forecasting the Beaufort Sea minimum sea ice extent, reached in September of each year. Monthly statistical models were created using SLR and CART. The following results were observed:

1. The forward method of SLR (as compared to the backward method of variable selection) created models which had more reasonable predictive variables as well as more consistent results. For this application, the forward method of SLR is likely more truthful in creating realistic and practical forecast models.
2. Overall, SAT, TI, and MYI were retained by the most models and can therefore be considered the most important predictor variables. This suggests that knowledge of the previous conditions of the sea ice and the surface temperatures of the Arctic throughout the year can provide useful information about the minimum sea ice extent in this region. Other variables that appeared in the final models include the EAWR teleconnection, PNA, and 300 hPa air temperature. Because these variables only appeared in a small number of the final models they are considered less important for future forecast skill.
3. Results from the CART analysis suggest that TI and SAT are the most important variables for predicting sea ice extent. These variables appeared as the first split for all final regression trees (Table 15). MYI also appears as an important variable for many months (Table 16), although it only appears as a split in the final regression tree for April. These results match well with the variables

retained by the SLR models for each forecast month, and therefore confirm the variable selection used in the SLR models.

4. The fit of the SLR models generally increases as predictions are made closer to the September minimum sea ice extent, with the best model fit during the summer months (June, July, and August). This fits with previous findings (Drobot and Maslanik 2003, Drobot 2007, Lindsay et al. 2008).
5. Although the poorest model fit is observed for the models created for the fall months, these months still provide some useful information regarding the September minimum sea ice extent (Tables 13 and 14). These models can speak to the nature of sea ice up to a year in advance and thus still have some use in understanding the ice conditions of the following summer.

IV.6.1 Comparison to Previous Studies

The most important variables retained in the statistical models created for this study do generally match with what has been found by previous research. Here, SAT, TI, and MYI are found to be the most important variables in predicting the minimum sea ice extent. Drobot and Maslanik (2003) found that TI, MYI, and the EA teleconnection index showed predictive ability in every forecast month. Although this study did not find that the EA was a significant contributor to the monthly forecasts, TI and MYI do match as important predictors. Drobot (2007) found that MYI was the most important predictor in the spring, while MYI, surface albedo, and TI were the most important predictors in the summer. Lindsay et al. (2008) indicated that ocean temperatures as well as varying teleconnection indices (primarily the AO) were significant predictors. Finally, Drobot et

al. (2009) found that ice concentration and FDD were the most influential predictors of sea ice conditions. Although there are some slight differences in the final predictor variables chosen in each study, TI and MYI appear consistently in all cases (where applicable).

Although the predictor variables do generally match between studies, the fit of the final forecast models created in previous studies and here show some discrepancy. In previous work, the final models created have higher R^2 and model fit values. Drobot and Maslanik (2003) create monthly models with R^2 values ranging from 0.74 in October to 0.92 in July. Drobot (2007) found an R^2 value of 0.52 for their spring model and 0.80 for their summer model. Lindsay et al. (2008) have R^2 values ranging from 0.81 in October to 0.95 in August. Drobot et al. (2009) successfully predicted the opening date of the Prudhoe Bay shipping season 60 percent of the time. These values can be compared to R^2 values ranging from 0.13 (forward method for May) to 0.72 (forward method for July) found in this study.

Differences in the results obtained in this work and previous studies can be explained by a number of factors. Different time periods are utilized by each study. This study, because it represents the most updated effort in creating forecast models, uses more recent data. Thus, it is possible that the predictive ability of these models has changed solely due to the inclusion of more data in this study. This study attempted to include a large number of predictor variables as inputs into the forecast models. In contrast, each of the previous studies only used some small subset of variables as inputs, which could create differences in the final models. Each of the previous studies utilized a

different measure to quantify the summer ice conditions of the Beaufort Sea. The amount of consistency between many of these measures is assessed in Chapter II. Because the sea ice conditions are being represented in different ways, the subsequent forecast models are of course different. This study incorporated data from the entire Arctic when compiling input data for the PCA analysis. Therefore, the variability of the entire Arctic is utilized to predict the Beaufort Sea minimum sea ice extent. Previous studies used data only over the defined Beaufort Sea study area. The variables included in this study change and interact on a large scale, and it is therefore important to consider the conditions of each variable over a larger area. Lastly, different methods of representing the predictor variables as inputs into the models were employed. For example, for determining the input values of TI, Drobot and Maslanik (2003) strangely chose to use the data from the single pixel within the Beaufort Sea that had the largest coefficient of determination between the BSI (their measure of summer sea ice conditions) and TI for each month. Drobot (2007) input the average value for each variable over the study area. Here, PCA is used to represent the most significant patterns of variability in each of the input variables. This method provides more useful and robust information regarding the spatial changes in each of the input variables and does not inflate the fit of the resulting forecast models. This is an important factor in why the models in this study show poorer model fit than previous studies.

CHAPTER V

SUMMARY AND CONCLUSIONS

This research addresses the question, what is the predictability of the Beaufort Sea minimum sea ice extent and which synoptic-scale climatological variables are most useful in making forecasts of summer sea ice conditions? This investigation answers this research question and addresses outstanding issues from previous studies through three distinct analyses. First, in studies of summer sea ice conditions in the Beaufort Sea, multiple measures of sea ice extent have been utilized. Each of these measures quantifies the conditions of sea ice in a different way, which makes comparisons between studies difficult. These measures include the Barnett Severity Index (BSI), the Beaufort Sea minimum sea ice extent (BS), and the Arctic-wide minimum sea ice extent (AW). Chapter II addresses this problem by providing a rigorous assessment of the consistency between these three measures. Second, previous studies have each focused on a small number of potential climatic predictor variables to predict summer sea ice conditions. A more comprehensive study incorporating all potential predictor variables was needed to fully understand the predictability of sea ice conditions in the Beaufort Sea. Chapter III offers a detailed evaluation of a large number of predictor variables, including atmospheric and surface variables, variables depicting the conditions of the sea ice itself, and teleconnection indices. Lastly, statistical forecast models created in previous studies use different data input methodologies, which have not been updated in many years. Chapter IV provides an updated assessment of the agreement between predictions and

observations up to a year in advance of the September minimum sea ice extent through monthly stepwise linear regression models. Information regarding the relative importance of the climatic predictor variables is provided through a classification and regression tree analysis.

V.1 Assessment of Measures of Sea Ice Extent

Three measures of sea ice conditions, the BSI, BS, and AW, are compared using the timing of light and heavy ice years, various goodness-of-fit measures, and linear regression. The BSI describes the summer sea ice conditions of the Beaufort Sea using information about the Beaufort Sea shipping season, including measures such as the opening date of the shipping lane and the distance to the ice edge on certain dates throughout the summer. The BS uses ice concentration data from the National Snow and Ice Data Center (NSIDC) and quantifies the minimum sea ice extent as the total area of grid cells within the Beaufort Sea with a sea ice concentration of 15% or greater. The AW uses this same methodology, but incorporates the entire Arctic.

The timing of light ice and heavy ice years for each measure were compared. For each measure, a light ice year was defined as any year with a standardized value less than or equal to 1, and a heavy ice year was any year with a standardized value greater than or equal to 1. Overall, the timing of these extreme years matched well between measures, with better agreement between measures for the light ice years as compared to the heavy ice years. Goodness-of-fit measures, such as the coefficient of determination (R^2), root mean square error (RMSE), and mean absolute error (MAE), were used to test the degree of association between measures. Overall, the best agreement was observed

between AW and the BSI, with slightly less agreement observed when either of these measures was compared to BS. Linear regression, performed for each measure, showed that all three measures have very similar slopes (-0.07 for BS, -0.09 for AW, and -0.08 for BSI), suggesting similarity between the measures.

Overall, these results suggest that all three measures show the same level of agreement. This means that it is reasonable to use any of these measures, and that the selection of the most appropriate measure can be made based on the specific goals of the study. BSI should be used when conditions of the sea ice throughout the entire summer are important for the analysis. AW should be used when larger-scale processes are being studied. BS, because it represents the minimum sea ice extent of this smaller region, is the most useful in studies attempting to predict the minimum extent for this smaller region.

V.2 Analysis of Predictor Variables

Sixteen predictor variables and ten teleconnection indices are examined using map analysis to determine which of these variables is expected to have the greatest predictive ability. The predictor variables include atmospheric air temperatures and geopotential heights at 300, 500, 700, and 850 hPa, surface air temperatures, freezing degree days, thawing degree days, sea level pressure, surface wind speed, surface wind direction, total ice concentration, and multiyear ice concentration. Teleconnection indices used include the Arctic Oscillation, the North Atlantic Oscillation, the Pacific-North American pattern, the East Atlantic pattern, the East Atlantic/Western Russia

patter, the East Pacific-North Pacific pattern, the Polar-Eurasia pattern, the Western Pacific pattern, the Southern Oscillation Index, and the Niño 3.4 index.

Examination of these variables was made using composite maps depicting the mean conditions of each variable for the five light ice and five heavy ice years, difference maps comparing the conditions of these two groups, anomaly maps comparing these mean values to the dataset average, and standard deviation maps assessing the consistency in the data within each composite group. This analysis was performed for each variable during each month of the year. Next, correlations assessed the relationship between the sixteen predictor variables and the ten teleconnection indices.

The results of this analysis suggest that of the sixteen predictor variables, the upper atmospheric air temperatures, surface air temperatures (including the monthly mean values, freezing degree days, and thawing degree days), sea level pressure, total ice concentration, and multiyear ice concentration show the greatest potential for predictive ability. These variables had the greatest significant differences between the light ice and heavy ice composites throughout the monthly analysis, suggesting that they may provide useful information regarding whether the sea ice for a given year will be heavy or light. Of the teleconnections studied, the Arctic Oscillation, North Atlantic Oscillation, Pacific-North America, and East Pacific-North Pacific patterns consistently showed the most grid cells with significant correlations with the predictor variables. These four teleconnection indices therefore may be driving the changes observed in the predictor variables and therefore may have some predictive ability.

V.3 Predicting September Sea Ice Extent

Monthly forecast models are created using both forward and backward stepwise linear regression. These models predict the Beaufort Sea September minimum sea ice extent beginning in October and going through August. To begin, all predictor variables and teleconnection indices are input into the models. To avoid over-fitting, these variables are tested for collinearity using correlation analysis between variables and variance inflation factors (VIFs). When two input variables were collinear, one of them was removed. The determination of which variable to remove was made based on the results obtained in Chapter III. The predictive ability of the final models was assessed using the coefficient of determination (R^2), root mean square error (RMSE), and mean absolute error (MAE).

Overall, surface air temperature, total ice concentration, and multiyear ice concentration were retained by the largest number of linear regression models. This suggests that these variables are the most important in predicting the September sea ice conditions in this region. The forecast skill of these models generally increased as predictions were made closer to the September minimum sea ice extent, which fit with the findings of previous studies. The best model fit was observed during the summer months (June, July, and August). Although the poorest model fit was observed in the fall models, these months still provide some useful information. This suggests that some knowledge of summer sea ice conditions can be obtained up to a year in advance of the September minimum sea ice extent.

Classification and regression trees were utilized for each forecast month to rank the input variables based on their relative importance. Results from this analysis suggest that total ice concentration and surface air temperature are the two most important predictor variables throughout the year. Multiyear ice concentration also appeared as an important predictor in many months. These results match the variables retained in the stepwise linear regression models.

Comparisons of the final models to previous studies yielded interesting results. Overall, there was agreement in the most important predictor variables, with antecedent ice conditions (total ice concentration and multiyear ice concentration) appearing as important predictors in many previous models. The fit of the forecast models obtained in this analysis, however, did differ from previous studies. In previous studies, forecast models show much greater potential predictive ability. This discrepancy in model fit can be explained by a number of factors. Most importantly, non-stationarity may affect this analysis, as it represents an updated assessment of the predictability of summer sea ice conditions in the Beaufort Sea, and therefore includes more recent data. With the inclusion of the last few years, where record minima in sea ice extent have been observed, the predictive ability of these linear forecast models have decreased. This suggests that the distribution of minimum sea ice extent may no longer be following a linear pattern, as suggested by Stroeve at al. (2011).

V.4 Final Conclusions

This assessment has contributed to the overall knowledge of sea ice conditions in the Beaufort Sea. The use of surface air temperature, total ice concentration, and

multiyear ice concentration as predictor variables was confirmed and a more current assessment of the model fit of linear regression models was performed. The results obtained in this analysis suggest that the predictive ability of linear forecast models has decreased in recent years. This confirms previous studies, which have suggested that changes in sea ice associated with Arctic Amplification have created a new climate regime in the Arctic, where sea ice is now responding to atmospheric conditions in a different way (National Research Council 2012, Maslanik et al. 2007b, Stroeve et al. 2007, Stroeve et al. 2011, Serreze and Francis 2006, Serreze et al. 2011).

REFERENCES

Abdi, H. and Williams, L.J. (2010) Principal component analysis. *WIREs Comp Stat*, 2: 433–459. doi: 10.1002/wics.101.

Alexander, M.A., Bhatt, U.S., Walsh, J.E., Timlin, M.S., Miller, J.S., Scott, J.D. (2004) The atmospheric response to realistic Arctic sea ice anomalies in an AGCM during winter. *Journal of Climate,* 17: 890–905.

Ballinger, T.J. and Sheridan, S.C. (2013) Associations between circulation pattern frequencies and sea ice minima in the western Arctic. *International Journal of Climatology*, 33.

Barnes, E.A. (2013) Revisiting the evidence linking Arctic amplification to extreme weather in midlatitudes. *Geophysical Research Letters*, 40: 4728–4733, doi:10.1002/grl.50880.

Barnett, D.G. (1980) A long-range forecasting method for the north coast of Alaska. *Sea ice processes and models*, R. Pritchard, Ed., University of Washington Press, 402–409.

Barnston, A.G., and Livezey, R.E. (1987) Classification, seasonality and persistence of low-frequency atmospheric circulation patterns. *Monthly Weather Review,* 115: 1083-1126.

Bhatt, U.S., Walker, D.A., Raynolds, M.K., Comiso, J.C., Epstein, H.E., Gia, G.-S., Gens, R., Pinzon, J.E., Tucker, C.J., Tweediw, C.E., Webber, P.J. (2010) Circumpolar Arctic tundra vegetative change is linked to sea ice decline. *Earth Interactions,* 14: 1–20.

Breiman, L., Freidman, J., Stone, C.J., Olshen, R.A. (1984) Classification and regression trees. Chapman and Hall/CRC, 1st edition.

Cavalieri, D., Parkinson, C., Gloersen, P., Zwally, H.J.. (1996) updated yearly. Sea ice concentrations from nimbus-7 SMMR and DMSP SSM/I-SSMIS passive microwave data. Boulder, Colorado USA: National Snow and Ice Data Center.

Chen, Y.U., (1982) Assessment of southern oscillation sea-level pressure indices. *Monthly Weather Review*, 110: 800-807

De'ath, G., and Fabricius, K.E. (2000) Classification and regression trees: A powerful yet simple technique for ecological data analysis. *Ecology,* 81(11): 3178-3192.

Deser, C., J.E. Walsh, and Timlin, M.S. (2000) Arctic sea ice variability in the context of recent atmospheric circulation trends. *Journal of Climate*, 13(3): 617-633.

---------- Thomas, R., Alexander, M., Lawrence, D. (2010) The seasonal atmospheric response to projected Arctic sea ice loss in the late 21st century. *Journal of Climate,* 23: 333–351. doi:10.1175/2009JCL13053.1.

Drobot, S. (2003) Long-range statistical forecasting of ice severity in the Beaufort-Chukchi Sea. *Weather and Forecasting*, 18(C3): 1161-1176. doi: 10.1175/1520-0434(2003)018<1161:LSFOIS>2.CO;2

---------- and J. A. Maslanik (2003) Interannual variability in summer Beaufort Sea ice conditions: Relationship to winter and summer surface and atmospheric variability. *Journal of Geophysical Research*, 108(C7). doi: 10.1029/2002JC001537.

---------- (2007) Using remote sensing data to develop seasonal outlooks for Arctic regional sea-ice minimum extent. *Remote sensing of environment*, 111(2-3): 136-147. doi:10.1016/j.rse.2007.03.024.

----------, J. A. Maslanik, and M. R. Anderson (2009) Interannual variations in the opening date of the Prudhoe Bay shipping season: Links to atmospheric and surface conditions. *International Journal of Climatology*, 29(2): 197-203.

Dumas, J. A., Flato, G.M., Weaver, A.J. (2003) The impact of varying atmospheric forcing on the thickness of Arctic multi-year sea ice. *Geophysical Research Letters*, 30(18). doi: 10.1029/2003GL017433.

Fowler, C., Emery, W.J., Maslanik, J. (2004) Satellite-derived evolution of Arctic sea ice age: October 1978 to March 2003. *IEEE Geoscience Remote Sensing Society Letters,* 1(2): 71.74.

Francis, J.A. and Hunter, E. (2006) New insight into the disappearing Arctic sea ice. *Eos, Transactions American Geophysical Union,* 87: 509–511.

----------, Chan, W.H., Leathers, D.J., Miller, J.R., Veron, D.E. (2009) Winter northern hemisphere weather patterns remember summer. *Geophysical Research Letters,* 36: L07503. doi:10.1029/2009GL037274.

---------- and Vavrus, S.J. (2012) Evidence linking Arctic amplification to extreme weather in mid-latitudes. *Geophysical Research Letters,* 39: L06801, doi: 10.1029/2012GL051000.

Griffiths, Franklyn. (1987) Politics of the northwest passage. Kingston: McGill-Queen's University Press.

Higgins, M.E., Cassano, J.J. (2009) Impacts of reduced sea ice on winter Arctic

atmospheric circulation, precipitation and temperature. *Journal of Geophysical Research*. 114, D16107. doi:10.1029/2009JD011884.

Holland, M.M. and Stroeve, J. (2011) Changing seasonal sea ice predictor relationships in a changing Arctic climate. *Geophysical Research Letters*, 38(18). doi: 10.1029/2011GL049303.

International Hydrographic Organization (IHO) (1953) Limits of oceans and seas, 3rd edition. Published online.

Kistler R., Kalnay, E., Collins, W., Saha, S., White, G., Woollen, J., Chelliah, M., Ebisuzaki, W., Kanamitsu, M., Kousky, V., van den Dool, H., Jenne, R., and Fiorino, M. (2001) The NCEP-NCAR 50-year reanalysis: Monthly means CD-ROM and documentation. *Bulletin of the American Meteorological Society*, 82(2): 247-268.

Klein, W.H., and Walsh, J.E. (1983) A comparison of pointwise screening and empirical orthogonal functions in specifying monthly surface temperature from 700 mb data. *Monthly Weather Review*, 111: 669-673.

Kunkel, K. E., Eastering, D. R., Wang, W. (1993) Upper air flow patterns associated with heavy precipitation: A comparison of observed and GCM data. *Proceedings of the Eighth Applied Climatology Conference of the American Meteorological Society, Anaheim, California*, 137-140.

Lawrence, D.M., Slater, A.G., Tomas, R.A., Holland, M.M., Deser, C. (2008) Accelerated Arctic land warming and permafrost degradation during rapid sea ice loss. *Geophysical Research Letters,* 35: L11506. doi:10.1029/2008GL033894.

Leathers, D.J., Yarnal, B., and Palecki, M.A. (1991) The pacific/north American teleconnection pattern and the United States climate. Part I: Regional temperature and precipitation associations. *Journal of Climate*, 4: 517-528.

Legates, D. R., and R. E. Davis (1997) The continuing search for an anthropogenic climate change signal: Limitations of correlation-based approaches, *Geophysical Research Letters* 24:2319–2322.

---------- and G. J. McCabe Jr. (1999) Evaluating the use of "goodness-of-fit" measures in hydrologic and hydroclimatic model validation. *Water Resources Research,* 35(1): 233-241.

Lemke, P., J. Ren, R. B. Alley, I. Allison, J. Carrasco, G. Flato, Y. Fuji, G. Kaser, P. Mote, R. H. Thomas and T. Zhang. (2007) Observations: Changes in snow, ice, and frozen ground. In: Climate change 2007: The physical science basis. Contribution of working group I to the fourth assessment report of the intergovernmental panel on

climate change [Solomon, S., D. Qin, M. Manning, Z. Chen, M. Marquis, K. B. Averyt, M. Tignor and H. L. Miller (eds.)]. Cambridge University Press, Cambridge, United Kingdom and New York, NY, USA.

L'Heureux, M. L., A. Kumar, G. D. Bell, M. S. Halpert, and R. W. Higgins (2008), Role of the Pacific-North American (PNA) pattern in the 2007 Arctic sea ice decline. *Geophysical Research Letters,* 35: L20701, doi:10.1029/2008GL035205.

Lindsay, R.W., and Shang, J. (2005) The thinning of Arctic sea ice, 1988-2003: Have we passed a tipping point? *Journal of Climate,* 18:4879-4894.

----------, Shang, J., Schweiger, A.J., Steel, M.A. (2008) Seasonal predictions of ice extent in the Arctic Ocean. *Journal of Geophysical Research*, 113(C2). doi: 10.1029/2007JC004259.

Liu, J., Curry, J., Wang, H. (2012) Impact of declining Arctic sea ice on winter snowfall. *Proceedings of the National Academy of Science (USA)*, 109(11): 4074–4079, doi:10.1073/pnas.1114910109.

Maslanik J.A., Fowler, C., Stroeve, J., Drobot, S., Zwally, H.J., Yi, D., Emery, W.J. (2007a) A younger,thinner ice cover: Increased potential for rapid, extensive ice loss. *Geophysical Research Letters,* 34: L24501.doi:10.1029/2007GL032043

----------, S. Drobot, C. Fowler, W. Emery, and R. Barry (2007b) On the Arctic climate paradox and the continuing role of atmospheric circulation in affecting sea ice conditions. *Geophysical Research Letters*, 34(3). doi: 10.1029/2006GL028269

---------- Stroeve, J., Fowler, C., and Emery, W. (2011) Distribution and trends in Arctic sea ice age through spring 2011. *Geophysical Research Letters*, 38: L13502, doi:10.1029/2011GL047735.

National Center for Atmospheric Research (NCAR). (2012) Southern oscillation index (SOI). Published online, http://www.cgd.ucar.edu/cas/catalog/climind/soi.html.

National Oceanic and Atmospheric Administration (NOAA) National Climatic Data Center. Teleconnections. Published online, http://www.ncdc.noaa.gov/teleconnections/.

National Research Council (2012) Seasonal-to-decadal predictions of Arctic sea ice: Challenges and strategies. Washington, DC: The National Academies Press.

National Weather Service (NWS) Climate Prediction Center (CPC). Teleconnections. Published online, http://www.cpc.ncep.noaa.gov/data/teledoc/telecontents.shtml.

Ogi, M. ,and Wallace, J.M. *(*2012) The role of summer surface wind anomalies in the summer Arctic sea ice extent in 2010 and 2011. *Geophysical Research Letters,* 39:L09704, doi*:*10.1029/2012GL051330*.*

Overland, J.E., Adams, J.M., Bond, N.A. (1998) Decadal variability of the Aleutian Low and its relation to high-latitude circulation. *Journal of Climate,* 12: 1542-1548.

----------, Wang, M. (2010) Large-scale atmospheric circulation changes are associated with the recent loss of Arctic sea ice. *Tellus,* 62A: 1–9.

Palecki, M. A., and Leathers, D. J. (1993) Northern hemisphere extratropical circulation anomalies and recent January land surface temperature trends .*Geophysical Research Letters,* 20:819-822.

Perovich, D.K., Light, B., Eicken, H., Jones, K.F., Runciman, K., Nghiem, S.V. (2007) Increasing solar heating of the Arctic Ocean and adjacent seas (1979-2005): Attribution and role in the ice-albedo feedback. *Geophysical Research Letters,* 34:L19505, doi: 10.1029/2007GL031480.

Petoukhov, V., Semenov, V.A. (2010) A link between reduced Barents-Kara sea ice and cold winter extremes over northern continents. *Journal of Geophysical Research,* 115: D21111. doi:10.1029/2009JD013568.

Polar Science Center (2010) Freezing degree-days (FDD) and thawing degree-days (TDD). Published online, http://psc.apl.washington.edu/nonwp_projects/landfast_ice/freezing.php.

Rigor, I. G., Wallace, J.M., Colony, R.L. (2002) Response of sea ice to the Arctic Oscillation. *Journal of Climate,* 15: 2648-2663.

Rogers, J. C. (1978). Meteorological factors affecting interannual variability of summertime ice extent in the Beaufort Sea. *Monthly Weather Review,* 106:890–897.

Screen J.A., Simmonds, I. (2010) The central role of diminishing sea ice in recent Arctic temperature amplification. *Nature,* 464. doi:10.1038/nature09051

Seierstad, I.A., Bader, J. (2008) Impact of a projected future Arctic sea ice reduction of extratropical storminess and the NAO. *Climate Dynamics*. doi:10.1007/s00382-008-0463-x.

Serreze, M.C., and Barry, R.G. (2005) The Arctic climate system. Cambridge University Press.

---------- and Barry, R. G. (2011) Processes and impacts of Arctic amplification: A research synthesis. *Global and Planetary Change,* 77: 85-96

----------, Holland, M.M., Stroeve, J. (2007a) Perspectives on the Arctic's shrinking sea ice cover. *Science,* 315:1533–1536

----------, Barrett, A.P., Slater, A.J., Steele, M., Zhang, J., Trenberth, K.E. (2007b) The large-scale energy budget of the Arctic. *Journal of Geophysical Research,*112:D11122. doi:10.1029/2006JD008230

----------, Francis, J.A. (2006) The Arctic amplification debate. *Climatic Change,* 76: 241–264.

----------, Barrett, A.P., Stroeve, J.C., Kindig, D.M., Holland, M.M. (2009) The emergence of surface-based Arctic amplification. *Cryosphere,* 3:11–19.

Stroeve, J., Holland M.M., Meier, W., Scambos, T., Serreze. M. (2007) Arctic sea ice decline: Faster than forecast. *Geophysical Research Letters*, 34(9). doi: 10.1029/2007GL029703.

----------, Serreze, M., Drobot, S., Gearheard, S., Holland, M., Maslanik, J., Meier, W., Scambos, T. (2008) Arctic sea ice extent plummets in 2007. *Eos, Transactions American Geophysical Union,* 89: 13–14.

----------, Serreze, M.C., Holland, M.M., Kay, J.E., Maslanik, J., Barrett, A.P. (2011) The Arctic's rapidly shrinking sea ice cover: A research synthesis. *Climatic Change*, published online.

Wallace, J.M., and Gutzler, D.S. (1981) Teleconnections in the geopotential height field during the Northern Hemisphere winter. *Monthly Weather Review,* 109: 784-812.

Walsh, J. E. (1980) Empirical orthogonal functions and the statistical predictability of sea ice extent. *Sea Ice Processes and Models*, edited by R. S. Pritchard, pp. 373-384, University of Washington Press, Seattle.

Willmott, C. J. (1984) On the evaluation of model performance in physical geography. *Spatial Statistics and Models*, edited by G. L. Gaile, and C. J. Willmott: 443–460.

---------- and Matsuura, K. (2005) Advantage of the mean absolute error (MAE) over the root mean square error (RMSE) in assessing average model performance. *Climate Research*, 30: 79-82.

Winton, M. (2006) Amplified Arctic climate change: What does surface albedo feedback

have to do with it? *Geophysical Research Letters,* 33: L03701. doi:10.1029/2005GL025244.

Wood, K. R., Overland, J.E., Salo, S.A., Bond, N.A., Williams, W.J., Dong, X. (2013) Is there a "new normal" climate in the Beaufort Sea? *Polar Research*, 32.

World Climate Research Programme: Climate and Cryoshpere (CLiC) Project. (2007) Integrated global observing strategy: A cryoshpere theme report.

Yamamato, K.Y., Tachibana, Y., Honda, M., Ukita, J. (2006) Intra-seasonal relationships between the Northern Hemisphere sea ice variability and the North Atlantic Oscillation. *Geophysical Research Letters*, 33: L14711. doi:10.1029/2006GL026286.